doi:10.1006/mthe.2001.0323, available online at http://www.idealibrary.com on IDEAL

Development of a FLP/frt System for Generating Helper-Dependent Adenoviral Vectors

Philip Ng,* Cindy Beauchamp,* Carole Evelegh,* Robin Parks,*,[1] and Frank L. Graham*,†,[2]

*Department of Biology and †Department of Pathology, McMaster University, Hamilton, Ontario, Canada L8S 4K1

Received for publication January 30, 2001; accepted in revised form April 3, 2001

Helper-dependent (HD) adenoviral vectors devoid of all viral coding sequences have a large cloning capacity and have been reported to provide long-term transgene expression *in vivo* with negligible toxicity, making them attractive vectors for gene therapy. Currently, the most efficient means of generating HD vectors involves co-infecting 293 cells expressing Cre with the HD vector and a helper virus bearing a packaging signal flanked by loxP sites. Cre-mediated excision of the packaging signal renders the helper virus genome unpackageable but still able to replicate and to provide helper functions for HD vector propagation. HD vector titer is increased by serial co-infections. Typically, helper virus contamination is ≤1% pre- and ≤0.1% postpurification by CsCl banding. While these contamination levels are low, further reduction is desirable. Alternative methods of selection against the helper virus may achieve this goal, especially when combined with Cre/loxP. We describe the development of a system for generating HD vectors based on site-specific recombination between frt sites catalyzed by FLP recombinase and show by direct comparison that the FLP/frt and Cre/loxP systems are equivalent with respect to HD vector amplification efficiency and helper virus contamination levels. Availability of a second recombinase system for HD vector production will enhance the utility and flexibility of HD vectors.

Key Words: **adenovirus; helper-dependent adenoviral vector; helper virus; FLP recombinase; Cre recombinase; gene therapy.**

Introduction

Adenoviruses (Ads) are excellent mammalian gene transfer vectors due to their ability to efficiently infect a wide variety of quiescent and proliferating cell types from various species to direct high-level gene expression. Consequently Ad vectors are extensively used as potential recombinant viral vaccines, for high-level protein production in cultured cells, and for gene therapy (1–4). First-generation Ad vectors typically have foreign DNA inserted in place of early region 1 (E1). E1-deleted vectors are replication deficient and are propagated in E1-complementing cells such as 293 (5). While these vectors remain very useful for many applications, it has become clear that transgene expression *in vivo* is only transient. Several factors contribute to this, including strong innate and inflammatory responses to the vector (6, 7), acute and chronic toxicity due to low level viral gene expression from the vector backbone (8), and generation of anti-Ad cytotoxic T-lymphocytes due to *de novo* viral gene expression (9–12) or processing of virion proteins (13). While high level transient transgene expression afforded by first-generation Ad vectors may be adequate, or even desirable, for many gene transfer and gene therapy applications, the transient nature of their expression kinetics renders these vectors unsuitable in cases in which prolonged, stable expression is required.

In principle, the simplest way to eliminate Ad-induced toxicity due to expression of viral proteins is to remove all viral coding sequences from the vector. Because cell lines that express the full array of adenoviral genes are currently not available, a "helper" Ad is required to provide all necessary functions *in trans* for propagation of these fully deleted, "helper-dependent" (HD) vectors. The only Ad sequences required *in cis* for vector propagation are the inverted terminal repeats (ITRs) necessary for DNA replication and the packaging signal (ψ) necessary for encapsidation of the vector genome. These *cis*-acting elements amount to only ~500 bp. HD vectors retain many of the

[1] Present address: Ottawa Health Research Institute, Room 4F102, 501 Smyth Road, Ottawa, Ontario, Canada K1H 8L6.

[2] To whom correspondence and reprint requests should be addressed. Fax: (905) 521-2955. E-mail: graham@mcmaster.ca.

1525-0016/01 $35.00

benefits of first-generation Ad vectors such as efficient transduction of a wide variety of dividing and nondividing cells from numerous species but have the added advantage of increased cloning capacity (~37 kb) and it is now becoming clear that they offer the potential for reduced toxicity and prolonged, stable transgene expression (14–21).

Currently, the most efficient means of generating HD vectors is the Cre/loxP system developed by Graham and co-workers (22). In this system, 293 cells expressing Cre are co-infected with the HD vector and a helper virus bearing a packaging signal flanked by loxP sites. Cre-mediated excision of the packaging signal renders the helper virus genome unpackageable but still able to provide all functions *in trans* for the propagation of the HD vector. The titer of the HD vector is increased by serial co-infection of Cre-expressing 293 cells with the HD vector and the helper virus. In the last step, the HD vector is purified by CsCl ultracentrifugation. While a number of factors can influence the yield and purity of HD vectors, typically about 10^{10} to 10^{11} vector particles are produced per 10^7 co-infected cells with a helper virus contamination level of ≤1 and ≤0.1% pre- and postpurification by CsCl ultracentrifugation (22, 24).

While these helper virus contamination levels are low, further reduction is desirable especially considering the high doses of HD vector that may be required as well as the inconvenience of CsCl ultracentrifugation for large-scale production of clinical-grade vectors. Alternative methods of selection against the helper virus may prove useful for achieving this goal, especially if used in conjunction with the Cre/loxP system. As a first step toward this goal, we have developed a system based on the yeast site-specific recombinase FLP, which catalyzes recombination between frt sites (23) for generating HD vectors, and have directly compared this system to the Cre/loxP system with respect to the efficiency of HD vector amplification and levels of helper virus contamination.

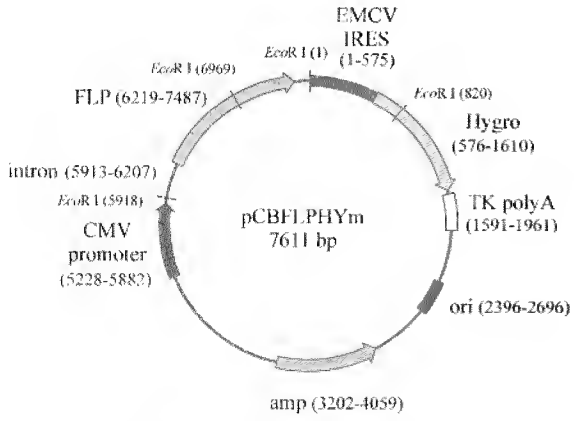

FIG. 1. The plasmid pCBFLPHYm was used to generate the FLP-expressing cell lines. The FLP coding sequence is separated from the hygromycin resistance coding sequence by the EMCV IRES. This bicistronic construct is expressed from the cytomegalovirus (CMV) immediate-early promoter. Other important features include an intron between the CMV promoter and the FLP coding sequence and a thymidine kinase (TK) poly(A).

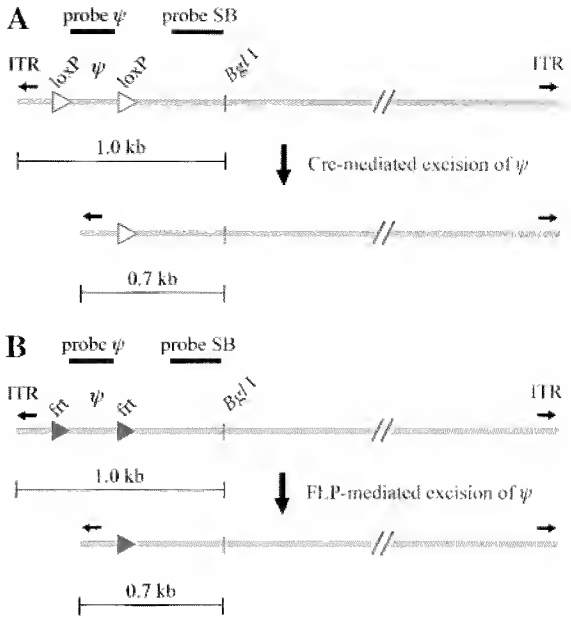

FIG. 2. (A) The helper virus AdLC8cluc has a packaging signal flanked by loxP sites. (B) The helper virus AdCBfrt3 has a packaging signal flanked by frt sites. The sizes of the relevant *BglI* fragments and the location of probe SB and probe ψ are shown.

Materials and Methods

Plasmids and viruses. The plasmid pCBFLPHYm contains the wild-type FLP (a generous gift from Dr. Volker Sandig, Merck Research Laboratories) and hygromycin resistance coding sequences, separated by the encephalomyocarditis virus (EMCV) internal ribosome entry site (IRES) (Fig. 1). The hygromycin protein contains a Leu (TCG) to Ser (TTG) substitution at amino acid position 239. This bicistronic construct is driven by the cytomegalovirus (CMV) immediate-early promoter. Other important features include an intron between the promoter and the FLP coding sequence and a thymidine kinase poly(A) 3′ of the hygromycin coding sequence. The helper virus AdLC8cluc has been previously described (Fig. 2A) (22). The helper virus AdCBfrt3 is identical to AdLC8cluc except that the packaging signal is flanked by frt instead of loxP sites (Fig. 2B). AdCBfrt3 was constructed by the same strategy used for the construction of AdLC8cluc (22) expect that synthetic oligonucleotides (5′-GAT CGA AGT TCC TAT ACT CTA GTA AGA ATA GGA ACT TCG AAT TC-3′ and 5′-GAT CGA ATT CGA AGT TCC TAT TCT TAC TAG AGT ATA GGA ACT TC-3′) containing an frt site instead of a loxP site were used. The helper-dependent vector backbone plasmid C4HSU has been described in detail elsewhere (24). The plasmid pC4HSULacZ (Fig. 3) was constructed by replacing the two adjacent *EheI* fragments in the plasmid C4HSU with the LacZ expression cassette, and the HD vector AdC4HSULacZ genome (Fig. 3) was liberated by digesting pC4HSULacZ with *PmeI*.

FLP-expressing cell lines. The FLP-expressing cell lines 293FLP and 293CreFLP were generated by transfecting 100-mm dishes of semiconfluent monolayers of 293 (25) and 293Cre4 cells (26), respectively, with 5 μg of pCBFLPHYm by calcium phosphate coprecipitation (27). Forty-eight hours posttransfection, cells were subjected to hygromycin selection (400 μg/ml for 293FLP cells and 175 μg/ml for 293CreFLP cells). Individual stable transformants were isolated 2 to 3 weeks posttransfection. FLP expression from the stable transformants was determined as follows: stable transformants were infected with AdCBfrt3 at an m.o.i. of 1, and total DNA was extracted from the cells 48 h postinfection, digested with *BglI*, and analyzed by Southern blot hybridization with probe fragment SB to determine the efficiency of FLP-mediated packaging signal excision as described below and in Fig. 5. Most transformants analyzed were similar with respect to efficiency of packaging signal excision and growth char-

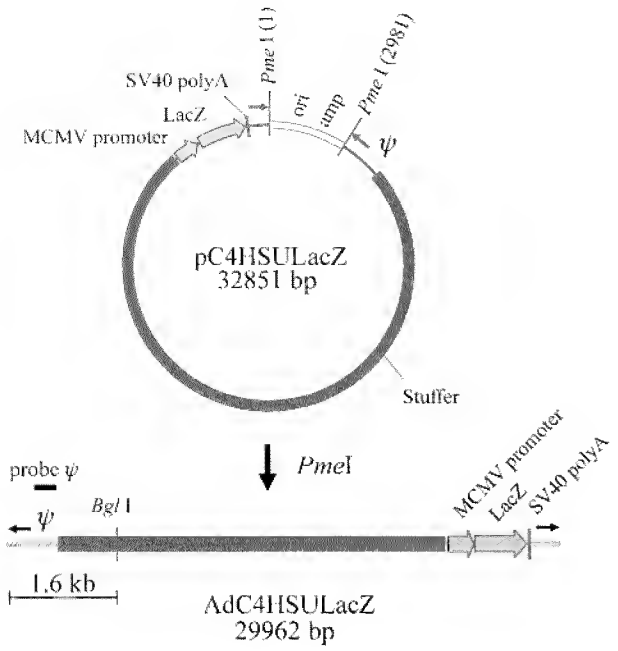

FIG. 3. The HD vector AdC4HSULacZ contains a LacZ reporter gene driven by the murine CMV immediate-early promoter, and the vector genome is released from the plasmid pC4HSULacZ by *PmeI* cleavage. The size of the relevant *BglI* fragment and the location of probe ψ are shown. Small black arrows represent the Ad inverted terminal repeats.

acteristics and two representative transformed cell lines, designated 293FLP and 293CreFLP, were chosen for further studies.

Analysis of HD vector amplifications. The HD vector AdC4HSULacZ was amplified according to the method of Parks *et al.* (22) with the following modifications: the same cell line (293Cre4, 293FLP, or 293CreFLP) was used for the initial HD vector rescue by transfection/infection (serial passage 0) as was used throughout the amplification, the helper virus was added at an m.o.i. of 1 for all serial passages except for passage 0 at which an m.o.i. of 5 was used, and 0.4 ml of each passage was used as inoculum for the subsequent passage. The titer of the HD vector, in blue-forming units (bfu)/ml, was measured at each serial passage as described (22). Total DNA, comprising cellular and both encapsidated and unencapsidated viral (HD vector and helper virus) DNA, was extracted from co-infected cells at each serial passage for Southern analysis as follows: when complete cytopathic effect was reached (48 h post-co-infection), the cells were scraped into the medium and 1 ml of the cell suspension was transferred to a microfuge tube. The infected cells were centrifuged, the supernatant was discarded, and the cell pellet was lysed by the addition of 0.2 ml of SDS–Pronase solution (0.5 mg/ml Pronase in 0.5% SDS, 10 mM Tris, pH 7.4, 10 mM EDTA, pH 8.0.) and incubation at 37°C overnight. The volume of the lysate was adjusted to 0.4 ml by the addition of TE and the DNA was precipitated by adding 1 ml 95% ethanol and recovered by centrifugation. The DNA pellet was washed twice with 70% ethanol and resuspended in TE. Virion DNA, comprising only encapsidated viral (HD vector and helper virus) DNA, was extracted as follows: infected cells were collected as described above and the infected cell pellet was resuspended in 400 μl of 100 mM Tris, pH 8.0. Cells were lysed by adding 50 μl of 5% sodium deoxycholate and incubating at 37°C for 1 h. $MgCl_2$ was then added to a final concentration of 20 mM. Cellular and unpackaged viral DNA and RNA were digested by adding DNase I and RNase A to a final concentration of 10 μg/ml each and incubating for 2 h at 37°C. EDTA and EGTA were then added to a final concentration of 5 mM each and virus particles were lysed and proteins digested by adding SDS to 0.5% and Pronase to a final concentration of 1 mg/ml and incubating for 1 h at 37°C. Following phenol, phenol/chloroform, and chloroform extraction, the virion DNA was precipitated by adding 95% ethanol. The DNA pellet was recovered by centrifugation, washed twice with 70% ethanol, and resuspended in TE. Probe SB is the 496-bp *SalI–BglI* fragment from the plasmid pDC411 (Microbix). Probe ψ is composed of two synthetic oligonucleotides (5′-CCG GTG TAC ACA GGA AGT GAC AAT TTT CGC GCG GTT TTA GGC GGA TGT TGT AGT AAA TTT GGG CGT AAC CGA GTA AGA TTT GGC CAT TTT CGC GGG AAA ACT GAA TAA GAG GAA GTG AAA TCT GAA TAA TTT TGT GTT ACT CAT AGC GCG TAA T-3′ and 5′-A TTA CGC GCT ATG AGT AAC ACA AAA TTA TTC AGA TTT CAC TTC CTC TTA TTC AGT TTT CCC GCG AAA ATG GCC AAA TCT TAC TCG GTT ACG CCC AAA TTT ACT ACA ACA TCC GCC TAA AAC CGC GCG AAA ATT GTC ACT TCC TGT GTA CAC CGG-3′) which are 100% homologous to the packaging signals of AdC4HSULacZ, AdLC8cluc, and AdCBfrt3.

Results and Discussion

Figure 4 presents an overview of the FLP/frt system for generating HD vectors. In this system, 293 cells expressing FLP are co-infected with the HD vector and a helper virus. The HD vector bears the transgene of interest and only those *cis*-acting viral elements required for DNA rep-

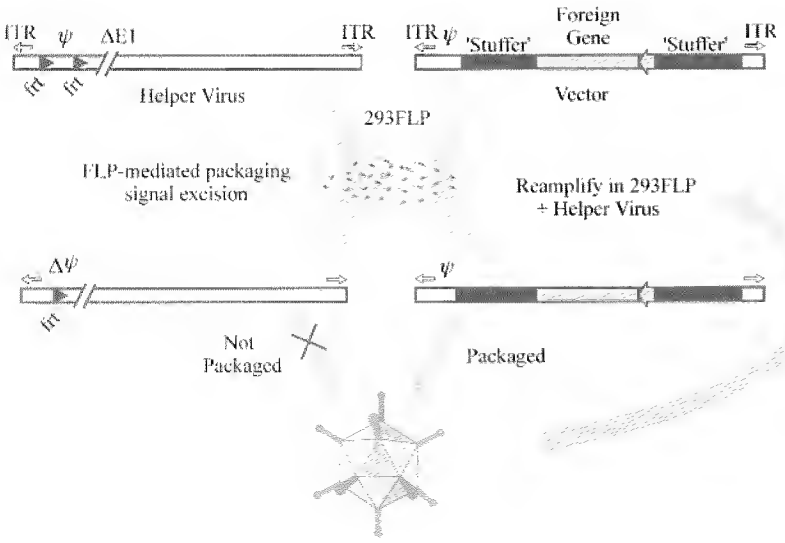

FIG. 4. The FLP/frt system for generating HD vectors. FLP-expressing 293 cells are co-infected with the HD vector and a helper virus bearing a packaging signal flanked by frt sites. FLP-mediated excision of the packaging signal renders the helper virus genome unpackageable but still able to replicate and provide all the *trans*-acting factors for the propagation of the HD vector. The titer of the HD vector is increased by serial co-infection of FLP-expressing 293 cells with the helper virus and the HD vector.

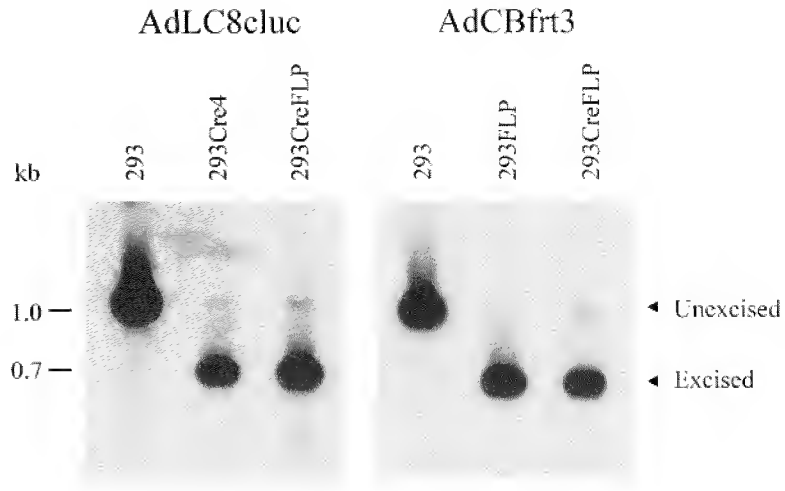

FIG. 5. Excision of the packaging signal from helper viruses following infection of cell lines expressing site-specific recombinases. Total DNA was extracted from the indicated cells 48 h postinfection with the indicated helper virus, digested with *BglI*, and analyzed by Southern blotting with probe SB.

lication (ITR) and encapsidation (ψ). The helper virus is an E1-deleted Ad bearing a packaging signal flanked by frt sites. Following co-infection, the packaging signal is excised from the helper virus genome by FLP-mediated site-specific recombination rendering it unpackageable but still able to replicate and provide all the *trans*-acting factors needed for the propagation of the HD vector. The titer of the HD vector is increased by serial co-infections and the HD vector is purified by CsCl banding.

Helper viruses and site-specific recombinase-expressing cell lines. The helper virus AdCBfrt3 bears a packaging signal flanked by frt sites (Fig. 2B). Except for the frt sites, AdCBfrt3 is identical to the helper virus, AdLC8cluc, used in the Cre/loxP system (Fig. 2A) (22). The cell lines 293FLP and 293CreFLP were generated by transfecting 293 and 293Cre4 cells, respectively, with the plasmid pCBFLPHYm as described under Materials and Methods. We first determined whether the packaging signal from AdCBfrt3 could be excised by FLP-mediated recombination following infection of 293FLP and 293CreFLP cells. For comparison, Cre-mediated packaging signal excision was also analyzed by infecting 293Cre4 cells with AdLC8cluc. We also determined the efficiency with which the packaging signal of AdLC8cluc could be excised by Cre-mediated recombination following infection of 293CreFLP cells. These analyses were accomplished by infecting the various cell lines with the relevant helper virus at an m.o.i. of 1. Total DNA was extracted from the cells 48 h postinfection, digested with *BglI*, and analyzed by Southern blotting with probe SB. In the absence of packaging signal excision the left end of the helper virus genome is present in a 1-kb *BglI* fragment (Fig. 2). Following packaging signal excision, this fragment is reduced to 0.7 kb (Fig. 2). The results of these analyses indicated that the efficiencies of FLP-mediated packaging signal excision using 293FLP or 293CreFLP cells and Cre-mediated packaging signal excision using 293Cre4 cells were all comparable (Fig. 5). As well, the results indicated that the efficiencies of Cre-mediated packaging signal excision using 293CreFLP cells or the parental 293Cre4 cells were comparable.

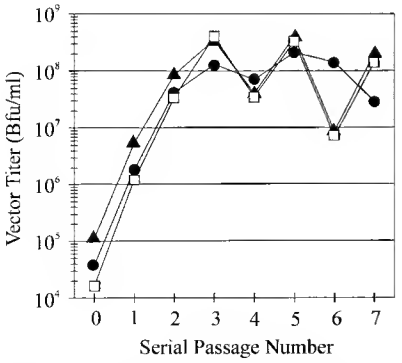

FIG. 6. Amplification of AdC4HSULacZ with the Cre/loxP system using AdLC8cluc and 293Cre4 cells (●) or with the FLP/frt system using AdCBfrt3 and 239FLP cells (□) or 293CreFLP cells (▲). The titer of AdC4HSULacZ, in blue forming units (bfu)/ml, was determined at each serial passage.

Efficiency of HD vector amplification. To directly compare the FLP/frt system with the Cre/loxP system with respect to the efficiency of HD vector amplification, the two systems were used to amplify the HD vector AdC4HSULacZ (Fig. 6) in parallel, and the titer of the HD vector was determined at each serial passage. As shown in Fig. 6, the FLP/frt system using AdCBfrt3 and either 293FLP or 293CreFLP cells was capable of efficiently amplifying AdC4HSULacZ. Maximum titers (2 to 5 × 10^8 bfu/ml) were reached by serial passage 3, which represented a yield of ~1000 to 2000 bfu/cell. Similar amplification kinetics were observed when AdC4HSULacZ was amplified with the Cre/loxP system using AdLC8cluc and 293Cre4 cells. These "side-by-side" comparisons indicate that the FLP/frt and the Cre/loxP systems can amplify a HD vector with comparably high efficiencies.

While the analysis presented in Fig. 6 is informative, it is limiting and incomplete. Specifically, most transgenes, unlike LacZ, cannot be easily assayed, thus rendering determination of the vector titer at each serial passage impractical. Furthermore, the analysis presented in Fig. 6 provides no information regarding the level of helper

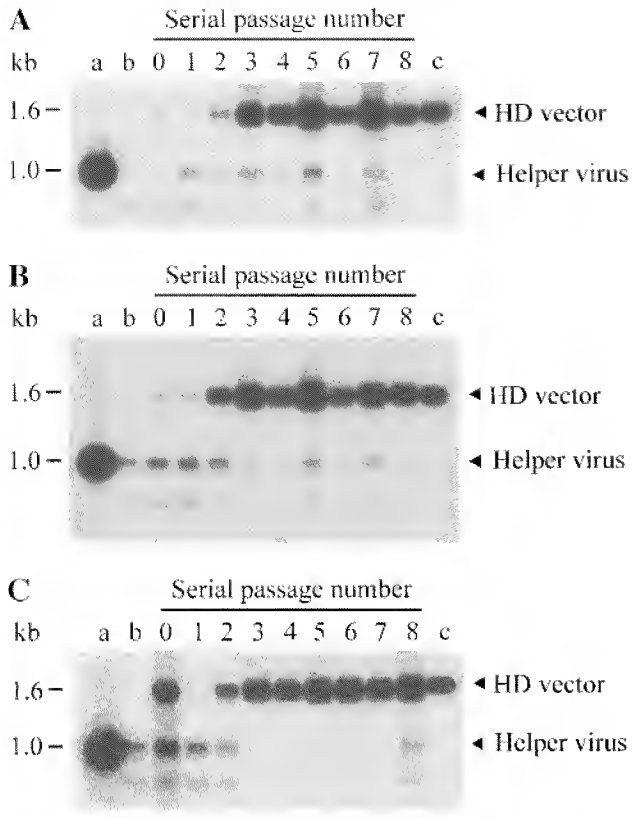

FIG. 7. Southern blot analysis of the AdC4HSULacZ amplifications. Total DNA was extracted from each serial passage, digested with *Bgl*I, and analyzed by Southern blotting with probe ψ. (A) Amplification of AdC4HSULacZ using AdCBfrt3 and 293FLP cells. Lane a contains total DNA extracted from 293 cells infected with AdCBfrt3 and lane b contains total DNA extracted from 293FLP cells infected with AdCBfrt3. (B) Amplification of AdC4HSULacZ using AdCBfrt3 and 293CreFLP cells. Lane a contains total DNA extracted from 293 cells infected with AdCBfrt3 and lane b contains total DNA extracted from 293CreFLP cells infected with AdCBfrt3. (C) Amplification of AdC4HSULacZ using AdLC8cluc and 293Cre4 cells. Lane a contains total DNA extracted from 293 cells infected with AdLC8cluc and lane b contains total DNA extracted from 293Cre4 cells infected with AdLC8cluc. In all three Southerns, lane c contains the plasmid pC4HSULacZ digested with *Pme*I and *Bgl*I. The band visible at ~0.7 kb is not packaged (unpublished results) and may represent the excised circular DNA bearing the packaging signal from the helper virus genome. The band at 1.6 kb visible at serial passage 0 represents DNA from the transfected plasmid pC4HSULacZ.

virus. Therefore, we sought to develop a more general technique to allow the replication of the HD vector as well as allowing the helper virus to be monitored during the amplification process, independent of transgene expression. To accomplish this, total DNA was extracted from each serial passage, digested with *Bgl*I, and analyzed by Southern blotting with a packaging signal probe (probe ψ). In this analysis, the packaging signal of the HD vector is present in a 1.6-kb *Bgl*I fragment (Fig. 3) while the packaging signal of the helper virus is present in a 1-kb *Bgl*I fragment (Fig. 2). The results of this analysis confirmed that the FLP/frt system is capable of efficiently amplifying AdC4HSULacZ, using either 293FLP (Fig. 7A) or 293CreFLP cells (Fig. 7B). In both cases, and consistent with the results presented in Fig. 6, the amount of HD vector increased from passage 0 to a peak by passage 3. Furthermore, this analysis revealed that in both cases, the amount of helper virus bearing an intact packaging signal remained low. Similar results were observed in the case in which AdC4HSULacZ was amplified using the Cre/loxP system (Fig. 7C). These results further indicate that the FLP/frt system is comparable to the Cre/loxP system in its ability to efficiently amplify a HD vector.

It is interesting to note, as shown in Figs. 6 and 7, that after reaching a peak titer at passage 3, the titer decreased at passage 4 and then peaked again at passage 5, followed by another decrease at passage 6. While we do not know what causes this cyclic fluctuation, it is typically observed and we speculate that it may be due to the effect of the m.o.i. of the HD vector. At peak titers, the m.o.i. of the HD vector used for the next passage is ~100–200 bfu/cell. It is possible that vector replication may be impeded with such a high m.o.i., perhaps due to cellular toxicity from virion proteins or overexpression of the transgene, thus resulting in a reduced yield of the HD vector and the helper virus (see lanes 4, 6, and 8 in Figs. 7A and 7B). The reduced HD vector titer, however, leads to a lower and perhaps more favorable m.o.i. of ~1–10 bfu/cell for the next passage, which in turn results in a peak HD vector yield. These results underscore the importance of the input HD vector m.o.i. for large-scale vector production since it can have a dramatic impact on the vector yield. To achieve maximal yield it is important that the m.o.i. of the HD vector be high enough to infect every cell. However, our results suggest that at excessive m.o.i. the yield of the HD vector can be reduced by as much as 10-fold.

Level of helper virus contamination. In addition to the efficiency of HD vector amplification, another important parameter of any system for generating HD vectors is the level of helper virus contamination. To accurately and objectively determine the level of helper virus contamination, the percentage of helper virus was determined for the HD vector amplified using the FLP/frt and the Cre/loxP system before HD vector purification by CsCl banding. Performing this analysis before CsCl banding is important because it avoids inconsistencies associated with collecting the HD vector from the CsCl gradient, a step that can result in final HD vector preparations with variable amounts of helper virus contamination, especially since the helper virus band is typically not visible. To accomplish this, encapsidated viral (HD vector and helper virus) DNA was isolated from virions at passage 5, in the absence of vector purification by CsCl ultracentrifugation, from the three amplification series illustrated in Fig. 7. The virion DNAs were digested with *Bgl*II and analyzed by Southern blotting with probe ψ. Total DNA (cellular, encapsidated, and nonencapsidated viral DNA) extracted from the same samples was also included for comparison. Phosphoimager analysis was used (Fig. 8) to quantitate the amount of HD vector and helper virus genomes in the virion DNA fraction and the percentage of helper virus contamination was calculated. The results revealed that the level of helper virus contamination was 0.6% when

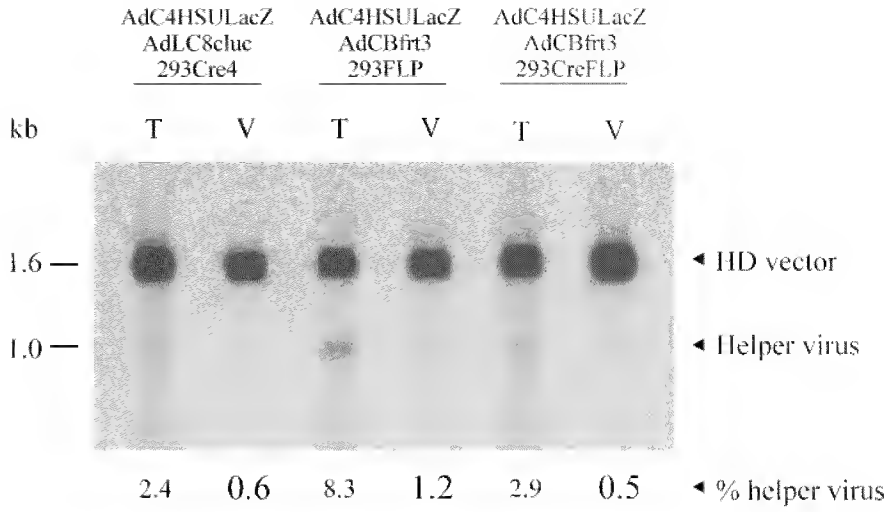

FIG. 8. Southern blot analysis to determine the percentage helper virus contamination before HD vector purification by CsCl ultracentrifugation. Total (T) and virion (V) DNAs were extracted from serial passage 5 from the amplifications shown in Fig. 7, digested with *Bgl*I, and analyzed by Southern blotting using probe ψ. Phosphoimager analysis was used to quantitate the amounts of HD vector and helper virus genomes in each lane. The percentage helper virus contamination was calculated from the amounts of HD vector and helper virus genome in the virion DNA fraction.

the HD vector was amplified using the Cre/loxP system. In the case of the FLP/frt system, the level of helper virus contamination was 1.2% when 293FLP cells were used and 0.5% when 293CreFLP cells were used. These results indicate that the HD vectors amplified using either the FLP/frt system or the Cre/loxP system had comparably low levels of helper virus contamination. In all cases, further reduction, typically 10-fold or more, in helper virus contamination can be achieved following HD vector purification by CsCl ultracentrifugation.

As mentioned above, total DNA, while not useful for determining the level of helper virus contamination, was also included for comparison in the analysis presented in Fig. 8. Interestingly, the percentage of helper virus genome in the total DNA fraction was consistently higher than in the virion DNA fraction; 2.4% with the Cre/loxP system and 8.3 and 2.9% with the FLP/frt system using 293FLP and 293CreFLP cells, respectively (Fig. 8). These results suggest that AdC4HSULacZ is preferentially packaged over the helper virus by four- to sevenfold. One possible explanation for the discrepancy between the total and the virion DNA may be due to the fact that the HD vector AdC4HSULacZ contains a wild-type packaging signal with all seven A repeats while the helper viruses AdCBfrt3 and AdLC8cluc contain only four intact A repeats. Another not mutually exclusive possibility is that the presence of the loxP or frt sites flanking the packaging signal may impede packaging of the helper virus.

This study demonstrates that the FLP/frt system can amplify a HD vector as efficiently as the Cre/loxP system, with comparably low levels of helper virus contamination. The observation that FLP functions as effectively as Cre is consistent with our previous study, which demonstrated that the two recombinases can be used to construct first-generation Ad vectors with equally high efficiencies (28). In addition, Cre-mediated packaging signal excision from AdLC8cluc following infection of 293CreFLP cells was comparable to that obtained following infection of the parental 293Cre4 cells. Indeed, using AdLC8cluc, we have been able to amplify AdC4HSULacZ with 293CreFLP cells at efficiencies comparable to those obtained using 293Cre4 cells (unpublished results). Therefore, it may now be possible to combine both Cre and FLP to further reduce the level of helper virus contamination by using the 293CreFLP cells and a helper virus with a packaging signal flanked by both loxP and frt sites. Furthermore, recombinase-controlled "molecular switches" (29) can now be adapted to HD vectors by using one site-specific recombinase system to inhibit helper virus growth and the other system to regulate transgene expression.

Acknowledgments

We thank Uma Sankar and Derek Cummings for their excellent technical assistance. This work was supported by grants from the National Institutes of Health, the Medical Research Council of Canada (MRC), and the National Cancer Institute of Canada (NCIC) and by Merck Research Laboratories. P.N. is supported by an MRC Postdoctoral Fellowship. Requests to obtain materials should be addressed to Dr. Susan H. Socher, Executive Director, External Scientific Affairs, Merck & Co., Inc., 770 Sumneytown Pike, P.O. Box 4, WP42-217, West Point, PA 19486. Fax: (215) 652-3143.

References

[1] Berkner, K. L. (1988). Development of adenovirus vectors for expression of heterologous genes. *Biotechniques* 6: 616–629.

[2] Graham, F. L., and Prevec, L. (1992). Adenovirus-based expression vectors and recombinant vaccines. In *Vaccines: New Approaches to Immunological Problems* (R. W. Ellis, Ed.), pp.363–389. Butterworth–Heinemann, Boston.

[3] Hitt, M., Addison, C. L., and Graham, F. L. (1997). Human adenovirus vectors for gene transfer into mammalian cells. *Adv. Pharmacol.* 40: 137–206.

[4] Hitt, M. M., Parks, R. J., and Graham, F. L. (1999). Structure and genetic organization of adenovirus vectors. In *The Development of Human Gene Therapy* (T. Friedman, Ed.), pp. 61–86. Cold Spring Harbor Laboratory Press, Cold Spring Harbor, NY.

[5] Graham, F. L., Smiley, J., Russell, W. C., and Nairn, R. (1977). Characteristics of a human cell line transformed by DNA from human adenovirus 5. *J. Gen. Viol.* 36: 59–72.

[6] Wolff, G., Worgall, S., van, R. N., Song, W. R., Harvey, B. G., and Crystal, R. G. (1997). Enhancement of in vivo adenovirus-mediated gene transfer and expression by prior depletion of tissue macrophages in the target organ. *J. Virol.* 71: 624–629.

[7] Worgall, S., Wolff, G., Falck-Pederson, E., and Crystal, R. G. (1997). Innate immune mechanisms dominate elimination of adenoviral vectors following in vivo administration. *Hum. Gene Ther.* 8:37–44.

[8] Morral, N., O'Neal, W., Zhou, H., Langston, C., and Beaudet, A. (1997). Immune responses to reporter proteins and high viral dose limit duration of expression with adenoviral vectors. Comparison of E2a wildtype and E2a deleted vectors. *Hum. Gene Ther.* 8: 1275–1286.

[9] Dai, Y., Schwartz, E. M., Gu, D., Zhang, W. W., Sarvetnick, N., and Verma, I. M. (1995). Cellular and humoral immune responses to adenoviral vectors containing factor IX gene. Tolerization of factor IX and vector antigens allows for long-term expression. *Proc. Natl. Acad. Sci. USA* 92: 1401–1405.

[10] Yang, Y., Nunes, F. A., Berencsi, K., Furth, E. E., Gonczol, E., and Wilson, I. M. (1994).

Cellular immunity to viral antigens limits E1-deleted adenoviruses for gene therapy. *Proc. Natl. Acad. Sci. USA* **91**: 4407–4411.

[11] Yang, Y., Li, Q., Ertl, H. C., and Wilson, J. M. (1995). Cellular and humoral immune responses to viral antigens create barriers to lung-directed gene therapy with recombinant adenoviruses. *J. Virol.* **69**: 2004–2015.

[12] Yang, Y., Xiang, Z., Ertl, H. C., and Wilson, J. M. (1995). Upregulation of class I major histocompatibility complex antigens by interferon gamma is necessary for T-cell-mediated elimination of recombinant adenovirus-infected hepatocytes in vivo. *Proc. Natl. Acad. Sci. USA* **92**: 7257–7261.

[13] Kafri, T., Morgan, D., Krahl, T., Sarvetnick, N., Sherman, L., and Verma, I. (1998). Cellular immune response to adenoviral vector infected cells does not require de novo viral gene expression: Implications for gene therapy. *Proc. Natl. Acad. Sci. USA* **95**: 11377–11382.

[14] Chen, H.-H., Mack, L. M., Kelly, R., Ontell, M., Kochanek, S., and Clemens, P. R. (1997). Persistence in muscle of an adenoviral vector that lacks all viral genes. *Proc. Natl. Acad. Sci. USA* **94**: 1645–1650.

[15] Morral., N., Parks, R. I., Zhou, H., Langston, C., Schiedner, G., Quinones, J., Graham, F. L., Kochanek, S., and Beaudet, A. L. (1998). High doses of a helper-dependent adenoviral vector yield supraphysiological levels of α1-antitrypsin with negligible toxicity. *Hum. Gene Ther.* **9**: 2709–2716.

[16] Morsy, M. A., Gu, M., Motzel, S., Zhao, I., Lin, J., Su, Q., Allen, H., Franlin, L., Parks, R. I., Graham, F. L., Kochanek, S., Bett, A. I., and Caskey, C. T. (1998). An adenoviral vector deleted for all viral coding sequences results in enhanced safety and extended expression of a leptin transgene. *Proc. Natl. Acad. Sci. USA* **95**: 7866–7871.

[17] Schiedner, G., Morral, N., Parks, R. I., Wu, Y., Koopmans, S. C., Langston, C., Graham, F. L., Beaudet, A. L., and Kochanek, S. (1998). Genomic DNA transfer with a high-capacity adenovirus vector results in improved in vivo gene expression and decreased toxicity. *Nat. Genet.* **18**: 180–183.

[18] Morral, N., O'Neal, W., Rice, K., Leland, M., Kaplan, J., Piedra, P. A., Zhou, H., Parks, R. I., Velji, R., Aguilar-Córdova, E., Wadsworth, S., Graham, F. L., Kochanek, S., Carey, K. D., and Beaudet, A. L. (1999). Administration of helper-dependent adenoviral vectors and sequential delivery of different vector serotype for long-term liver directed gene transfer in baboons. *Proc. Natl. Acad. Sci. USA* **96**: 12816–12821.

[19] Balague, C., Zhou, J., Dai, Y., *et al.* (2000). Sustained high-level expression of full-length human factor VIII and restoration of clotting activity in hemophilic mice using a minimal adenovirus vector. *Blood* **95**: 820–828.

[20] Cregan, S. P., MacLaurin, J., Gendron, T. F., Callaghan, S. M., Park, D. S., Parks, R. I., Graham, F. L., Morley, P., and Slack, R. S. (2000). Helper-dependent adenovirus vectors. Their use as a gene delivery system to neurons. *Gene Ther.* **14**: 1200–1209.

[21] Maione, D., Wiznerowicz, M., Delmastro, P., Cortese, R., Ciliberto, G., La Monica, N., and Savino, R. (2000). Prolonged expression and effective readministration of erythropoietin delivered with a fully deleted adenoviral vector. *Hum. Gene Ther.* **11**: 859–868.

[22] Parks, R. I., Chen, L., Anton, M., Sankar, U., Rudnicki, M. A., and Graham, F. L. (1996). A helper-dependent adenovirus vector system. Removal of helper virus by Cre-mediated excision of the viral packaging signal. *Proc. Natl. Acad. Sci. USA* **93**: 13565–13570.

[23] Broach, J. R., Guarascio, V. R., and Jayaram, M. (1982). Recombination with the yeast 2μ plasmid is site specific. *Cell* **29**: 227–234.

[24] Sandig, V., Youil, R., Bett, A. I., Franlin, L. L., Oshima, M., Maione, D., Wang, F., Metzker, M. L., Savino, R., and Caskey, C. T. (1999). Optimization of the helper-dependent adenovirus system for production and potency in vivo. *Proc. Natl. Acad. Sci. USA* **97**: 1002–1007.

[25] Graham, F. L., Smiley, J., Russell, W. C., and Nairn, R. (1977). Characteristics of a human cell line transformed by DNA from human adenovirus 5. *J. Gen. Viol.* **36**: 59–72.

[26] Chen, L., Anton, M., and Graham, F. L. (1996). Production and characterization of human 293 cell lines expressing the site-specific recombinase Cre. *Somatic Cell Mol. Genet.* **22**: 477–488.

[27] Graham, F. L., and van der Eb, A. J. (1973). A new technique for the assay of infectivity of human adenovirus 5 DNA. *Virology* **52**: 456–467.

[28] Ng, P., Cummings, D. T., Evelegh, C. M., and Graham, F. L. (2000). The yeast recombinase flp functions effectively in human cells for construction of adenovirus vectors. *Biotechniques* **29**: 524–6, 528.

[29] Anton, M., and Graham, F. L. (1995). Site-specific recombination mediated by an adenovirus vector expressing the Cre recombinase protein: A molecular switch for control of gene expression. *J. Virol.* **69**: 4600–4606.

Transgenic Research **10:** 317–328, 2001.

FLP/*FRT*-mediated restoration of normal phenotypes and clonal sectors formation in *rolC* transgenic tobacco

David Gidoni*, Moshe Bar & Nehama Gilboa
Department of Plant Genetics, Institute of Field and Garden Crops, ARO, The Volcani Center, P.O. Box 6, Bet Dagan 50250, Israel

Received 2 October 2000; revised 11 December 2000; accepted 13 December 2000

Key words: site-specific recombination, transgene excision, clonal leaf and lateral shoot sectors, periclinal chimeras, fertility restoration

Abstract

Site-specific recombination systems have been shown to excise transgene DNA sequences positioned between their cognate target sites, and thus be used to generate clonal sectors in transgenic plants. Here we characterized clonal sectors derived from genetic reversion of *rolC* (*A. rhizogenes*) – induced vegetative and reproductive phenotypes, mediated by FLP recombinase from *S. cerevisiae*, in tobacco. The constitutive expression of *rolC* induces pleiotropic effects including reduced apical dominance and plant height, lanceolate and pale green leaves and small, male-sterile flowers. Two transgenic male-sterile tobacco lines (*N. tabacum*, Samsun NN) expressing a *35s*P-*rolC* gene construct flanked by two *FRT* (FLP recombinase target) sites, were cross-pollinated with pollen from a constitutive *35s*P-*FLP* expressing line. Three main phenotypes were generated in result of recombinase-mediated excision of the *35s*P-*rolC* locus in the F_1 (*FLP* × *FRT-35s*P-*rolC-FRT*) hybrid progenies: (a) restoration of male fertility, associated with reversion to normal leaf phenotypes prior to flower bud formation, (b) development of normal and fertile lateral shoot sectors on the background of rolC-type plants, (c) restoration of partially fertile flowers, associated with display of peripheral normal leaf sectors surrounding rolC-type inner-leaf tissues, consistent with periclinal chimeras. These results, supported by DNA molecular analysis, indicate that site-specific recombination might be used as a relatively efficient tool for generation of transgenic periclinal chimeric plants.

Introduction

Site-specific recombination systems such as Cre/*lox* from bacteriophage P1 of *E. coli*, R/*RS* from the SR1 plasmid of *Zygosaccharomyces rouxii* and FLP/*FRT* from the 2 μm plasmid of *Saccharomyces cerevisiae*, can mediate an accurate recombination reaction in heterologous organisms through interaction between a single recombinase and its cognate two 34 bp target sites, placed in the host genome (reviewed in Kilby et al., 1993; Odell & Russell, 1994; Sauer, 1994; Ow, 1996; Ow & Medberry, 1995; Sauer & Henderson, 1988). Using both selectable and visual marker genes in plants, these systems were shown to mediate either gain of a new phenotype as a result of excision of a target-site bounded blocking DNA from a silent marker gene, and/or loss of a phenotypic trait as a result of removal of an expressed transgene that was bounded by directly oriented recombination target-sites (Dale & Ow 1990; Odell et al., 1990; Dale & Ow, 1991; Bayley et al., 1992; Russell et al., 1992; Lloyd & Davis, 1994; Kilby et al., 1995; Lyznik et al., 1995, 1996; Onouchi et al., 1995; Bar et al., 1996; Stuurman et al., 1996; Davies et al., 1999). Both constitutive (Onouchi et al., 1995; Gidoni D, Bar M, Leshem B, unpublished data), tissue-specific (Odell et al., 1994) and induced (Kilby et al., 1995, 2000) recombinase-mediated activation of a previously blocked either *gusA* or *Spec* (Davies et al., 1999) markers, produced GUS-active and spectinomycin-resistant visual sectors

* Author for Correspondence: *E-mail:* gidoni@netvision.net.il

in *Arabidopsis* and tobacco, respectively. These results indicate that site-specific recombination systems can potentially be used as a tool in clonal sectors formation and lineage studies in plants. However, GUS assays are invasive and mostly detrimental to plant tissues and spectinomycin resistance can only be scored in cotyledons. These marker characteristics limit visualization of sectors to young plantlet stages.

In order to study recombinase-mediated clonal sectors formation during later vegetative and reproductive stages, we employed the *rolC* gene from *Agrobacterium rhizogenes* as marker. When *rolC* is expressed under control of the CaMV *35s* promoter (*35s*P), it causes pleiotropic altered phenotypes, such as dwarfism, reduced apical dominance, reduced female fertility, lanceolate and pale-green leaves and small, male sterile flowers in transgenic tobacco (Schmulling et al., 1988) and potato (Fladung, 1990). *rolC*-induced male sterility is dominant and is based on impaired microsporogenesis, which leads to the formation of nonfunctional pollen (Schmulling et al., 1988). The reduction in chlorophyll content in leaves was used as visual, cell autonomous marker system, to monitor *Ac* transposon excision from a transcriptionally blocked *35s*P-*Ac*-*rolC* locus (Spena et al., 1989). *Ac* excision events occurring during leaf development, resulted in reconstruction of a transcriptionally active *35s*P-*rolC* locus and gave rise to generation of pale-green leaf sectors in transgenic tobacco (Spena et al., 1989), tomato (Jones et al., 1992) and aspen (Fladung & Ahuja, 1997). These phenotypic characteristics enabled visualization of periclinal sector formation during *Agrobacterium*-mediated transformation in tobacco (Oono et al., 1993; Schmulling & Schell, 1993) and due to *Ac* transposition in aspen (Fladung & Ahuja, 1997).

In the present study, reversion of the pleiotropic phenotypic effects of *rolC* was used as a developmental, whole-plant visual marker system, to further monitor FLP recombinase-mediated clonal sectors in tobacco. Cross-pollination with pollen from a *35s*P-*FLP*-expressing line have brought FLP into the target lines carrying *FRT-35s*P-*rolC-FRT* loci and the phenotypic outcome of the function of FLP on these target loci was characterized. Three main phenotypes were generated in result of recombinase-mediated excision of the *35s*P-*rolC* loci

(a) Restored wild-type appearance and fertility,

(b) Development of normal and fertile lateral shoot sectors on the background of rolC-type progeny,

(c) Generation of peripheral and inner leaf sectorial phenotypes associated with partially restored fertile flowers.

PCR analysis of leaf DNA samples from all progeny plants and sectorial tissues displayed the presence of both excised and non-excised *rolC* target loci, indicating that recombinase-mediated clonal sectors in plants can be periclinal chimeras.

Materials and methods

DNA modifications and plasmid constructions

Molecular cloning procedures were carried out as described by Maniatis et al. (1982). The FLP target plasmid construct, pFCF (Figure 1B) was generated by inserting a 1.5 kb *Eco*RI–*Bam*HI fragment from pPCV002-CaMVC containing *35s*P-*rolC* (Spena et al., 1987) into *Eco*RI–*Bam*HI restriction sites of pFNF. pFNF was generated by inserting a 1.55 kb *Nsi*I-*Hin*dIII fragment from pNeoβGal containing *FRT-npt-FRT* (Stratagene, La Jolla, CA) into *Pst*I-*Hin*dIII restriction sites of pPCV002 (Koncz & Schell, 1986) after the *Bam*HI and *Eco*RI restriction sites of pPCV002 had been eliminated (blunt-ended with the Klenow fragment of DNA polymerase I and religated).

Construction of the FLP expression construct, pJFLO, was described in Luo et al. (2000). During the construction of pJFLO and pFCF, all the newly formed 5′ and 3′ junctions were confirmed by DNA sequencing.

Formation and manipulation of transgenic plants

The pJFLO and pFCF binary constructions (Figure 1), each containing a linked neomycin phosphotransferase (*nptII*) expression cassette were introduced into *Agrobacterium tumefaciens* GV3101-pMP90RK (Koncz & Schell, 1986) by means of the freeze-thaw procedure (An et al., 1988). *Agrobacterium* clones were used to transform leaf disks of *N. tabacum* L. samsun NN (SNN) according to Horsch et al. (1985). Kanamycin-resistant (Kan^R) plants were regenerated and transferred to the greenhouse. The number of genomic loci of the integrated DNA was evaluated by both Southern-blot analysis and the germination of T_1 seeds from selfing of the pJFLO primary transformed parent line. The copy numbers of transgenic loci in the pFCF transgenic lines were confirmed only by

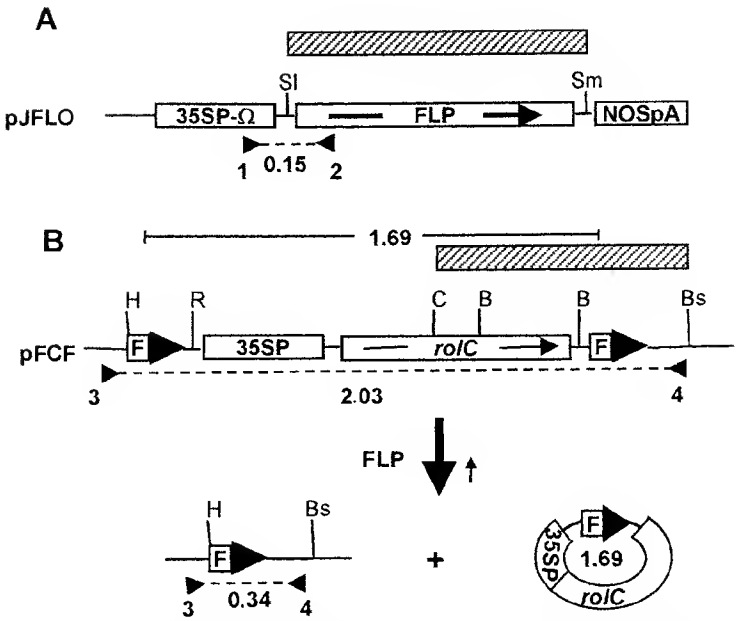

Figure 1. Schematic diagrams of the FLP recombinase and target-site constructs. A. In the FLP expression binary-vector constructs, pJFLO, *FLP* is positioned under the control of the CaMV *35s* gene promoter and the Ω translation enhancer sequence of TMV (Gallie et al., 1989) as well as the nopaline synthase polyadenylation signal. Positions of the PCR primers 1 and 2 are indicated by small arrows and the *35s*PΩ-*FLP* PCR product (in kb) by broken lines. B. In the *FRT* recombination-target binary vector construct, pFCF, the *35s*P-*rolC* expression unit is flanked by *FRT* target sites (*F*) and its expression confer rolC traits to transgenic plants. Excision of the 1.69-kb *FRT-35s*P-*rolC-FRT* DNA results in elimination of its expression and restoration of normal or sectorial phenotypes. Positions of the PCR primers 3 and 4 are indicated by small arrows and the *FRT-35s*P-*rolC-FRT* pre- and post-recombination PCR products (in kb) by broken lines. The probes for Southern blot hybridization analysis of PCR products are shown by striped bars and relevant RE sites. Abbreviations are: SI–*Sal*I; Sm–*Sma*I; H–*Hin*dIII; R–*Eco*RI; C–*Cla*I; B–*Bam*HI and Bs–*Bst*EII. Each of the above two T-DNA constructs is linked to a kanamycin-resistance selection marker construct (Koncz & Schell, 1986).

Table 1. Segregation of Kanamycin resistance (Kan^R) and *FCF* and *JFLO* loci in FCF × JFLO hybrid seedling progeny

Hybrid[1]	Tested progeny	Kan^R +/*FCF*[2]	Kan^R +/*JFLO*[2]	*FCF*/*JFLO*[2]	Kan^R: Kan^S	Expected ratio
FCF(107)×SNN	86	25			0.41:1	1:1
FCF(109)×SNN	137	30			0.28:1	1:1
FCF(107)×JFLO(811)	87	5	46	11	2.48:1	3:1
FCF(109)×JFLO(811)	96	9	44	9	1.82:1	3:1

[1]Hemizygous FCF parent lines were cross-pollinated with pollen from either SNN (wild-type) or a hemizygous JFLO(811) plant.
[2]Kanamycin resistant progeny were analyzed by PCR for the presence/absence of *FCF* and *JFLO* loci (Figure 2).

Southern-blot analysis since the presence of the *rolC* gene reduced female gamete viability (Schmulling et al., 1988) and estimation of Kan^R segregation was lower than expected (Table 1).

Cross-pollination of transgenic plants hemizygous for pJFLO (FLP paternal parent, called JFLO(811)), with hemizygous two pFCF transformed lines [target construct maternal parents, called FCF(107 or 109)] yielded hybrids JFLO(811) × FCF(107) and JFLO(811) × FCF(109), respectively.

Scoring pollen viability and restoration of male fertility

Pollen was collected from five flowers of each plant at anthesis and germinated for 4 h in a germination

medium consisting of 10% sucrose, 100 mg/l H_3BO_3, 300 mg/l $Ca(NO_3)_2 \cdot 4H_2O$, 200 mg/l $MgSO_4 \cdot 7H_2O$, 100 mg/l KNO_3 (Schmulling et al., 1993; Bruce & Williams, 1986). Pollen that gave rise to tube growth of at least twice the length of the pollen grain diameter, was defined viable (Bruce & Williams, 1986). The percentage of viable pollen was determined microscopically.

Restoration of fertility was determined in each hybrid plant by testing the ability of flowers to self-fertilize and cross-pollinate pre-emasculated flowers of wild-type plants. All emasculated and pollinated flowers were bagged in order to prevent access to other pollen. Five flowers were included in each test and the number of seed in the corresponding seed capsules was averaged.

Plant DNA extraction and PCR analysis

Total DNA was isolated from leaf tissue of greenhouse plants (Doyle & Doyle, 1990) and then subjected to PCR/Southern analysis. The primers (Figure 1A) used to detect the *JFLO* locus were: (i) 5′-ATTTGGAGAGGACAGGCTTC-3′, specific for the CaMV-*35s* promoter; and (ii) 5′-ACTGACGAACAACAAGCACCTTAGGTG-3′, specific for the 5′ end region of *FLP*. The primers (Figure 1B) used to differentiate between pre- and post-recombination *FCF* locus were: (i) 5′-GAAAAGTGCCACCTGACGTCTAAG-3′, specific to the immediate upstream region of the left *FRT*; and (ii) 5′-CTCAATTAGTCAGCAACCATAGTC-3′, specific to the immediate downstream region of the right *FRT*. PCR amplification was performed using a Thermal Controller (M-J Research Inc., Watertown, MA). Cycling conditions were 1 min at 94 °C; 25 cycles of 1 min at 94 °C, 1 min at 56 °C and 4 min at 72 °C; and extension at 72 °C for 10 min. The reactions involved 5–10 ng of DNA template, 0.2 mM of dNTPs, 160 ng of each primer and 1.5 U of *Taq* DNA polymerase (Boehringer-Mannheim, GmbH, Germany) in a final reaction volume of 50 µl. PCR products were resolved by electrophoresis in 1% agarose gels, blotted onto a Hybond N^+ nylon membrane (Amersham, UK) and hybridized to ^{32}P-labeled either *JFLO*- or *FCF*-specific probes (Figure 1A and B, respectively). The DNA products used as probes were radiolabled by random priming with a kit from Boehringer–Mannheim. Following hybridization at 65 °C, according to manufacturer's instructions, the membranes were washed twice for 15 min in 2 × SSPE (0.18 M NaCl, 10 mM NaH_2PO_4, 1 mM EDTA, pH 7.7) and 0.1% SDS at room temperature, for 30 min in 1 × SSPE and 0.1% SDS at 42 °C, and once for 30 min in 0.1 × SSPE and 0.1% SDS at 65 °C. Southern blotting products were visualized by X-ray autoradiography.

Statistics

Data were analyzed by a one-way analysis of variance using the general linear model procedure (PROC–GLM) of the SAS package (SAS Institute, 1989). Treatments were compared by Duncan's multiple range test at the 0.05 protection level. Normal distribution of data was confirmed by the Shapiro–Wilk test.

Results

Experimental strategy and parental JFLO and FCF transgenic lines

The experimental strategy used in this study is schematically described in Figure 1. The yeast FLP recombinase gene is positioned under the control of the CaMV *35s* promoter (*35s*P) and omega leader (Ω) in pJFLO (Luo et al., 2000; Figure 1A). The FLP coding sequence in pJFLO was derived from pOG44 (O'Gorman et al., 1991) and the sequence immediately upstream to the ATG initiation codon was modified from CACC to AACA, consistent with the consensus sequence for plants (Lutcke et al., 1987).

The FLP recombinase target construct, pFCF, contains a *35s*P-*rolC* expression cassette (Spena et al., 1987) that is positioned between directly oriented *FRT* sites (Figure 1B, top). The expression of rolC from pFCF in tobacco is expected to induce characteristic rolC pleiotropic phenotypes, mainly dwarfism, reduction in apical dominance and in female fertility and generation of lanceolate and pale-green leaves and small, male sterile flowers (Schmulling et al., 1988). *FCF* was designed to serve as a target locus for FLP-excisional recombination activity (Figure 1B, bottom), thus to enable studying the reversion of the rolC-induced vegetative and reproductive traits in the *FCF/JFLO* hybrid progenies in result of excision of the genomic *35s*P-*rolC* expression cassette.

The binary vector plasmids pJFLO and pFCF were introduced into tobacco plants via *Agrobacterium*-mediated leaf disk transformation and the hemizygous, single-locus lines, JFLO(811), FCF(107) and FCF(109) were selected for further study. Both FCF

lines displayed the characteristic rolC pleiotropic phenotypes described above (Figures 3A and B, left), while JFLO(811) plant phenotypes were normal (Figures 3A and B, right).

FLP-mediated excision recombination of the FCF target loci in the JFLO/FCF hybrid progeny

To study the effect of FLP activity on the target *FCF* loci, the *JFLO* locus was brought into the same plants as *FCF* loci, by cross-pollination of the FCF(107) and FCF(109) lines with pollen from JFLO(811). Germination of the FCF(107) × JFLO(811) and FCF(109) × JFLO(811) hybrid seed progeny on kanamycin-containing media is expected to yield Kan^R:Kan^S segregation ratio of 3:1, however, the actual ratios were 2.5:1 and 1.8:1, respectively (Table 1). The lower than expected number of Kan^R plants in both these and FCF × SNN out-crosses (Table 1) may be ascribed to the fact that female gametes containing the *35s*P-*rolC* cassette in FCF are less viable as compared to wild-type (Schmulling et al., 1988).

In order to monitor recombination activity in the FCF × JFLO progenies, total DNA, extracted from leaf-sample homogenates of the 62 Kan^R individuals from each cross (Table 1), was PCR amplified with both *JFLO*- and *FCF*-specific primers (Figures 1A and B, respectively, Materials and methods) and the PCR products were resolved on agarose gels. To confirm identity of the products, the DNA was blot-hybridized to either a 1.28-kb *Sal*I-*Sma*I *FLP*-specific probe from pJFLO or a 1.1-kb *Cla*I-*Bst*EII *rolC*-specific probe from pFCF (Figures 1A and B, respectively). An expected 2.03 kb fragment, characteristic of the intact, non-recombined *FCF*-target locus was detected in parental FCF lines (Figure 2A, lane 1) and in the progeny shown in Figure 2A lanes 2,3,6,7, 9–12. Additionally, an expected *JFLO*-specific 0.15-kb PCR/Southern product was detected in the parental JFLO plant (Figure 2B, lane 13) and in the progeny shown in Figure 2B lanes 3–8, 10, 12. An amplification product of 0.34 kb, expected from excision recombination and loss of the 1.69-kb *35s*P-*rolC* cassette of *FCF* is restricted to the hybrid progeny containing both the 2.03-kb *FCF* target locus and the 0.15-kb fragment that designates the *JFLO* locus (Figure 2A and B, lanes 3,6,7,10,12). This confirms *FRT* site-specific recombination at the FCF genomic locus and is consistent with FLP-mediated deletion of the *35s*P-*rolC* expression cassette from the genome of *FCF/JFLO* progenies.

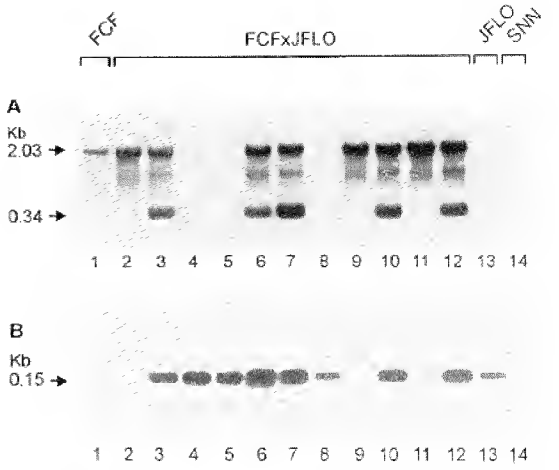

Figure 2. PCR/Southern analysis of *FCF*- and *FLP*- specific loci in the parental lines FCF(107) (lane 1) and JFLO(811) (lane 13) and their cross progeny. A. The 2.03-kb and 0.34-kb *FCF*-specific pre- and post-recombination products. B. The 0.15-kb *FLP*-specific product, representing the *JFLO* locus. Lanes 2,9,11 represent rolC-type progeny and lanes 4–8 represent normal-type progeny. Lanes 3 and 10 represent samplings from a dark green and a light green leaf sectors shown in Figure 5D, and lane 12 represents a leaf sample from a normal-type lateral shoot sector shown in Figure 6C. SNN: non-transformed *N. tabacum* L. Samson NN (lane 14). PCR products were fractionated on agarose gels and blot hybridized to either a 1.1-kb *Cla*I-*Bst*EII probe from pFCF corresponding to the 3′ region of *rolC* and adjacent *FRT* (A) or a 1.28 kb *Sal*I-*Sma*I *FLP* probe from pJFLO (B), (Figure 1).

The results in Figure 2 indicate the segregation of FCF × JFLO Kan^R progeny into three genotypes: +/*FCF*, +/*JFLO* and *FCF*/*JFLO*, however, the ratio between these groups is deviated from the expected 1:1:1 (Table 1). The expected numbers of +/*FCF* and *FCF*/*JFLO* genotypes were lower as compared to the +/JFLO genotype, consistent with the lower from the expected 3:1 Kan^R:Kan^S segregation ratio among the progeny of these crosses (Table 1).

Restoration of fertility and other wild-type traits in FCF/JFLO hybrid progeny

Of the 124 Kan^R progeny from the two FCF × JFLO crosses (Table 1), 14 carried a +/*FCF* genotype and displayed the typical *rolC* pleiotropic phenotypes, while the 90 +/*JFLO* plants were normal. Restoration of fertility was studied both by the ability of pollen to germinate *in vitro* in a pollen germination medium and the ability of hybrid plants to either self or

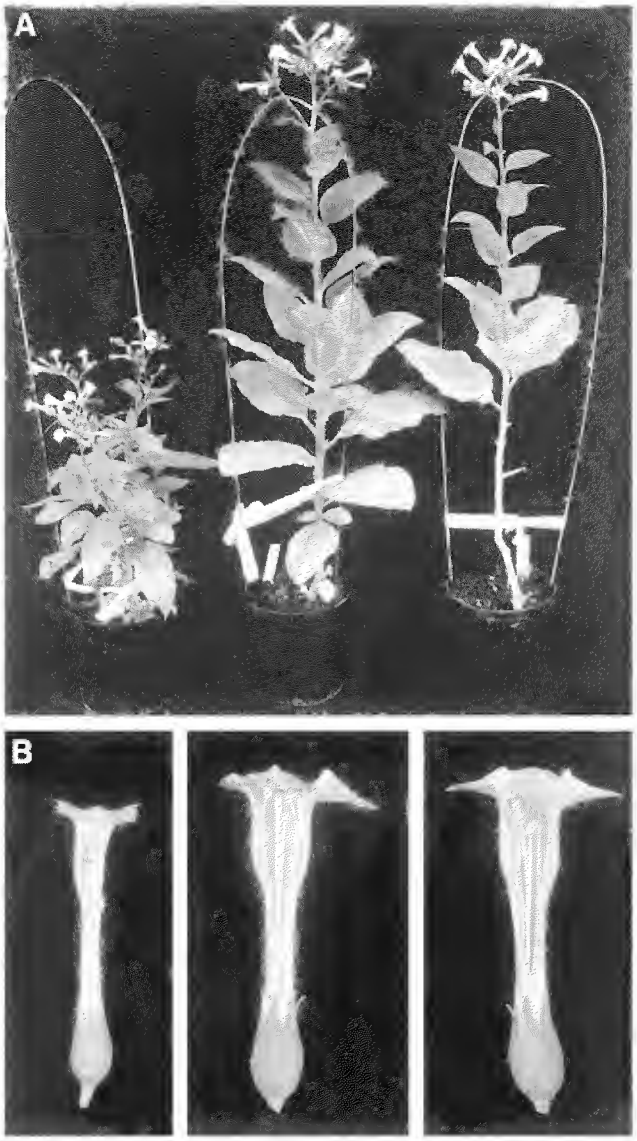

Figure 3. A representation of reversion to normal-type growth (A) and flower (B) morphologies in hybrid progeny (middle), derived from crosses of a FCF(107) target line (left) with the *FLP*-expressing line JFLO(811) (right).

cross-fertilize wild-type plants. While no germination was evident with pollen derived from FCF parent lines (Figure 4A), above 90% of pollen were capable of germination when derived from wild-type and $+/JFLO$ plants (Table 2). Consistently, seed yield per capsule in self-fertilized FCF, JFLO(811) and wild-type plants was zero, 1760 ± 121 and 1824 ± 118, respectively, similar to the yields derived from crosses of each with wild-type plants (Table 2)

The phenotypes displayed by the 20 progeny having a *FCF/JFLO* genotype, can be divided essentially into three main groups:

(a) Restoration of wild-type appearance and fertility,

(b) Sectorial leaf phenotypes and partially restored fertile flowers, and

(c) rolC-type, no restoration of wild-type traits, however, with the potential to develop normal and

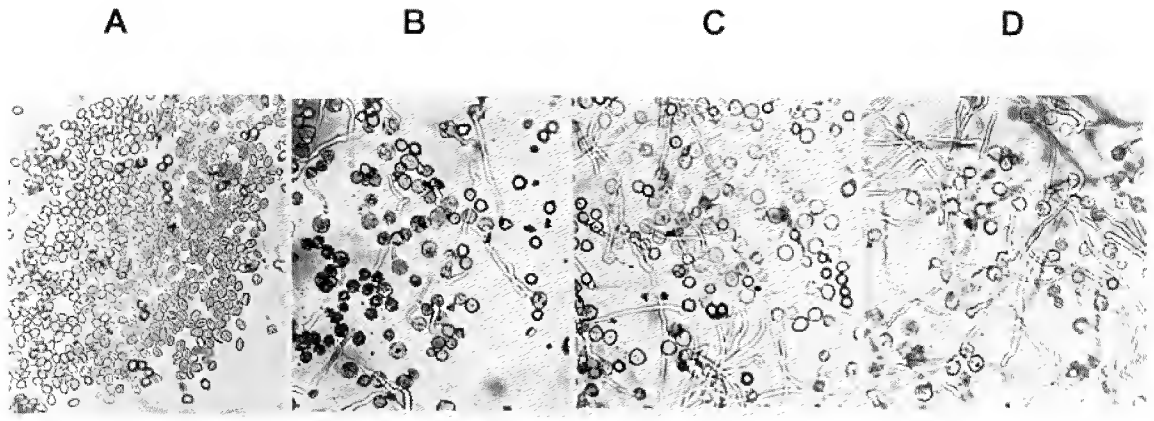

Figure 4. Representative pictures of pollen germination tests showing zero germination in FCF(107) (A), 20–30% (B) and 60–70% germination (C) in two partially restored FCF(107) × JFLO(811) progeny and >90% germination (D) in a normal-type restored hybrid progeny.

fertile shoots from lateral buds as a result of pruning.

Ten progeny (group a) developed fertile flowers with pollen viability score of>90%, similar to wild-type and JFLO lines (Figure 4D; Table 2, plants F_1(107)-36, 44, 45, 58 and F_1(109)-2, 8, 9, 17, 47, 59) while two additional plants (group a') scored 70–80% (Table 2, plants F_1(107)-38,42). Seed yield derived from self-cross and out-cross tests of group a plants ranged between 1485 ± 130–1962 ± 172 and 1307 ± 128–1817 ± 201, respectively, not significantly different ($p < 0.05$) from wild-type (1824 ± 118–1964 ± 169). These results indicate restoration of both female and male fertility, similar to wild-type. The only exception, however, was F_1(109)-17 which after self-crossing, yielded 960 ± 125 seeds per capsule, 53% of wild-type. This very likely reflects reduced female fertility, as pollen fertility was similar to wild-type, yielding 1530 ± 212 seed per capsule on an out-crossing test (Table 2). The plants in this group displayed normal leaf phenotypes either at the whole-plant (represented in Figure 3A and B, middle) or in some cases, normal leaves replaced chimeric leaves during plant development (Table 2). Stem height ranged from 44 to 74 cm (63–100%) compared to 66–76 cm of wild-type (Table 2). PCR analysis of phenotypic normal leaf DNA that was sampled from the plants' upper part indicated excision of the *35s*P-*rolC* expression cassette from part, but not all cells (Figure 2, lanes 6,7).

Plant heights in group a' (Table 2, plants F_1(107)-38,42) were 53 and 68 cm, respectively. Pollen viability was 70–80% and seed yields were 807 ± 94 and 975 ± 172 in self-cross, and 1020 ± 143 and 1231 ± 172 in out-cross tests, respectively. This indicates restoration of male fertility to 52–63% of wild-type (1964 ± 169). In the six hybrid progeny of group b (Fig. 4BC; Table 2, plants F_1(107)-8,59,60 and F_1(109)-1,38,41), however, pollen viability was 5–30% and seed yields were 7–53% and 19–41% of wild-type, in self and out-cross tests, respectively. These plants characteristically, displayed chimeric leaf phenotypes throughout their whole vegetative and reproductive stages (described bellow) and their stem heights ranged between 40 and 52 cm. In comparison, both plants of group c (Figures 3A and B, left; Figure 4A; Table 2, F_1(107)-17,61) maintained essentially all pleiotropic rolC characteristic vegetative and reproductive traits, with stem height of 28–32 cm and male sterile flowers, similar to their corresponding FCF parents. The pruning of these plants, however, induced growth of lateral shoot sectors of normal phenotypes (described below).

Chimeric phenotypes and clonal sectors formation in FCF/JFLO hybrid progeny

FCF/JFLO hybrid progeny (both groups a, a' and b) produced visible chimeric leaf phenotypes, displaying various shapes and sizes of mosaics of dark green (wild-type) sectors on the background of surrounding light green (rolC) leaf tissue (Figure 5A–F). All plants developed a single predominant stem, indicating restoration of apical dominance. Chimeric leaves displayed wrinkled and dark green margins, surrounding a smooth, pale green central region (Figures 5C and 6A,B). In some plants, peripheral dark

Table 2. Leaf types, stem height, pollen viability and seed yield of tobacco wild-type (SNN) plants, FCF maternal parent, JFLO paternal parent and FCF × JFLO cross progeny

Plant no.	Leaf type[2]	Stem height[3]	Pollen viability[4]	Self seed set[5]	Cross seed set[5]
FCF	rC	28–35	0	0^{f}	0^{f}
JFLO(811)	N	70	>90	1760 ± 121^{a}	1724 ± 143^{a}
SNN (WT)	N	66–76	>90	1824 ± 118^{a}	1964 ± 168^{a}
$F_1(107)$[1] -					
8	Ch	40	10–20	348 ± 139^{de}	470 ± 57^{de}
17	rC	30	0	0^{f}	0^{f}
17/L[6]	N	55	60–70	541 ± 84^{cd}	698 ± 123^{cd}
36	Ch/N	45	>90	1527 ± 187^{ab}	1677 ± 191^{a}
38	Ch/N	53	70–80	975 ± 172^{bc}	1231 ± 172^{ab}
42	Ch/N	68	70–80	807 ± 94^{cd}	1020 ± 143^{bc}
44	N	74	>90	1860 ± 129^{a}	1653 ± 111^{a}
45	N	55	>90	1718 ± 172^{a}	1643 ± 166^{a}
58	N	65	>90	1514 ± 112^{ab}	1728 ± 177^{a}
59	Ch	47	20–30	676 ± 94^{cd}	811 ± 151^{cd}
60	Ch	52	10–20	595 ± 152^{cd}	675 ± 143^{cd}
61	rC	32	0	0^{f}	0^{f}
61/L[6]	N	65	>90	775 ± 126^{cd}	1326 ± 157^{ab}
$F_1(109)$[1] -					
1	Ch	47	20–30	443 ± 107^{cde}	620 ± 65^{cd}
2	Ch/N	47	>90	1862 ± 172^{a}	1689 ± 190^{a}
8	Ch/N	48	>90	1885 ± 184^{a}	1801 ± 213^{a}
9	Ch/N	51	>90	1916 ± 174^{a}	1817 ± 201^{a}
17	Ch/N	44	>90	960 ± 125^{bc}	1530 ± 212^{ab}
38	Ch	40	20–30	628 ± 124^{cd}	759 ± 119^{cd}
41	Ch	52	5–10	135 ± 31^{e}	380 ± 89^{de}
47	N	72	>90	1485 ± 130^{ab}	1711 ± 169^{a}
59	N	68	>90	1562 ± 135^{ab}	1307 ± 128^{ab}

[1] $F_1(107)$ and $F_1(109)$ progeny correspond to the crosses of FCF(107) and FCF(109) with JFLO(811), respectively.
[2] Leaf phenotypes: N–normal; rC–rolC; Ch–chimeric; Ch/N–chimeric phenotypes were replaced by normal phenotypes during plant development.
[3] In centimeters at the time when the first flower opened.
[4] Percentage of germinating pollen *in vitro*; average of five flowers.
[5] Average number of seed in five seed capsules derived from selfing or cross-pollination of wild-type (SNN) plants; low case letters ($a - f$) represent significance differences at $p < 0.05$.
[6] Represent pruned and grown from lateral buds.

green sectors were combined with half-leaf or inner-leaf penetrations of dark green tissue (Figures 5D and F, respectively). Other phenotypes consisted mainly of dark green small sectors and spots scatters over both peripheral and central leaf regions (Figure 5E). In some cases, indicative of groups a and a′, chimeric leaves at early stages were replaced by normal leaf phenotypes during plant development, whereas the chimeric formations in group b were inherited to younger leaves throughout the whole course of plant growth. PCR/Southern analysis of recombination of DNA samples from dark and light green leaf sectors from each plant indicated the presence of both recombined and non-recombined *FCF*-target loci (represented in Figure 2, lanes 3,10).

An additional type of plant chimera was induced by cutting of phenotypic rolC-type shoots, made in the two plants of group c. The presence of both pre- and post-recombination *FCF* loci in these plants, as revealed by PCR analysis of leaf total DNA (data

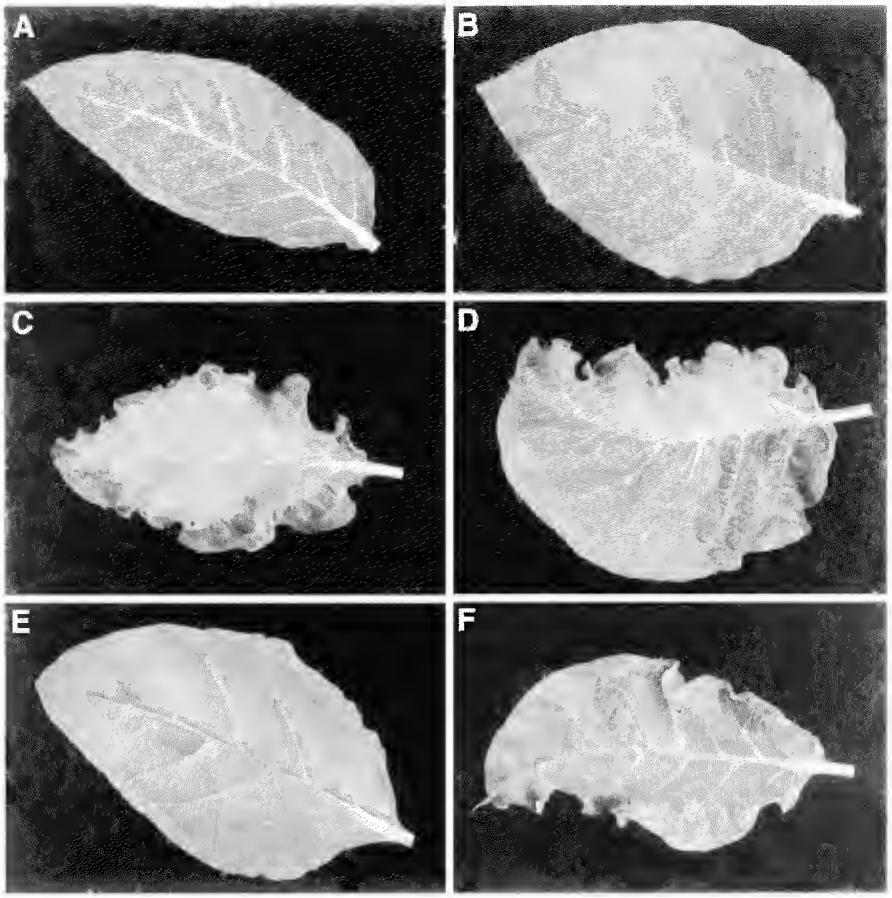

Figure 5. Visible chimeric leaf phenotypes in FCF × JFLO cross-hybrids. A: FCF(107), B: JFLO(811), C: Dark green and wrinkled periphery surrounding a smooth, pale green central region, D: One half is dark green and the other half is as in C, E: Small dark green sectors and spots scattered over both peripheral and central regions, F: Penetration of dark green sectors from the periphery inside.

not shown), indicated a chimeric status of recombination while no alteration of phenotype could be observed. However, cuttings have induced the development of a normal and fertile lateral shoot in each plant (Figure 6C). The lateral shoots of both plants displayed normal leaf phenotypes and heights of 55 and 65 cm (Table 2, F_1(107)-17/L and 61/L, respectively). Additionally, fertility was restored to 60–70%, 541 ± 84 and 698 ± 123 for F_1(107)-17/L and >90%, 775 ± 126 and 1326 ± 157 for F_1(107)-61/L, as indicated by pollen viability test and seed yield in self- and cross-fertilized flowers, respectively (Table 2). PCR/Southern analysis of DNA, sampled from phenotypic normal leaves revealed the presence of both pre- and post-recombined *FCF* loci (Figure 2, lane 12). Such chimeras were not observed from repetitive cuttings made in FCF parental lines, suggesting that recombination reactions may have occurred in the auxiliary bud meristem, in sufficient number of cells that gave rise to the development of restored normal and fertile lateral shoots in the F_1(107)-17 and F_1(107)-61 progenies.

Discussion

The constitutive expression of *35s*P-*rolC* in transgenic tobacco causes pleiotropic altered phenotypes, such as dwarfism, reduced apical dominance, reduced female fertility, lanceolate and pale-green leaves and small, male sterile flowers (Schmulling et al., 1988). In the present study, cross pollination with pollen from a constitutive *FLP*-expressing line was used to deliver FLP recombinase into two *FRT*-flanked *35s*P-*rolC* tar-

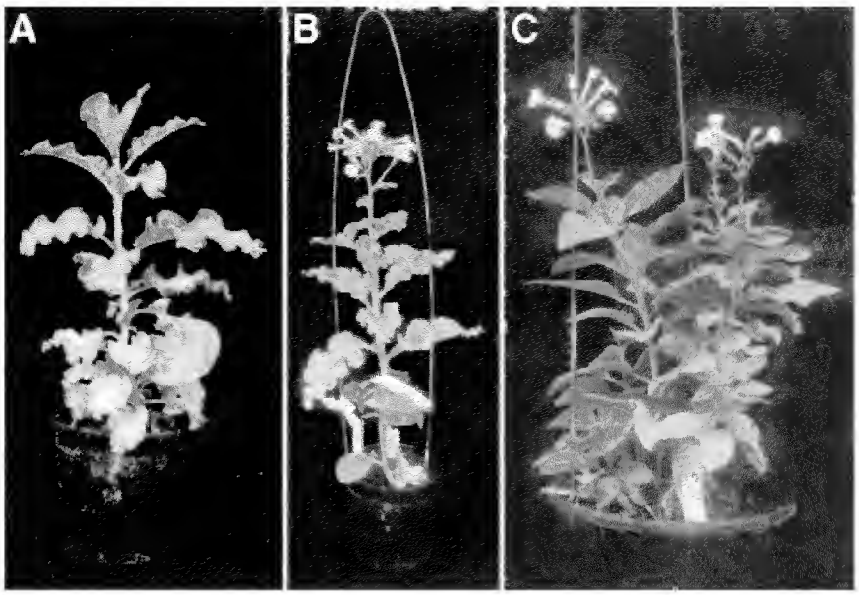

Figure 6. Representation of FCF × JFLO hybrid progeny displaying whole-plant leaf chimera (A,B) and a normal-type lateral shoot sector (C). The latter was derived from cuttings of a hybrid progeny that originally displayed rolC-type phenotypes.

get lines, and the recombination-mediated excision of the *35s*P-*rolC* cassette restored normal phenotypes or produced clonal leaf and lateral shoot sectors in the hybrid progenies. A potential strategy to restore fertility in hybrid plants was described by Schmulling et al. (1993) after crossing of male sterile *rolC* plants with plants that express *rolC* antisense RNA. However, seed setting was only partially restored in these plants. Here, the reversion of rolC-induced leaf morphologic traits was associated with restoration of fertility and seed setting, ranging between 52% and 93% or 20% and 41% in progenies displaying normal or sectorial leaf phenotypes, respectively. This implies that reversion to normal leaf phenotypes (of both marginal and central regions) prior to flower bud formation, is necessary for efficient restoration of male fertility and seed setting in the *rolC*-transgenic plants. These results are consistent with the cell autonomous activity of the rolC gene product.

PCR analysis of DNA from normal leaves and dark green leaf sectors indicated a chimeric state, carrying both excised and non-excised *FRT-35s*P-*rolC-FRT* target loci. A possible explanation to this situation is differential excision of *35s*P-*rolC* from different shoot apical meristem layers, giving rise to different composition of tissue layers as describes for periclinal chimeras (Poethig, 1989). In angiosperms, the outer L_1 layer gives rise mainly to the leaf and stem epidermis tissue, whereas the L_2 and L_3 layers contribute mainly to the subepidermal mesophyll, cortical and vascular tissues (Poethig, 1989). In tobacco, L_2 produces all the mesophyll tissue at the leaf periphery (Tilney-Bassett, 1986). The phenotypic display of mutations in the chlorophyll pathway in L_2 layer is white periphery surrounding a central green region, while mutations in both L_2 and L_3 give rise to fully white leaves. The peripheral leaf dark green sectors described in the present report (Figure 5C) may have originated from L_2 layer cells that undergone excision of the *35s*P-*rolC* expression cassette while normal leaf phenotype and the green sectors that occupy both peripheral and central leaf regions (Figure 5D,F) could have originated either from excision events in both L_2 and L_3 layers, and/or from penetrations of L_2 cells into the L_3 layer during leaf development (Poethig, 1989). Consistent with periclinal chimeras, leaf sectors were usually inherited to younger leaves (Figure 6A,B). In some cases, however, sectorial leaves were replaced by phenotypic normal leaves, suggesting that either additional cells in the shoot apical meristem had undergone recombination or *35s*P-*rolC*-excised cells had replaced the *35s*P-*rolC*-containing cells, during plant development. Transgenic periclinal chimeras of *35s*P-*rolC*-expressing tissues have been previously obtained by *Agrobacterium*-mediated transformation of tobacco in approximately 6.5–15% of the regenerated

plants (Oono et al., 1993; Schmulling & Schell, 1993). In similar to the described in the present report, chimeric leaves were characterized by a wrinkled, dark green periphery and a pale green central region. While the difference in pigmentation was ascribed to the lower content of chlorophyll in rolC-expressive tissues (Schmulling et al., 1988) the peripheral wrinkled morphology was referred mainly to an inhibitory effect of *35s*P-*rolC* on cell division in developing leaves, giving rise to difference in cell number and therefore causing physical tension between the dark and pale green regions (Oono et al., 1993). Molecular DNA and RNA analysis implied that the inner region was derived from transformed shoot meristem L_3 layer while the periphery was developed from non-transformed cells that incorporated into the outer L_2 layer of the shoot meristem during regeneration. A different type of periclinal chimera was reported by Fladung and Ahuja (1997) in which excision of the maize *Ac* transposon from a silent *35s*P-*Ac*-*rolC* locus restored *rolC* activity in green leaf tissue in transgenic aspen. This event, found in one out of 385 regenerated plants, indicated expression of rolC in the L_1 derived colorless epidermal tissue.

The results presented in this report also showed that cuttings of rolC-type shoots of *JFLO/FCF* genotype, induced the development of normal and fertile shoots from lateral buds. In angiosperms, lateral shoots originate from lateral shoot meristems that arise regularly at the base of each leaf (Poethig, 1989). Cuttings provide a mechanical means to induce differentiation of lateral shoot meristems into shoots. It is therefore reasonable to assume that the arising of normal and fertile, yet genotypically chimeric lateral shoots (Figure 6C; Table 2, F_1(107)-17/L and 61/L), originated from an excised *FCF* lineage that populated the L_2 and L_3 layers of the lateral bud meristem.

Among the potential usage of site-specific recombination systems in plants, elimination of selectable marker genes (Dale & Ow, 1991; Russell et al., 1992), fertility restoration by excision of a sterility-inducing transgene (Luo et al., 2000), conversion of complex transgene integration structures to single-copy units (Srivastava et al., 1999) and activation of clonal sectors (Odell et al., 1994; Kilby et al., 1995, 2000; Onouchi et al., 1995; Davies et al., 1999) have been demonstrated. In conjunction with the latter application, the present report indicates that recombinase-mediated excision of *rolC* can be used as a relatively efficient tool for generation of clonal leaf and lateral shoot sectors and for production of transgenic periclinal chimeras. Thus, establishment of conditions for excision of *rolC* via induced activation of FLP recombinase at specific developmental stages might be useful to study further the effects of rolC on plant vegetative and reproductive developmental processes.

Acknowledgements

Our special thanks to Jeff Schell, Csaba Koncz, Thomas Schmulling and Angelo Spena for their kind gifts of the pPCV002-CaMVC and pPCV002 plasmids. This study was supported partly by a grant from the Chief Scientist of the Israeli Ministry of Agriculture and partly by a grant (No. US-2651-95) from BARD (US-Israel Binational Agricultural Research and Development Fund) to David Gidoni. Contribution from the Agricultural Research Organization, The Volcani Center, Institute of Field Crops, Bet Dagan, Israel, No. 144/2000.

References

An G, Ebert PR, Mitra A and Ha SB (1988) Binary vectors. *In*: Gelvin SB, Schilperoot RA and Vernma DPS (eds.), Plant Molecular Biology Manual. (pp. A3/1–A3/19) Kluwer Academic Publishers, Dordrecht.

Bar M, Leshem B, Gilboa N and Gidoni D (1996) Visual characterization of recombination at *FRT-gusA* loci in transgenic tobacco mediated by constitutive expression of the native FLP recombinase. *Theor Appl Genet* **93**: 407–413.

Bayley CC, Morgan M, Dale EC and Ow DW (1992) Exchange of gene activity in transgenic plants catalyzed by the Cre-lox site-specific recombination system. *Plant Mol Biol* **18**: 353–361.

Bruce R and Williams EG (1986) Pollen, pistil and reproductive function in crop plants. *Plant Breed Rev* **4**: 9–79.

Dale EC and Ow DW (1990) Intra- and inter-molecular site-specific recombination in plant cells mediated by bacteriophage P1 recombinase. *Gene* **91**: 79–85.

Dale EC and Ow DW (1991) Gene transfer with subsequent removal of the selection gene from the host gene genome. *Proc Natl Acad Sci USA* **88**: 10558–10562.

Davies GJ, Kilby NJ, Riou-Khamlichi C and Murray JAH (1999) Somatic and germinal inheritance of an FLP-mediated deletion in transgenic tobacco. *J Exp Bot* **50**: 1447–1456.

Doyle JJ and Doyle JL (1990) Isolation of plant DNA from fresh tissue. *Focus* **12**: 13–15.

Fladung M (1990) Transformation of diploid and tetraploid potato clones with the *rolC* gene of *Agrobacterium rhizogenes* and characterization of transgenic plants. *Plant Breed* **104**: 295–304.

Fladung M and Ahuja MR (1997) Excision of the maize transposable element *Ac* in periclinal chimeric leaves of *35s-Ac-rolC* transgenic aspen-*Populus*. *Plant Mol Biol* **33**: 1097–1103

Gallie DR, William JL and Walbot V (1989) Visualizing mRNA expression in plant protoplasts: factors influencing efficient mRNA uptake and translation. *Plant Cell* **1**: 301–311.

Horsch RB, Fry JE, Hoffmann NL, Eichholz D, Rogers SG and Fraley RT (1985) A simple and general method for transferring genes into plants. *Science* **227**: 1229–1231.

Jones JDG, Bishop G, Carroll B, Dickinson M, English J, Harrison K et al. (1992) Prospects for establishing a tomato gene tagging system using the maize transposon *Activator (Ac). Proc R Soc Ebinb* **99B**: 107–119.

Kilby NJ, Snaith MR and Murray JAH (1993) Site-specific recombinases: tools for genome engineering. *Trends Genet* **9**: 413–421.

Kilby NJ, Davies GJ, Snaith MR and Murray JAH (1995) FLP recombinase in transgenic plants: constitutive activity in stably transformed tobacco and generation of marked cell clones in *Arabidopsis*. *Plant J* **8**: 637–652.

Kilby NJ, Fyvie MJ, Sessions RA, Davies GJ and Murray JAH (2000) Controlled induction of GUS marked clonal sectors in *Arabidopsis*. *J Exp Bot* **51**: 853–863.

Koncz C and Schell J (1986) The promoter TI-DNA gene 5 controls the tissue-specific expression of chimeric genes carried by a novel type of *Agrobacterium* binary vector. *Mol Gen Genet* **204**: 383–396.

Lloyd AM and Davis RW (1994) Functional expression of the yeast FLP/*FRT* site-specific recombination system in *Nicotiana tabacum*. *Mol Gen Genet* **242**: 653–657.

Luo H, Lyznik LA, Gidoni D and Hodges TK (2000) FLP-mediated recombination for use in hybrid plant production. *Plant J* **23**: 423–430.

Lutcke HA, Chow KC, Mickel FS, Moss KA, Kern HF and Scheele GA (1987) Selection of AUG initiation codons differ in plants and animals. *EMBO J* **6**: 43–48.

Lyznik LA, Hirayama L, Rao KV, Abad A and Hodges TK (1995) Heat-inducible expression of *FLP* gene in maize cells. *Plant J* **8**: 177–186.

Lyznik LA, Rao KV and Hodges TK (1996) FLP-mediated recombination of FRT sites in the maize genome. *Nucl Acids Res* **24**: 3784–3789.

Maniatis T, Fritsch EF and Sambrook J (1982) Molecular Cloning: A Laboratory Manual. Cold Spring Harbor Laboratory, Cold Spring Harbor, New York.

Odell JT, Caimi PG, Sauer B and Russell SH (1990) Site-directed recombination in the genome of transgenic tobacco. *Mol Gen Genet* **223**: 369–378.

Odell JT, Hoopes JL and Vermerris W (1994) Seed-specific gene activation mediated by the Cre/*lox* site-specific recombination system. *Plant Physiol* **106**: 447–458.

Odell JT and Russell SH (1994) Use of site-specific recombination in the genome systems in plants. *In*: Paszkowski J (ed.) *Homologous Recombination and Gene Silencing in Plants*. (pp. 219–270) Kluwer Academic Publishers, Dordrecht.

O'Gorman S, Fox DT and Wahl GM (1991) Recombinase-mediated gene activation and site-specific integration in mammalian cells. *Science* **251**: 1351–1355.

Onouchi H, Nishihama R, Kudo M, Machida Y and Machida C (1995) Visualization of site-specific recombination catalyzed by a recombinase from *Zygosaccharomyces rouxii* in *Arabidopsis thaliana*. *Mol Gen Genet* **247**: 653–660.

Oono Y, Suzuki T, Toki S and Uchimiya H (1993) Effects of the over-expression of rolC gene on leaf development in transgenic periclinal chimeric plants. *Plant Cell Physiol* **34**: 745–752.

Ow DW and Medberry SL (1995) Genome manipulation through site-specific recombination. *Critic Rev Plant Sci* **14**: 239–261.

Ow DW (1996) Recombinase-directed chromosome engineering in plants. *Curr Opin Biotechnol* **7**: 181–186.

Poethig S (1989) Genetic mosaics and cell lineage analysis in plants. *Trend Genet* **5**: 273–277.

Russell SH, Hoopes JL and Odell JT (1992) Directed excision of a transgene from the plant genome. *Mol Gen Genet* **234**: 49–59.

Sauer B and Henderson N (1988) Site-specific DNA recombination in mammalian cells by the Cre recombinase of bacteriophage P1. *Proc Natl Acad Sci USA* **85**: 5166–5170.

Sauer B (1994) Site-specific recombination: development and applications. *Curr Biol* **5**: 521–527.

Schmülling T, Schell J and Spena A (1988) Single genes from *Agrobacterium rhizogenes* influence plant development. *EMBO J* **7**: 2621–2629.

Schmülling T, Röhrig H, Pilz S, Walden R and Schell J (1993) Restoration of fertility by antisense RNA in genetically engineered male sterile tobacco plants. *Mol Gen Genet* **237**: 385–394.

Schmülling T and Schell J (1993) Transgenic tobacco plants regenerated from leaf disks can be periclinal chimeras. *Plant Mol Biol* **21**: 705–708.

Spena A, Schmülling T, Koncz C and Schell JS (1987) Independent and synergistic activity of *rol A, B* and *C* loci in stimulating abnormal growth in plants. *EMBO J* **6**: 3891–3899.

Spena A, Aalen R and Schulze SC (1989) Cell-autonomous behavior of the rolC gene of *Agrobacterium rhizogenes* during leaf development in transgenic plants. *Plant Cell* **1**: 1157–1164.

Srivastava V, Anderson OD and Ow DW (1999) Single-copy transgenic wheat generated through the resolution of complex integration patterns. *Proc Natl Acad Sci USA* **96**: 11117–11121.

Stuurman J, de Vroomen MJ, Nijkamp HJJ and van Haaren MJJ (1996) Single-site manipulation of tomato chromosomes *in vitro* and *in vivo* using Cre-*lox* site-specific recombination. *Plant Mol Biol* **32**: 901–913.

Stuurman J, Nijkamp HJJ and van Haaren MJJ (1998) Molecular insertion-site selectivity of Ds in tomato. *Plant J* **14**: 215–223.

Tilney-Bassett RAE (1986) *Plant Chimeras*. Edward Arnold, London.

ELSEVIER

Gene 212 (1998) 77–86

GENE
AN INTERNATIONAL JOURNAL ON GENES AND GENOMES

A broad-host-range Flp-*FRT* recombination system for site-specific excision of chromosomally-located DNA sequences: application for isolation of unmarked *Pseudomonas aeruginosa* mutants

Tung T. Hoang, RoxAnn R. Karkhoff-Schweizer, Alecksandr J. Kutchma, Herbert P. Schweizer *

Department of Microbiology, Colorado State University, Fort Collins, CO 80523, USA

Received 26 December 1997; received in revised form 23 February 1998; accepted 2 March 1998; Received by J. Wild

Abstract

An improved method for gene replacement in *Pseudomonas aeruginosa* was developed. The method employs several new gene replacement vectors that incorporate (1) the counterselectable *sacB* marker, (2) a *lacZα*-allele for blue–white screening, (3) the pUC18/19 vectors multiple cloning site with 10 unique restriction sites, (4) an *oriT* for conjugation-mediated plasmid transfer and (5) carbenicillin, gentamicin (Gm) and tetracycline selectable markers. A cassette was constructed that contains a Gm^R selectable marker next to the green fluorescent protein structural gene, with both markers being flanked by Flp recombinase target (*FRT*) sites. The *FRT* cassette was used to insertionally inactivate the cloned *P. aeruginosa pabC* gene encoding aminodeoxychorismate lyase. After conjugal transfer into *P. aeruginosa*, plasmid integrants were selected, and deletion of unwanted DNA sequences was promoted by sucrose counterselection. The *FRT* cassette was excised with high frequencies (close to 100%) from the chromosome after conjugal transfer of a Flp recombinase-expressing plasmid; this *sacB*-containing plasmid was subsequently cured by sucrose counterselection, resulting in an unmarked *P. aeruginosa ΔpabC* strain.

Keywords: *Saccharomyces cerevisiae*; Cassette; Gene replacement; Mutagenesis

1. Introduction

Analyses of cloned genes and their products from bacteria in the environments of their native chromosomes necessitate methods that enable the genetic exchange of mutated, plasmid-borne DNA with the respective genomes. Our laboratory was the first to develop a gene replacement system for *Pseudomonas aeruginosa* that allowed for positive selection of all steps involved in the gene replacement process (Schweizer, 1992). This system included the *Bacillus subtilis sacB* gene as counter-selectable marker (Schweizer, 1992), allowing for positive selection of the segregation of true mutants from the more frequently occurring merodiploids on medium containing 5% sucrose. This selection process greatly facilitated the genetic exchange not only of selectable markers but also of screenable markers, e.g. *lacZ*- or *xylE*-based gene fusions (Schweizer and Hoang, 1995; Schweizer et al., 1996), and Ts-conferring alleles (Hoang and Schweizer, 1997). The latest improvement included a gene replacement vector, pEX100T, which was genetically engineered to facilitate

* Corresponding author. Tel: +1 970 491 3536; Fax: +1 970 491 1815; e-mail: hschweiz@cvmbs.colostate.edu

Abbreviations: *aacC1*, Gm acetyltransferase 3-1 encoding gene; Ap, ampicillin; *B.*, *Bacillus*; βGal, β-galactosidase; bhr, broad-host-range; *bla*, gene encoding β-lactamase; bp, base pair(s); cI_{857}, gene encoding Ts λ repressor; Cb, carbenicillin; Δ, deletion; dNTP, deoxyribonucleoside triphosphate(s); *E.*, *Escherichia*; Flp, *S. cerevisiae* recombinase; *FLP*, Flp structural gene; *FRT*, Flp recombinase target; GFP, green fluorescent protein; *GFP*, GFP-encoding gene; Gm, gentamicin; kb, kilobase(s) or 1000 bp; Km, kanamycin; *lacZα*, βGal α peptide-encoding gene; *lacZpo*, *lac* promoter-operator; LB, Luria–Bertani (medium); MCS, multiple cloning site(s); nt, nucleotide(s); oligo, oligodeoxyribonucleotide; *ori*, pMB1-based origin of DNA replication; ori_{1600}, bhr replicon; *oriT*, origin of transfer; *P.*, *Pseudomonas*; PABA, *p*-amino benzoic acid; PBS, phosphate-buffered saline; PCR, polymerase chain reaction; PIA, *Pseudomonas* isolation agar; Pol, polymerase; *R*, resistance/resistant; *rep*, ori_{1600} replication protein; ^{S}, sensitive; *S.*, *Saccharomyces*; *sacB*, *B. subtilis* levansucrase-encoding gene; TBE, Tris-borate-EDTA; *tet*, Tc^R-encoding gene; Tc, tetracycline; Ts, temperature sensitive; u, unit(s); wt, wild type; XGal, 5-bromo-4-chloro-3-indolyl-β-D-galactopyranoside; ::, novel junction (fusion or insertion).

0378-1119/98/$19.00
PII: S0378-1119(98)00130-9

the cloning and genetic manipulation of virtually any DNA fragment (Schweizer and Hoang, 1995). This was achieved by incorporating into a single vector (1) the counterselectable *sacB* marker; (2) a *lacZα*- allele for blue–white screening on XGal-containing media; (3) an *oriT* for conjugation-mediated plasmid transfer and (4) unique cloning sites for *Sma*I and the rare-cutting meganuclease I-*Sce*I. By site-specific mutagenesis and subcloning, most restriction sites within the vector were eliminated giving greater access to restriction sites within the cloned fragment, thus facilitating the construction of insertions, deletions and frameshifts.

Although, in its present form, this vector is very versatile and has been used by many laboratories to introduce marked and unmarked mutant alleles into the *P. aeruginosa* chromosome, it suffers from some drawbacks: (1) even though the presence of very few restriction enzyme cleavage sites facilitates mutagenesis of cloned fragments, lack of a MCS hampers cloning of previously mutagenized fragments; (2) the current replacement vector utilizes Ap^R as the selectable marker, and β-lactams are not applicable in many other bacteria. Being the sole selectable plasmid marker, it also precludes the use of Ap^R/Cb^R conferring cassettes in insertional mutagenesis experiments (Schweizer et al., 1996). One goal of the present studies was to further extend the usefulness of this vector system by addressing these shortcomings.

Besides construction of versatile suicide delivery vectors, efforts aimed at optimizations of existing gene replacement systems must also include development of methods that allow generation of chromosomal insertions of heterologous DNA segments eventually devoid of any selection marker, as is currently required for metabolic engineering of novel phenotypes for environmental applications and development of live vaccine strains (De Lorenzo, 1994). Useful methods previously employed in other bacteria to excise unwanted marker sequences from the chomosome involve various site-specific recombination systems, in particular the Cre-*lox* system of the phage/plasmid P1 (Sternberg et al., 1981; Ayres et al., 1993), the ParA-*res* system of RP4 (Kristensen et al., 1995), the TnpR-*res* system of the γδ transposon (Camilli et al., 1994) and the *Saccharomyces cerevisiae* Flp-*FRT* system (Cherepanov and Wackernagel, 1995). These systems are useful tools for genetic engineering due to the high specificity of the respective recombinases, which enables directed operations in vivo on DNA molecules as large as bacterial or eukaryotic chromosomes. Of all of these systems, the Flp-*FRT* recombination system (Sadowski, 1995) is perhaps the most versatile, since it is the least restrictive in terms of host-range, functioning in bacteria (Cherepanov and Wackernagel, 1995), yeasts (Sadowski, 1995), plants (Lyznik et al., 1996) and mammalian cells (Dymecki, 1996). The Flp enzyme is a site-specific recombinase that promotes recombination at a specific 13-bp site within a 65-nt sequence, termed *FRT* (see Fig. 2B) (Cox, 1983).

In this study, we adapted the *S. cerevisiae* Flp-*FRT* system for use in bacteria other than *E. coli*. This included construction of a new Gm^R-*FRT* cassette and a broad-host-range (bhr) Flp recombinase-expressing vector.

2. Materials and methods

2.1. Bacterial strains, plasmids, media and culture conditions

The bacterial strains and plasmids used in this study are listed in Table 1. LB medium was used as the rich medium for both *E. coli* and *P. aeruginosa*. The minimal medium used for *P. aeruginosa* was VBMM. VBMM is VB medium containing 0.3% citrate and is selective for *P. aeruginosa* since *E. coli* cannot utilize citrate (Hoang and Schweizer, 1997). For growth of *pabC* mutants, VBMM was supplemented with 10 μg PABA per ml. Antibiotics were used in selection media at the following concentrations: for *E. coli*, Ap (100 μg/ml); Gm (10 μg/ml); Tc (10 μg/ml); and for *P. aeruginosa*, Cb (500 μg/ml); Gm (100–200 μg/ml); Tc (50 μg/ml). Lactose phenotypes were screened on LB plates containing 40 μg Xgal per ml. Hemolysin production of *P. aeruginosa* cells was screened on sheep blood agar plates (BBL Microbiology Systems, Cockeysville, MD). Sucrose-resistant colonies were obtained by streaking *P. aeruginosa* merodiploids or cells containing plasmids with *sacB* on VBMM or LB or PIA (Difco, Detroit, MI) plates supplemented with 5% sucrose.

2.2. DNA manipulations

Restriction enzymes, T4 DNA ligase, T4 polynucleotide kinase and T4 DNA Pol were purchased from Gibco-BRL (Gaithersburg, MD) and used as recommended by the supplier, except the T4 DNA Pol, which was used for blunt-ending DNA fragments in the respective restriction enzyme incubation buffers in the presence of 100 μM dNTPs (Sambrook et al., 1989). *Taq* and *Taq*$^+$ Pol were purchased from Quiagen (Santa Clarita, CA) and Stratagene (La Jolla, CA), respectively, and were used as recommended by the suppliers. Small-scale isolations of plasmid DNA from *E. coli* and *P. aeruginosa* were achieved utilizing the QUIAprep spin miniprep kit (Quiagen, Santa Clarita, CA), and DNA transformations were done as previously described (Hoang and Schweizer, 1997). DNA restriction fragments were eluted from agarose gels by utilizing the Geneclean procedure (BIO 101, San Diego, CA). For genomic Southern analysis, chromosomal *P. aeruginosa*

Table 1
Bacterial strains and plasmids

		Relevant genotype or description	Source or reference
Strains			
E. coli	DH5αF′	[F$^+$ ϕ80 *lacZ*ΔM15] Δ(*lacZYA-argF*)U169 *recA*1 *endA*1 *hsdR*17 [$r_K^- m_K^+$] *supE*44 *thi*-1 *gyrA relA*1	Gibco-BRL, Gaithersburg, MD
	SM10	*thi*-1 *thr leu tonA lacY supE recA*::RP4-2-Tc::Mu (Km^R)	De Lorenzo and Timmis (1994)
P. aeruginosa	PAO1	Prototroph	B.H. Holloway
	PAO205	PAO1 with Δ(*pabC-orf*)::Gm^R-*GFP FRT*	This study
	PAO206	PAO1 with unmarked Δ(*pabC-orf*)	This study
Plasmids			
	pΔH-1	Ap^R; 3.4-kb *Bam*HI fragment with Δ*plcH*	M.L. Vasil
	pALB2	Ap^R, Tc^R; source of *sacB*$^+$ gene	Schweizer and Hoang (1995)
	pALTER-1	Tc^R; source of *tet* gene	Promega, Madison, WI
	pCP16	Ap^R; source of *FRT* sequences	Cherepanov and Wackernagel (1995)
	pEX100T	Ap^R; *oriT*$^+$ *sacB*$^+$ gene replacement vector	Schweizer and Hoang (1995)
	pGEM-T*oriT*	Ap^R; source of *oriT*	Schweizer et al. (1996)
	pGFPmut1	Ap^R; source of *GFP* gene	Cormack et al. (1996)
	pMMC6	Ap^R; source of inducible Flp recombinase	Cox (1983)
	pUCGM	Ap^R, Gm^R; source of Gm^R cassette	Schweizer (1993a)
	pUC18/19	Ap^R; cloning vectors	Yanisch-Perron et al. (1985)
	pUC1918	Ap^R; cloning vector with duplicated pUC18/19 MCS	Schweizer (1993b)
	pUCP20T	Ap^R; mobilizable broad-host-range cloning vector	Schweizer et al. (1996)
	pEX18Ap[a]	Ap^R; *oriT*$^+$ *sacB*$^+$, gene replacement vector with MCS from pUC18	This study
	pEX18Gm[a]	Gm^R; *oriT*$^+$ *sacB*$^+$, gene replacement vector with MCS from pUC18	This study
	pEX18Tc[a]	Tc^R; *oriT*$^+$ *sacB*$^+$, gene replacement vector with MCS from pUC18	This study
	pFGS1	Ap^R, Gm^R; replacement of a 1.9-kb *Hpa*I fragment from the *tet* genes of pCP16 with a 0.83-kb *Sma*I fragment from pUCGM	This study
	pFLP1	Ap^R; ligation of a blunt-ended 2.5-kb pMMC6 *Cla*I+*Xba*I fragment into the blunt-ended *Aff*III site of pGEM-T*oriT*	This study
	pFLP2	Ap^R; 2.6-kb *Bam*HI–*Sph*I fragment from pALB2 ligated between the same sites of pPS908	This study
	pPS681	Ap^R; 6.7-kb fragment containing the *P. aeruginosa acpP* region	Laboratory collection
	pPS698	Ap^R; 3-kb *Bam*HI–*Hin*dIII *pabC*$^+$–*orf*$^+$ fragment from pPS681 ligated between the same sites of pUC18	This study
	pPS747	Ap^R; pUCP20T with 0.7-kb *Pst*I–*Xba*I fragment from pGFPmut1	This study
	pPS838	Ap^R, Gm^R; 1.5-kb blunt-ended pFGS1 *Hin*dIII–*Sma*I fragment ligated into the blunt-ended pUC1918 *Eco*RI	This study
	pPS854	Ap^R; religated 2.9-kb reverse PCR fragment from pPS838	This study
	pPS856	Ap^R, Gm^R; 0.83-kb blunt-ended *Sac*I fragment from pUCGM ligated into the *Eco*RV site of pPS854	This study
	pPS858	Ap^R, Gm^R; blunt-ended pPS747 *Pst*I–*Xba*I fragment ligated into the blunt-ended *Eco*R1 site of pPS856	This study
	pPS908	Ap^R; 2.5-kb blunt-ended pMMC6 *Cla*I–*Xba*I fragment ligated into the *Sma*I site of pUCP20T	This study
	pPS953	Ap^R, Gm^R; replacement of a 1.3-kb pPS698 *Stu*I fragment with a 1.8-kb blunt-ended pPS858 *Sac*I fragment	This study
	pPS955	Ap^R, Gm^R; ligation of a 3.6-kb *Bam*H1–*Hin*dIII fragment from pPS953 between the same sites of pEX18Ap	This study

[a]The corresponding pEX19Ap, pEX19Gm and pEX19Tc vectors contain the pUC19 MCS.

DNA was isolated utilizing the IsoQuick nucleic acid extraction kit (ORCA Research, Bothell, WA), digested with various restriction endonucleases, electrophoresed on a 1% agarose gel in 0.5× TBE buffer and transferred to Photogene nylon membranes (Gibco BRL, Gaithersburg, MD) as previously described (Sambrook et al., 1989). Plasmid DNA was biotinylated by random hexamer priming following the NEBlot™ Phototype™ kit protocol (New England Biolabs, Beverly, MA). Following transfer and ultraviolet fixation (Sambrook et al., 1989), the membranes were probed with the biotinylated DNA fragment according to the Phototype™ detection kit protocol (New England Biolabs, Beverly, MA). Automated nucleotide sequencing was performed as previously described (Hoang and Schweizer, 1997).

2.3. Plasmid constructions

Details on the construction of selected plasmids not evident from the information given in Table 1 are as follows.

To obtain the gene replacement vectors pEX18Ap and pEX19Ap, 1791-bp *Pvu*I fragments from pUC18 or pUC19 (Yanisch-Perron et al., 1985), respectively, were gel-purified and ligated to the large *Pvu*I fragment of pEX100T (Schweizer and Hoang, 1995), from which the overlapping *Sph*I and *Nsi*I had been eliminated by digestion with *Nsi*I, followed by blunt-ending and ligation. The vectors pEX18Gm and pEX18Tc were obtained from pEX18Ap in several steps. First, two primers (APU2, 5′-GTTGAATACTCATACTCTTC and APD, 5′-catcgaTTGTCAGACCAAGTTTACTCAT) were synthesized. These primers are complimentary to nt 5630–5650 (APU2) and 4780–4760 [capital letters of APD; lower-case letters denote nt that were inserted to generate a *Cla*I site (underlined)] of pEX18Ap. Primers APD and APU2 were used to prime synthesis from pEX18Ap DNA in a 50-μl reaction mixture containing 1× *Taq*$^+$ buffer (Stratagene, La Jolla, CA), 200 μM of each dNTP, 30 pmol of each primer, ~10 pmol plasmid DNA and 2.5 u *Taq*$^+$ Pol (Stratagene, La Jolla, CA). The reaction mixture was subjected to the following thermal cycles: one cycle at 96°C for 1.5 min; 30 cycles (95°C, 1 min; 58°C, 25 s; 72°C, 2.5 min) and a final extension at 72°C for 5 min. A similar reaction was set up with pEX19Ap template DNA. All reactions yielded single, linear 5-kb fragments that were treated (20 min; 37°C) with 2.5 u T4 DNA Pol in the presence of 100 μM dNTPs and purified by agarose gel electrophoresis. For construction of pEX18Gm/pEX19Gm and pEX18Tc/pEX19Tc, the 5-kb PCR fragments from the pEX18Ap/pEX19Ap reactions were ligated to a 830-bp blunt-ended *Sac*I fragment from pUCGM (Schweizer, 1993a) or to a 1348-bp blunt-ended *Cla*I–*Sty*I fragment from pALTER-1 (Promega, Madison, WI), respectively. Only those isolates containing the *aacC*1 and *tet* genes in the same transcriptional orientation as the originally present *bla* gene were retained.

The Gm^R-*GFP* FRT cassette contained on pPS858 was assembled in several steps. First, two primers (FSGA, 5′-tagaattcCATTGAGTAAGTTTTTAAGCACATC and FSGB, 5′-gatatcCATTGCT-GTTGACAAAGGGAATCA) were synthesized and phosphorylated by T4 polynucleotide kinase. These oligos primed just inside the *FRT* sequences contained on pPS838 and either introduced an *Eco*RI site (underlined lower-case letters in FSGA) or an *Eco*RV site (underlined lower-case letters in FGSB). The phosphorylated FSGA and FSGB oligos were used to prime synthesis from pPS838 DNA in a reverse PCR reaction as described above. However, the reaction mixtures were subjected to the following thermal cycles: one cycle at 96°C for 40 s; 30 cycles (95°C, 40 s; 54°C, 12 s; 72°C, 2 min and 20 s) an a final extension at 72°C for 5 min. The single 2.9-kb reaction product was gel-purified and then religated to form pPS854. The final vector, pPS858, was derived from pPS854 by insertion of the Gm^R-encoding cassette from pUCGM and the *GFP* cassette from pPS747 in successive steps, as detailed in Table 1.

2.4. Gene replacement and in-vivo marker excision in P. aeruginosa

For gene replacement, the previously *sacB*-based described strategy (Schweizer and Hoang, 1995) was employed.

For isolation of Δ*plcH* mutants, a 3.4-kb *Bam*HI fragment from pΔH-1 containing an unmarked 2-kb *Sma*I-deletion of the *plcH* coding sequence (Pritchard and Vasil, 1986) was cloned into the *Bam*HI site of all pEX vectors. The recombinant plasmids were conjugated from *E. coli* SM10 into PAO1, and Cb^R, Gm^R or Tc^R plasmid-integrants were selected on VBMM medium containing the appropriate antibiotic. Merodiploids were resolved by plating on VBMM medium containing 5% sucrose. The hemolysin phenotypes of sucrose^R mutants were screened on blood agar plates, and putative Δ*plcH* mutants showing no zones of hemolysis after 36 h were counted.

For the isolation of a Δ(*pabC-orf*) mutant, pPS955 was conjugally transferred from *E. coli* SM10 into PAO1 (Schweizer, 1992), followed by selection of Gm^R colonies on VBMM+Gm medium. The merodiploid colonies were plated on VBMM+PABA+Gm medium containing 5% sucrose. The chromosomal restriction patterns of sucrose^R, putative Δ(*pabC-orf*)::Gm^R-*GFP FRT* mutants were verified by genomic Southern analysis utilizing as the probes either the biotin-labeled 3-kb chromosomal insert of pPS698 (*pabC-orf* probe) or the biotin-labeled 0.83-kb insert of pUCGM (*aacC*1 or Gm probe). Strain PAO205 containing the correct insertion was retained for the excision experiment.

Deletion of the chromosomally integrated Gm^R-*GFP* markers by Flp recombinase-catalyzed excision was achieved by conjugally transferring the Flp-expressing pFLP2 from *E. coli* SM10 into *P. aeruginosa* PAO205 at 37°C. The mating mixtures were suspended in 1 ml PBS (Miller, 1992). Aliquots (100 μl) of the undiluted, 10^{-1}, 10^{-2} and 10^{-3} diluted (in PBS) cell suspension were plated on VBMM+PABA+Cb medium and incubated at 37°C until single colonies were discernible. Twenty single colonies were screened for Gm^s on VBMM+PABA±Gm plates. Plasmid pFLP2 was cured by generously streaking cells from four patches containing Gm^S colonies on VBMM+PABA medium supplemented with 5% sucrose, followed by incubation at 37°C. Loss of pFLP2 was tested by patching 20

sucrose^R colonies on VBMM + PABA ± Cb medium, and then verified by subjecting eight LB-grown sucrose^R, Cb^S and Gm^S cells to plasmid mini-prep isolation and agarose gel electrophoresis of 10-μl aliquots of 'DNA' (using a replicative Cb^R-conferring plasmid as a positive control).

Excision events were initially assessed by performing colony PCR on four Gm^R isolates utilizing two *aacC1*-specific primers (Gm-Up, 5′-TGGAGCAG-CAACGATGTTAC and Gm-Down, 5′-TGTTAGGT-GGCGGTACTTGG). To do this, cells from an entire patch were transferred to a microfuge tube containing 50 μl H_2O, and the cell suspension was boiled for 5 min. Lysates (5 μl) were then transferred to tubes containing (in 45 μl) 1 × PCR buffer (Quiagen, Santa Clarita, CA), 200 μM of each dNTP and 30 pmol of each Gm-Up and Gm-Down primer. The reaction mixtures were denatured in a thermal cycler at 96°C for 5 min before addition of 2.5 u *Taq* Pol (Quiagen, Chatsworth, CA) and subjecting the mixtures to 34 cycles of amplification (96°C, 35 s; 54°C, 20 s; 72°C, 1 min) followed by a final extension at 72°C for 5 min. Five microliters of the 50-μl reaction mixtures were analyzed on an agarose gel.

The mutants were then further verified or by isolating chromosomal DNAs from the same four colonies used in PCR analysis and by performing genomic Southern analyses utilizing the above described biotin-labeled *pabC-orf* and *aacC1* probes.

3. Results and discussion

3.1. Construction of new gene replacement vectors

To extend the usefulness of the *sacB*-based gene replacement system, several new vectors were constructed (Fig. 1). Besides incorporating all the features of pEX100T, the vectors also contain a MCS in *lacZα* in two orientations with respect to *lacZpo*, each containing 10 unique restriction sites. To expand the use of the vectors to other bacteria where the Ap^R/Cb^R marker may not be applicable, derivatives were constructed that contain either Gm^R or Tc^R selectable markers.

To test the usefulness of these vectors for the introduction of unmarked mutant alleles into the *P. aeruginosa* chromosome, we decided to mutate *plcH*, encoding heat labile hemolysin, a phenotypic trait that can be easily scored on blood agar plates (Pritchard and Vasil, 1986). The same unmarked Δ*plcH* mutant allele was cloned into all pEX vectors, the recombinant plasmids were conjugated into PAO1 and Cb^R, Gm^R or Tc^R plasmid-integrants were selected. Sucrose^R selection yielded unmarked Δ*plcH* mutants at frequencies ranging from 5 to 25%, as indicated by the lack of zones of hemolysis on blood agar plates. Selected putative mutants were analyzed by colony PCR utilizing nested primers and all of these lacked the *plcH* coding sequence (data not shown).

3.2. Design of an FRT cassette vector and construction of a Gm^R selectable FRT cassette

The recently described *FRT* cassettes (Cherepanov and Wackernagel, 1995) were not useful in *P. aeruginosa* for various reasons. First, the Km^R cassette was not useful because of the high intrinsic resistance of *P. aeruginosa* to Km. Second, the Tn*10*-derived Tc^R cassette, although potentially useful, does confer Tc^R only when present in single copy or in a few copies per cell. Thus, insertions of this cassette into multicopy plasmids cannot be monitored by Tc^R. In addition, both of these cassettes contain redundant DNA sequences, and they cannot be easily isolated due to a lack of duplicated flanking restriction sites.

Our goals, therefore, were to develop an *FRT* cassette vector that (1) would allow easy excision of the cassette from its vector and (2) would contain a basic *FRT* cassette possessing unique restriction sites for insertion of desired marker genes, thus allowing construction of customized *FRT* cassettes. To do this, pPS854 (Fig. 2A) was constructed as detailed in Materials and methods (Section 2.3) and in Table 1. This plasmid contains the *FRT* sites flanked, in inverted order, by unique recognition sites for eight enzymes that can be utilized to liberate the *FRT* cassette from the vector backbone. The region separating the *FRT* sites (68 bp) contains unique *Eco*RI and *Eco*RV restriction sites, separated by 2 bp (Fig. 2B). These two sites facilitate the construction of customized *FRT* cassettes by insertion of selectable and/or screenable markers, or addition of other desirable features, e.g. polystop codons or transcription termination/initiation sequences. The *FRT* cassette can be easily excised from its vector since the two *FRT* sites are flanked, in inverted order, by unique *Sac*I, *Kpn*I, *Sma*I, *Bam*HI, *Sal*I, *Pst*I, *Sph*I and *Hin*dIII sites.

This *FRT* cassette vector was then used to construct pPS858 (Section 2.3; Fig. 2C). Plasmid pPS858 carries a *FRT* cassette containing the selectable Gm^R marker and the screenable GFP; the GFP gene is transcribed from the *aacC1* promoter. It should be noted that although the GFP marker has proved useful to monitor loss of the entire Gm^R-*GFP* cassette in *E. coli*, its use in *P. aeruginosa* may be limited to cells grown under conditions where the production of endogenous fluorescent pigments is restricted, e.g. in the presence of high concentrations of iron. It did not prove to be useful for the experiments described in this study due to the intense fluorescence of *P. aeruginosa* cells grown on VBMM medium. Alternatively, the *FRT* cassettes could be equipped with the widely applicable *xylE* screenable marker (Schweizer, 1993b).

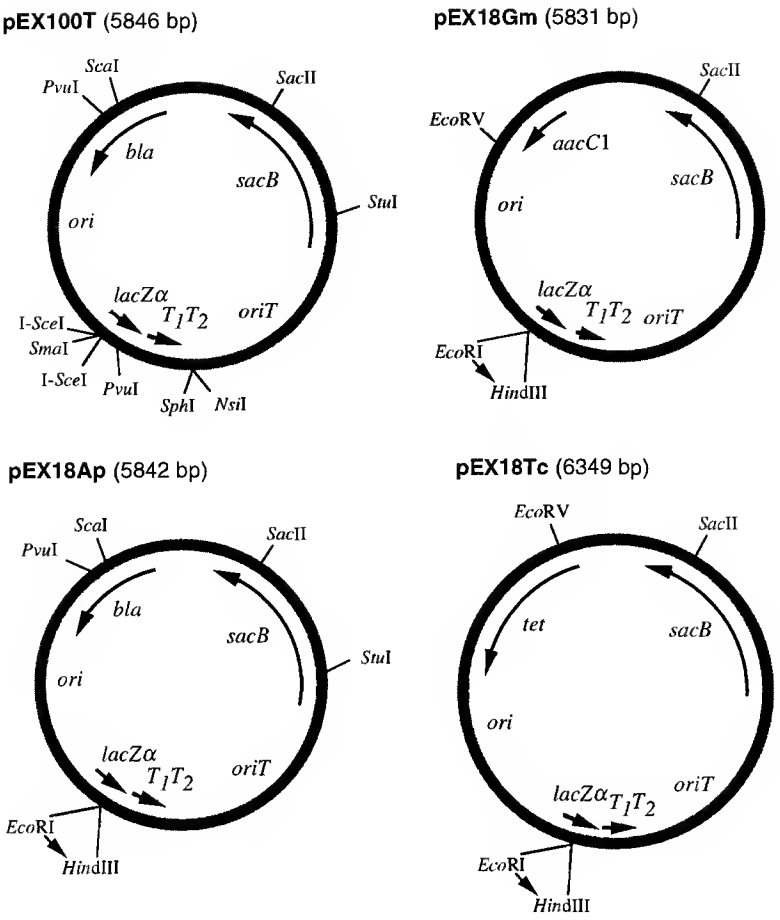

Fig. 1. Maps of gene replacement vectors. Plasmids are drawn to scale. The locations of genes and their transcriptional orientations are shown, including the double transcriptional terminators T_1 and T_2, and 5S rRNA gene from *E. coli*. The restriction sites of the MCS in all plasmids, in counterclockwise order, are: *Eco*RI–*Sac*I–*Kpn*I–*Sma*I–*Bam*HI–*Xba*I–*Sal*I–*Pst*I–*Sph*I–*Hin*dIII. In the corresponding pEX19Ap, pEX19Gm, and pEX19Tc vectors, the order of the sites of the MCS is reversed. The nt sequences of pEX100T, pEX18Ap, pEX18Gm and pEX18Tc were deposited in GenBank and were assigned the Accession Nos U17500, AF004910, AF047518, and AF047519, respectively.

3.3. Construction of a bhr Flp recombinase-producing plasmid

None of the hitherto available Flp recombinase-producing vectors was either mobilizable or able to replicate in bacteria other than *E. coli*, thus necessating the construction of such vectors.

Since some recombinases are sufficiently active to promote excision when transiently expressed in the bacterium of interest from a non-replicative, mobilizable plasmid (Kristensen et al., 1995), we first constructed pFLP1 (Table 1). This plasmid contains the recombinase structural gene, *FLP*, under transcriptional control of the strong but regulatable rightward λ promoter, λp_R. In addition, *FLP* is fused to the initiation codon of the *cro* structural gene, encoding the efficiently translated λ Cro antirepressor. Since the insert also contains cI_{857}, the gene encoding the thermo-labile λ repressor, all the elements required for efficient and regulated transcription, and translation of Flp are present (Cox, 1983). When transformed into *E. coli* mobilizer strain SM10, pFLP1 was efficiently transferred between *E. coli* strains. However, when utilizing this plasmid in excision experiments from the *P. aeruginosa* chromosome, we observed excision of the *FRT* cassette only at very low frequencies (0.5–1%) (Schweizer, 1998). Although the exact reasons for this observation remain unknown, it was presumably because in the absence of any selective pressure, we could not control the number of recipient cells that temporarily received the Flp-producing, non-replicative pFLP1. Since changes of various parameters known to effect conjugation efficiencies, e.g. time of conjugation, growth rate of bacteria, media composition, etc., did not lead to marked and consistent improvements of excision frequencies, we decided to construct pFLP2 (Fig. 3). This replicative bhr plasmid contains the Flp-expressing cassette from pMMC6, is mobilizable and is curable from its host by sucrose^R selection since it carries the counterselectable *sacB* marker. Its use and effectiveness are described in the next paragraph.

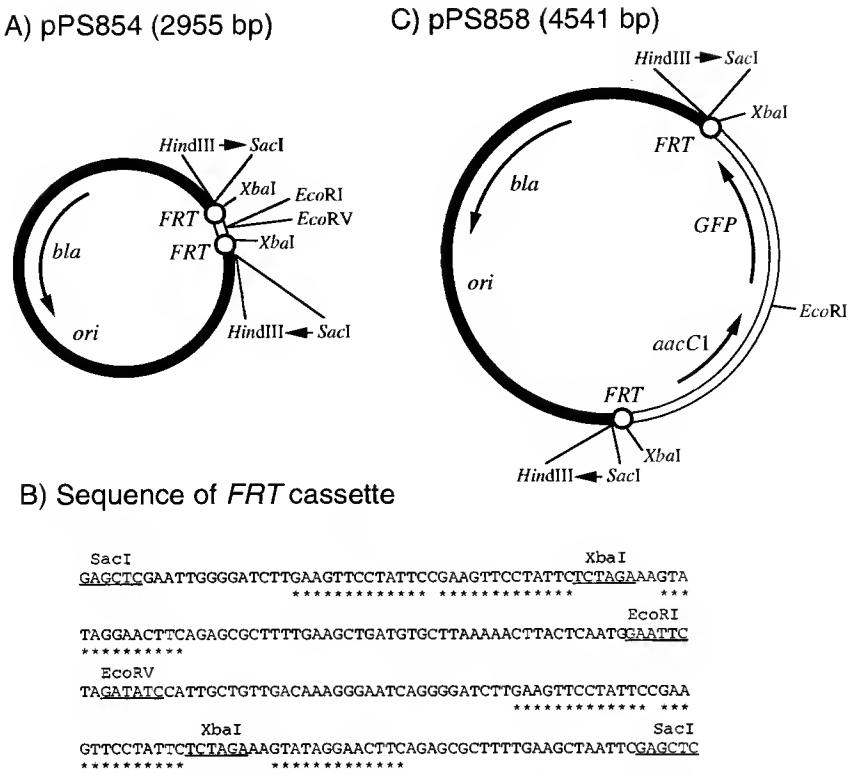

Fig. 2. Physical maps of *FRT* cassette vectors and sequence of *FRT* cassette. Plasmids are drawn to scale. (**A**) The basic *FRT* cassette vector pPS854 was derived as described in Section 2.3. The locations of selected restriction enzyme cleavage sites and genes are shown. (**B**) Nt sequence of the region located between the *Sac*I sites of pPS854. Asterisks underline the *FRT* sequences. (**C**) pPS858 was derived from pPS854 by insertion of the Gm^R determinant from pUCGM (Schweizer, 1993b) and the *GFP* from pPS747 (Table 1) into the *Eco*RI and *Eco*RV sites, respectively. *Hin*dIII→*Sac*I, *Hin*dIII–*Sph*I–*Pst*I–*Sal*I–*Xba*I–*Bam*HI–*Sma*I–*Kpn*I–*Sac*I.

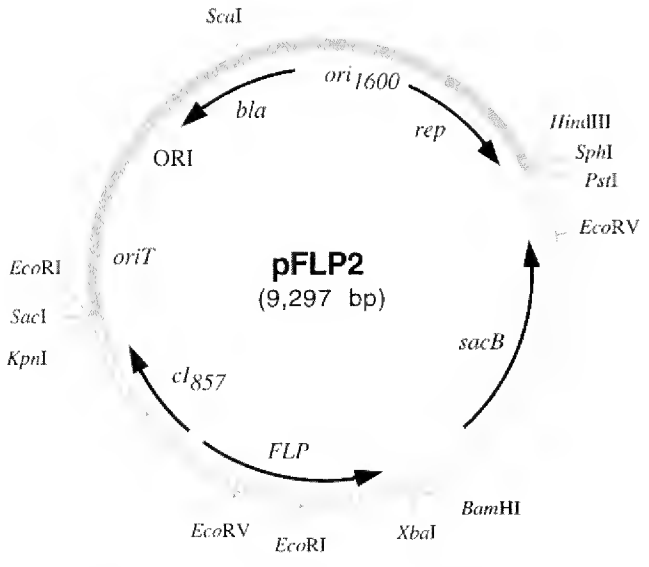

Fig. 3. Physical map of the bhr Flp vector pFLP2. Only selected restriction enzyme cleavage sites are shown. Expression of *FLP* is driven by the strong, rightward λ promoter (located in the *FLP*-cI_{857} intergenic region) and is regulated by the Ts, cI_{857}-encoded λ repressor. Efficient Flp translation is achieved by its fusion to the λCro ATG initiation codon (Cox, 1983). The nt sequence of pFLP2 was deposited in GenBank and was assigned the Accession No. AF048702.

3.4. *Isolation of an unmarked* P. aeruginosa *ΔpabC mutant*

To examine the usefulness of the tools described in this study, we decided to isolate an unmarked Δ*pabC* mutant. The putative *P. aeruginosa pabC* gene is one of the genes delimiting a fatty acid biosynthetic gene cluster that is currently being studied in our laboratory (unpublished results). In *E. coli*, the *pabC* gene product, aminodeoxychorismate lyase, is required for PABA synthesis, and *pabC* mutants are PABA auxotrophs (Green et al., 1992). As is the case in *E. coli*, the *P. aeruginosa pabC* gene lies next to a gene (*orf*) that encodes a putative protein of unknown function (Fig. 4A) and whose inactivation in *E. coli* did not result in a detectable phenotype (Green et al., 1992).

A defined pPS955-borne Δ(*pabC-orf*) was constructed as described in Table 1, and the deletion was returned to the *P. aeruginosa* chromosome as illustrated in Fig. 4A. After conjugal transfer of the non-replicative pPS955 from *E. coli* SM10 into PAO1, merodiploids were obtained by selecting Gm^R. From these, colonies having undergone Δ1 were selected as $sucrose^R$, Gm^R and Cb^R. The unmarked Δ(*pabC-orf*) mutant PAO206 was then derived from the Gm^R-*GFP* integrant PAO205

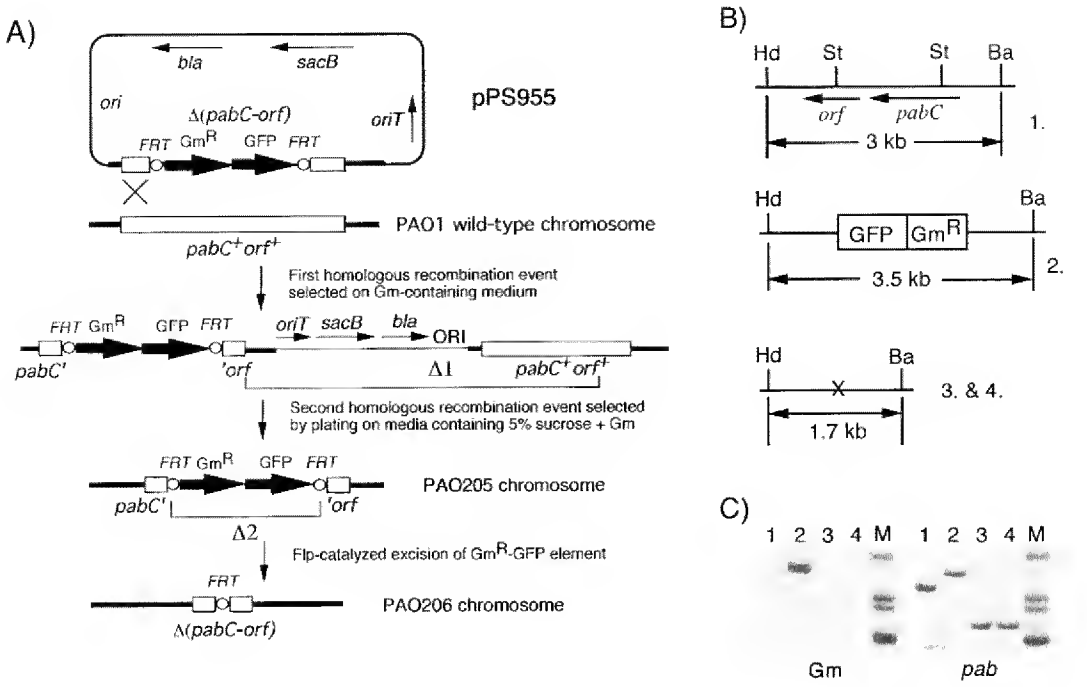

Fig. 4. Strategy for isolation of an unmarked Δ(*pabC-orf*) mutation. (**A**) For gene replacement, the previously described *sacB*-based strategy (Schweizer and Hoang, 1995) was employed, as detailed in Section 2.4. Colonies having undergone Δ1 were screened as sucrose^R, Gm^R and Cb^S. The unmarked Δ(*pabC-orf*) mutant was then derived from the Gm^R-*GFP* integrant by Flp-catalyzed excision (Δ2) of the Gm^R-*GFP* markers. The *orf* indicates a *P. aeruginosa* gene of unknown function. (**B**) Genomic organization of the PAO1 *pabC*$^+$-*orf*$^+$ region (1) and of Δ(*pabC-orf*) mutants PAO205 (2) and PAO206 (isolates 3 and 4). The relative positions of *Bam*HI (Ba) and *Hin*dIII (Hd) sites, as well as the lengths of *Bam*HI–*Hin*dIII fragments expected after digestion of the respective chromosomal DNAs are shown. The *Stu*I (St) sites shown in (1) delimit the Δ(*pabC-orf*) mutation, and the X in (3 and 4) marks the position of the *FRT* sequence in the unmarked Δ(*pabC-orf*) strain. (**C**) Genomic Southern analysis. Nylon membranes containing electrophoretically separated genomic DNA fragments from the isolates depicted in panel *B* were probed either with a biotinylated DNA *pabC-orf* fragment (panel labeled *pab*) or with a *aacC*1 fragment (panel labeled Gm), as described in Materials and methods. DNA in lanes 1, 2, 3 and 4 corresponds to *Bam*HI–*Hin*dIII fragments from the strains shown in (B). Lane M shows (top to bottom) biotinylated λ *Hin*dIII (4.3, 2.4, and 2.04-kb) markers and a biotinylated 1.35-kb ϕX *Hae*III marker.

by Flp-catalyzed excision of the Gm^R-*GFP* markers. During its expression in the recipient, Flp recombinase acted at the *FRT* sites to catalyze excision of the Gm^R-*GFP* element (marked with Δ2) at very high frequencies (all 20 colonies tested were Gm^S), leaving behind a short *FRT*-containing sequence. It should be noted that although Flp production from pFLP2 is under control of the temperature-labile λ repressor (Cox, 1983), complete excision was observed even at 30°C, corroborating similar observations previously made by Cherepanov and Wackernagel (1995). The pFLP2 vector was efficiently cured from the Gm^S cells by sucrose selection; all 20 of the Gm^S colonies tested had lost the plasmid as indicated by their Cb^S phenotypes and absence of DNA in plasmid mini-preps. Since basal levels of Flp expression seemed sufficient for complete excision, all steps involved in the excision process, i.e. conjugal transfer of pFLP2 and selection of Cb^R exconjugants, were performed at 37°C.

Successful execution of the steps labeled Δ1 and Δ2 in Fig. 4A was monitored by colony PCR analysis utilizing *aacC*1-specific primers, as detailed in Section 2.4. All four PAO205 colonies analyzed showed a single fragment of ~550 bp, which was absent from the parental strain PAO1 and two isolates of the putative PAO206 excision mutants (data not shown). To further verify the genetic make up of the the putative unmarked Δ(*pabC-orf*) mutants, a genomic Southern analysis was performed (Fig. 4B and C). From the results presented in Fig. 4C, it is evident that both deletion events produced the desired restriction patterns. Probing with a *pabC-orf* specific probe (panel labeled *pab*) revealed deletion of a 1.3-kb region from the PAO1 wt chromosome in both the Δ(*pabC-orf*)::Gm^R-*GFP* insertion mutant PAO205 (lane 2) and the unmarked Δ(*pabC-orf*) mutant PAO206 (lanes 3 and 4). The size of the 3-kb *Bam*HI–*Hin*dIII fragment observed in wt PAO1 (lane 1) was increased to a 3.5-kb fragment (3-kb minus 1.3-kb genomic DNA plus 1.8-kb Gm^R-*GFP* fragment) (lane 2) in the insertion mutant PAO205, and reduced to 1.7 kb (lanes 3 and 4) in the unmarked deletion mutant PAO206. Probing with a *aacC*1-specific probe (panel labeled Gm) revealed the presence of the 1.8-kb Gm^R-*GFP* FRT cassette only in the Δ(*pabC-orf*)::Gm^R-*GFP* insertion mutant PAO205 on a 3.5-kb *Bam*HI–*Hin*dIII fragment (lane 2). As expected,

the *aacC1* sequences were absent from wt PAO1 genomic DNA (lane 1), and they were deleted from the excision mutant PAO206 (lanes 3 and 4).

3.5. *Isolation of other mutations in* P. aeruginosa *and* E. coli

Clearly, the efficiency and adaptability of the procedure make it ideal for routine isolation of unmarked chromosomal mutants in various bacteria. To date, utilizing the gene replacement vectors and strategies described above, we have utilized it for isolation of unmarked *P. aeruginosa* Δ(*pabC-orf*) (this study), Δ*asd* (Hoang et al., 1997) and Δ(*mexAB-oprM*) (Schweizer, 1998) mutants. The same procedure was also utilized for construction of an unmarked *E. coli* Δ*asd* mutant strain (our unpublished data), except that a plasmid with a Ts *ori* was utilized as the suicide delivery vector.

4. Conclusions

(1) This paper describes an efficient procedure for isolation of unmarked mutant alleles in the *P. aeruginosa* chromosome, utilizing a combination of versatile gene replacement vectors and a bhr version of the *S. cerevisiae* Flp-*FRT* recombination system. With a few modifications, the method is also applicable in other bacteria, e.g. *E. coli*.

(2) Supporting this system are several new mobilizable gene replacement vectors. They contain the MCS and the *lacZα* from the popular pUC18/19 cloning vectors and facilitate the cloning and manipulation of DNA fragments, followed by their transfer into the *P. aeruginosa* chromosome. Since they are available with Ap (Cb), Gm and Tc selectable markers, they will be applicable in a wide range of bacteria.

(3) A versatile *FRT* cassette vector was constructed. This high copy number, pUC-based vector contains unique *Eco*RI and *Eco*RV restriction sites flanked by two *FRT* sites. Based on this vector, a *FRT* cassette was constructed that provides a Gm^R selectable and a GFP screenable marker. In concert with a newly constructed Flp recombinase-expressing bhr vector, several unmarked *P. aeruginosa* mutants, as well as an unmarked *E. coli* mutant, were constructed.

(4) The technique described in this paper provides a method for gene replacement/in-vivo excision that complements existing, similar techniques (Ayres et al., 1993; Kristensen et al., 1995) but has the added advantage that the Flp-*FRT* system is functional in all bacterial systems studied to date.

(5) In bacteria, such as the pseudomonads, that exhibit a high intrinsic resistance to many antibiotics, one could envision employing a single *FRT* cassette with a workable selectable marker for isolation of consecutive chromosomal mutations in the same strain. The only possible drawback to such an approach may be that recombination between *FRT* sites placed in the same chromosome could lead to a deletion or inversion of a large chromosomal segment, depending on the orientation of the *FRT* sites and the distance between them (Wild et al., 1996). Although such large rearrangements are unlikely, especially when selecting mutants on minimal media, it is advisable when integrating a cassette into a second gene in the same host to place the second cassette in the same orientation as the first. With the advent of genome sequencing, such experiments will be possible, and optimized *FRT* cassettes will be valuable tools for micro- and macro-manipulations of entire bacterial chromosomes (Wild et al., 1996).

Acknowledgement

This work was supported by a grant from the Research Council of the College of Veterinary Medicine and Biomedical Sciences at Colorado State University and, in part, by start up funds from the Department of Microbiology. We wish to thank Dr W. Wackernagel, University of Oldenburg, and Dr M.L. Vasil, University of Colorado Health Sciences Center, for the provision of bacterial plasmids.

References

Ayres, E.K., Thomson, V.J., Merino, G., Balderes, D., Figurski, D., 1993. Precise deletions in large bacterial genomes by vector-mediated excision (VEX): the *trfA* gene of promiscous plasmi RK2 is essential for replication in several Gram-negative hosts. J. Mol. Biol. 230, 174–185.

Camilli, A., Beattie, D.T., Mekalanos, J., 1994. Use of genetic recombination as a reporter of gene expression. Proc. Natl. Acad. Sci. USA 91, 2634–2638.

Cherepanov, P.P., Wackernagel, W., 1995. Gene disruption in *Escherichia coli*: Tc^R and Km^R cassettes with the option of Flp-catalyzed excision of the antibiotic-resistance determinant. Gene 158, 9–14.

Cormack, B., Valdivia, R., Falkow, S., 1996. FACS-optimized mutants of the green fluorescent protein (GFP). Gene 173, 33–38.

Cox, M.M., 1983. The FLP protein of the yeast 2-μm plasmid: expression of a eukaryotic genetic recombination system in *Escherichia coli*. Proc. Natl. Acad. Sci. USA 80, 4223–4227.

De Lorenzo, V., 1994. Designing microbial systems for gene expression in the field. Trends Biotechnol. 12, 365–371.

De Lorenzo, V., Timmis, K.N., 1994. Analysis and construction of stable phenotypes in Gram-negative bacteria with Tn*5* and Tn*10*-derived transposons. Meth. Enzymol. 235, 386–405.

Dymecki, S.M., 1996. A modular set of Flp, FRT and *lacZ* fusion vectors for manipulating genes by site-specific recombination. Gene 171, 197–201.

Green, J.M., Merkel, W.K., Nichols, B.P., 1992. Characterization and sequence of *Escherichia coli pabC*, the gene encoding aminodeox-

ychorismate lyase, a pyridoxal phosphate-containing enzyme. J. Bacteriol. 174, 5317–5323.

Hoang, T., Williams, S., Schweizer, H.P., 1997. Molecular genetic analysis of the region containing the essential *Pseudomonas aeruginosa asd* gene encoding aspartate-β-semialdehyde dehydrogenase. Microbiology 143, 899–907.

Hoang, T.T., Schweizer, H.P., Fatty acid biosynthesis in *Pseudomonas aeruginosa*: cloning and characterization of the *fabAB* operon encoding β-hydroxydecanoyl-acyl carrier protein dehydratase (FabA) and β-ketoacyl-acyl carrier protein synthase I (FabB). 1997. J. Bacteriol. 179, 5326–5332.

Kristensen, C.S., Eberl, L., Sanchez-Romero, J.M., Givskov, M., Molin, S., De Lorenzo, V., 1995. Site-specific deletions of chromosomally located DNA segments with the multimer resolution system of broad-host-range plasmid RP4. J. Bacteriol. 177, 52–58.

Lyznik, L.A., Rao, K.V., Hodges, T.K., 1996. Flp-mediated recombination of FRT sites in the maize genome. Nucleic Acids Res. 24, 3784–3789.

Miller, J.H., A Short Course in Bacterial Genetics, Cold Spring Harbor Laboratory Press, Cold Spring Harbor, NY, 1992.

Pritchard, A.E., Vasil, M.L., 1986. Nucleotide sequence and expression of a phosphate-regulated gene encoding a secreted hemolysin of *Pseudomonas aeruginosa*. J. Bacteriol. 167, 291–298.

Sadowski, P., 1995. The Flp recombinase of the 2-microns plasmid of *Saccharomyces cerevisiae*. Prog. Nucleic Acids Res. Mol. Biol. 51, 53–91.

Sambrook, J., Fritsch, E.F., Maniatis, T., Molecular Cloning. A Laboratory Manual, Cold Spring Harbor Laboratory Press, Cold Spring Harbor, NY, 1989.

Schweizer, H.P., 1992. Allelic exchange in *Pseudomonas aeruginosa* using novel ColE1-type vectors and a family of cassettes containing a portable *oriT* and the counter-selectable *Bacillus subtilis sacB* marker. Mol. Microbiol. 6, 1195–1204.

Schweizer, H.P., 1993a. Small broad-host-range gentamycin resistance cassettes for site-specific insertion and deletion mutagenesis. BioTechniques 15, 831–833.

Schweizer, H.P., 1993b. Two plasmids, X1918 and Z1918, for easy recovery of the *xylE* and *lacZ* reporter genes. Gene 134, 89–91.

Schweizer, H.P., Hoang, T., 1995. An improved system for gene replacement and *xylE* fusion analysis in *Pseudomonas aeruginosa*. Gene 158, 15–22.

Schweizer, H.P., Klassen, T.R., Hoang, T., Improved methods for gene analysis and expression in *Pseudomonas*. In: Nakazawa, T., Furukawa, K., Haas, D., Silver, S. (Eds.), Molecular Biology of Pseudomonads. American Society for Microbiology, Washington, DC, 1996, pp. 229–237.

Schweizer, H.P., Intrinsic resistance to inhibitors of fatty acid biosynthesis in *Pseudomonas aeruginosa* is due to efflux: application of a novel technique for generation of unmarked chromosomal mutations for the study of efflux systems. 1998. Antimicrob. Agents Chemother. 42, 394–398.

Sternberg, N., Hamilton, D., Hoess, R., 1981. Bacteriophage P1 site-specific recombination. II. Recombination between *loxP* and the bacterial chromosome. J. Mol. Biol. 150, 487–507.

Wild, J., Hradecna, Z., Posfai, G., Szybalski, W., 1996. A broad-host-range in vivo pop-out and amplification system for generating large quantities of 50–100-kb genomic fragments for direct DNA sequencing. Gene 179, 181–188.

Yanisch-Perron, C., Vieira, J., Messing, J., 1985. Improved M13 cloning vectors and host strains: nucleotide sequences of the M13mp18 and pUC19 vectors. Gene 33, 103–119.

EXHIBIT 4

Disruption of neural signal transducer and activator of transcription 3 causes obesity, diabetes, infertility, and thermal dysregulation

Qian Gao*†‡, Michael J. Wolfgang*†, Susanne Neschen§, Katsutaro Morino§, Tamas L. Horvath¶, Gerald I. Shulman§‖, and Xin-Yuan Fu*,**

Departments of *Pathology and §Internal Medicine and Cellular and Molecular Physiology and ¶Department of Obstetrics and Gynecology and Reproductive Science and ‖Howard Hughes Medical Institute, Yale University School of Medicine, New Haven, CT 06520

Edited by Jeffrey M. Friedman, The Rockefeller University, New York, NY, and approved January 21, 2004 (received for review June 26, 2003)

Signal transducer and activator of transcription (STAT)3 is widely expressed in the CNS during development and adulthood. STAT3 has been implicated in the control of neuron/glial differentiation and leptin-mediated energy homeostasis, but the physiological role and degree of involvement of STAT3 in these processes is not defined and controversial because of the lack of a direct genetic model. To address this, we created mice with a neural-specific disruption of STAT3 ($STAT3^{N-/-}$). Surprisingly, homozygous mutants were born at the expected Mendelian ratio without apparent developmental abnormalities but susceptible to neonatal lethality. Mutants that survived the neonatal period were hyperphagic, obese, diabetic, and infertile. Administering a melanocortin-3/4 receptor agonist abrogated the hyperphagia and hypothalamic immunohistochemistry showed a marked reduction in proopiomelanocortin with an increase in neuropeptide Y and agouti-related protein. Mutants had reduced energy expenditure and became hypothermic after fasting or cold stress. $STAT3^{N-/-}$ mice are hyperleptinemic, suggesting a leptin-resistant condition. Concomitant with neuroendocrine defects such as decreased linear growth and infertility with accompanying increased corticosterone levels, this CNS knockout recapitulates the unique phenotype of *db/db* and *ob/ob* obese models and distinguishes them from other genetic models of obesity. Thus, STAT3 in the CNS plays essential roles in the regulation of energy homeostasis and reproduction.

Signal transducer and activator of transcription (STAT) proteins are a group of cytokine-activated signaling molecules that can directly bind to DNA and activate or repress transcription of target genes. A myriad of cytokines activate STAT proteins through receptor-associated kinases. Activation of STATs occurs through tyrosine phosphorylation that is required for SH2 domain-mediated dimerization and DNA binding. Most STAT proteins have specific effects, but STAT3, the most ancient STAT, is broadly expressed and activated by a diverse array of cytokines and stresses (1–3). It was initially described as an acute phase protein involved in various biological and pathological processes. STAT3 deletion causes embryonic lethality before gastrulation via an unknown mechanism (4). STAT3 has unusually pleiotropic effects regulating murine embryonic stem cell maintenance (5), macrophage function (6, 7), immune regulation (8), and peripheral neuron survival after axotomy (9, 10) among others.

In the CNS, STAT3 is expressed during embryonic development, mostly at ventricular areas, where neuronal proliferation and differentiation take place. Consistently, STAT3 is strongly suggested by *in vitro* studies to play an instructive role in glial and neuron differentiation (11–14). In adults, STAT3 has long been implicated in the regulation of energy homeostasis through the fat-derived cytokine leptin. Although leptin can activate several STAT proteins, including STAT3, 5, and 6, *in vitro* (15), only STAT3 is activated in the hypothalamus *in vivo* upon leptin administration (16, 17). These data strongly suggest that STAT3 plays a role in leptin mediated energy balance.

Leptin regulates energy homeostasis and physiology by affecting diverse functions such as food intake, energy expenditure, and reproduction (18) through distinct proopiomelanocortin (POMC)- and neuropeptide Y (NPY)-related neuronal circuitry in hypothalamic nuclei (19, 20). Activation of STAT3 in response to leptin within the hypothalamus can be detected in both networks that mediate anorexogenic (POMC and CART) and orexogenic [NYP and agouti-related protein (AgRP)] physiology. Leptin signaling down-regulates NPY/AgRP and up-regulates POMC/CART neurons, thus limiting food intake and signaling peripheral energy stores. The biological evidence supporting a major role for STAT3 in energy homeostasis comes from the weight reducing effects of other STAT3 activating cytokines such as IL-6 (21) and ciliary neurotrophic factor (22), and leptin receptor point mutations (23), However, no direct test of STAT3 function in energy homeostasis has been conducted.

Multiple signaling pathways are activated by ligand activation of the leptin receptor including mitogen-activated protein kinase (24) and phosphatidylinositol 3-kinase (25, 26), which has been shown to control feeding. In addition, immediate electrical changes can be detected in hypothalamic neurons after leptin administration in a manner not amendable to transcriptional modification (27, 28). Other signals, such as insulin (29, 30) and long chain fatty acid (31, 32), can also affect energy metabolism through hypothalamic neuronal circuitry. This raises questions on the role and degree of involvement of STAT3 in leptin function. To address (*i*) the participation of STAT3 in the CNS and (*ii*) the degree to which STAT3 is involved in energy homeostasis, we generated a neural-specific deletion of STAT3 by using gene targeting to create a conditional STAT3 allele. We found that STAT3 can account for all of the essential effects of leptin action on energy balance and neuroendocrinology because neural STAT3 mutant mice recapitulate leptin receptor (*db/db*) and ligand deficiency (*ob/ob*).

Methods

Animals. Generation of mice with a conditional knockout (KO) of STAT3 has been described (7). Exons 18–20, which contain the SH2 domain of STAT3, were flanked by two lox P sites. Nestin-Cre transgenic mice [The Jackson Laboratory mice database: B6.Cg(SJL)-TgN(Nes-cre)IKln] expressing Cre under the control of a rat nestin promoter/enhancer were described (34). The Nestin-Cre;$STAT3^{f/f}$ mutant mice, designated as

This paper was submitted directly (Track II) to the PNAS office.

Abbreviations: STAT, signal transducer and activator of transcription; POMC, proopiomelanocortin; KO, knockout; NPY, neuropeptide Y; AgRP, agouti-related protein.

†Q.G. and M.J.W. contributed equally to this work.

‡Present address: Department of Obstetrics and Gynecology, Yale University School of Medicine, New Haven, CT 06511.

**To whom correspondence should be addressed. E-mail: xin-yuan.fu@yale.edu.

NEUROSCIENCE

$STAT3^{N-/-}$, were generated through Nestin-Cre;$STAT3^{f/+}$ mice crossed to $STAT3^{f/f}$ mice. The genotype was determined by PCR as described (7). All experiments were done in a C57BL/6 background. All procedures were performed in accordance with the National Institutes of Health Guide for the Care and Use of Laboratory Animals and under the approval of the Yale Medical School Animal Care and Use Committee.

Immunoblotting. Immunoblotting was done as described with an anti-STAT3 or anti-STAT1 Ab (Santa Cruz Biotechnology) (33). Next, a horseradish peroxidase-conjugated secondary anti-rabbit Ab was used and visualized by using SuperSignal chemi-illuminescent substrate (Pierce).

Histological Analysis. Tissue was collected and fixed in 4% paraformaldehyde for 4 h, then snap frozen in OCT, and sectioned or paraffin embedded. Frozen sections (10 μm) were cut, washed in PBS, and stained with hematoxylin and eosin by using standard techniques. Immunohistochemistry was performed by using anti-β-endorphin for POMC neurons (Chemicon) 1:5,000, anti-AgRP (Calbiochem) 1:5,000, and anti-NPY (Peninsula Laboratories) 1:10,000 by using standard techniques.

Plasma Parameters. Blood samples were taken from cut tailtips of conscious mice either in the fasting (≈14 h) or fed state at 1000 hours. Plasma was collected for measurement of glucose (glucose oxidase method; Analyzer 2, Beckman Coulter), insulin (double Ab RIA, Linco Research Immunoassay, St. Charles, MO), leptin (RIA, Linco Research Immunoassay), corticosterone (double Ab RIA, ICN), triglycerides (enzymatic method, Sigma), and nonesterified fatty acids (enzymatic method, NEFA-C, Wako Pure Chemicals, Osaka).

Glucose Tolerance Test. The i.p. glucose tolerance tests were performed. After 14 h of fasting, mice received a single i.p. injection of 20% glucose solution (1 g/kg), time 0. Plasma samples for glucose and insulin measurement were taken at −30, 15, 30, 60, and 120 min from cut tailtips.

Results

Neural-Specific STAT3 Deletion Results in Severe Obesity. To study the physiological role of STAT3 in the brain, we generated a neural-specific deletion of STAT3 by using gene targeting to create a conditional STAT3 allele. We initially generated a floxed STAT3 allele (7) that was mated to a rat nestin-Cre transgenic mouse (34) to generate a neural-specific STAT3 deletion. The rat nestin-Cre transgene expresses cre-recombinase in neuroepithelium as early as embryonic day 10.5 (29, 35) and yields a broad neural deletion of STAT3 in the brain as measured by immunoblotting (Fig. 1*a*), but not in other organs, such as liver and pancreas (data not shown). Embryonic day 14.5 fibroblast growth factor 2-responsive neurospheres derived from $STAT3^{N-/-}$ forebrain exhibited no detectible STAT3, supporting a complete deletion of STAT3 in early neuronal precursors (data not shown). To our surprise, $STAT3^{N-/-}$ mice were born alive at the expected Mendelian ratio with no apparent developmental abnormalities although STAT3 has been implicated in the control of gliogenesis (11, 12). They appeared to locomote and suckle normally but were susceptible to neonatal lethality. Upon necropsy, these pups were found to contain dramatically reduced milk in their stomachs. Reducing pup numbers to lower the competition for milk and to minimize neonatal stress was able to rescue a substantial proportion of the mutants.

The $STAT3^{N-/-}$ animals that survived the neonatal period started to develop an obese phenotype ≈6–8 weeks of age (Fig. 1*b*) and weighed twice as much as their littermates at adulthood (Fig. 2*a*). The accumulated mass was nearly exclusively adipose

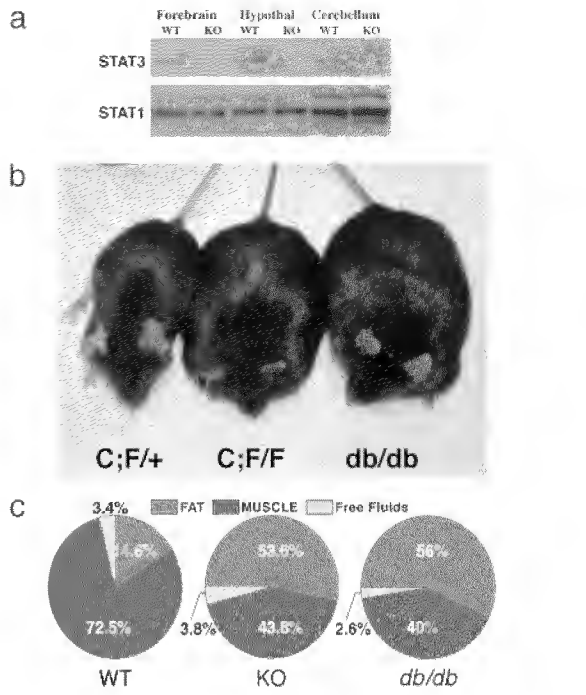

Fig. 1. Neural deletion of STAT3 results in severe obesity. (a) Western blot analysis of STAT3 in forebrain, hypothalamus, and cerebellum in WT and KO animals. The blot was stripped and reprobed with a STAT1 Ab as a control. (*b*) Heterozygous and obese homozygous Nestin-Cre; $STAT3^{f/f}$ ($STAT3^{N-/-}$) animals compared to a *db/db* mutant. (*c*) NMR imaging by using a minispec MQ10 analyzer (Bruker, Woodlands, TX) of WT, KO, and *db/db* animals ($n = 4$) showing total fat and lean mass as well as free fluid. Data are given as percentage of total body weight.

tissue revealed by a quantitative analysis of body composition done on live adults by using NMR imaging (minispec MQ10 analyzer). Total fat content of $STAT3^{N-/-}$ mice increased 5-fold compared to littermate controls to comprise >50% of their body weight, which is equal to the body composition of *db/db* mutants (Fig. 1*c*). In contrast, lean mass expressed as absolute weight was unchanged.

The livers of $STAT3^{N-/-}$ mice were severely enlarged with greatly increased fat deposits (Fig. 2 *c–e*) despite no local genetic defect of STAT3. In contrast, a hepatocyte-specific STAT3 KO under the same diet did not result in increased fat deposits in the liver (data not shown) consistent with selective KO of the leptin receptor (36). The restricted phenotypes resemble the dysfunction of hypothalamic leptin signaling, demonstrating STAT3 as a central and not peripheral mediator of energy homeostasis. No anatomical defects were detected in hypothalamic nuclei by histochemical analysis of serial brain sections in $STAT3^{N-/-}$ mice (data not shown).

CNS STAT3 Is Necessary for Satiety Signals. As with leptin receptor-deficient (*db/db*) mice, $STAT3^{N-/-}$ mice are hyperphagic (Fig. 2*b*) in a hyperleptinemic background (see Fig. 4*a*) reflecting the increased fat mass and block of leptin signaling. The hyperphagia is a consequence of an imbalance in anorexogenic and orexogenic neuropeptides due to the disruption of leptin signaling. Physiologically, leptin signaling up-regulates anorexogenic neuropeptides, including α-melanocyte-stimulating hormone, a cleavage product of POMC, which functions to inhibit food intake mainly through the G protein-coupled melanocortin-4 receptor (MC4R) (37). POMC was suggested to be a direct STAT3 downstream target gene (38). In both WT and leptin-signaling mutants, one i.p. injection of the MC3/4R agonist,

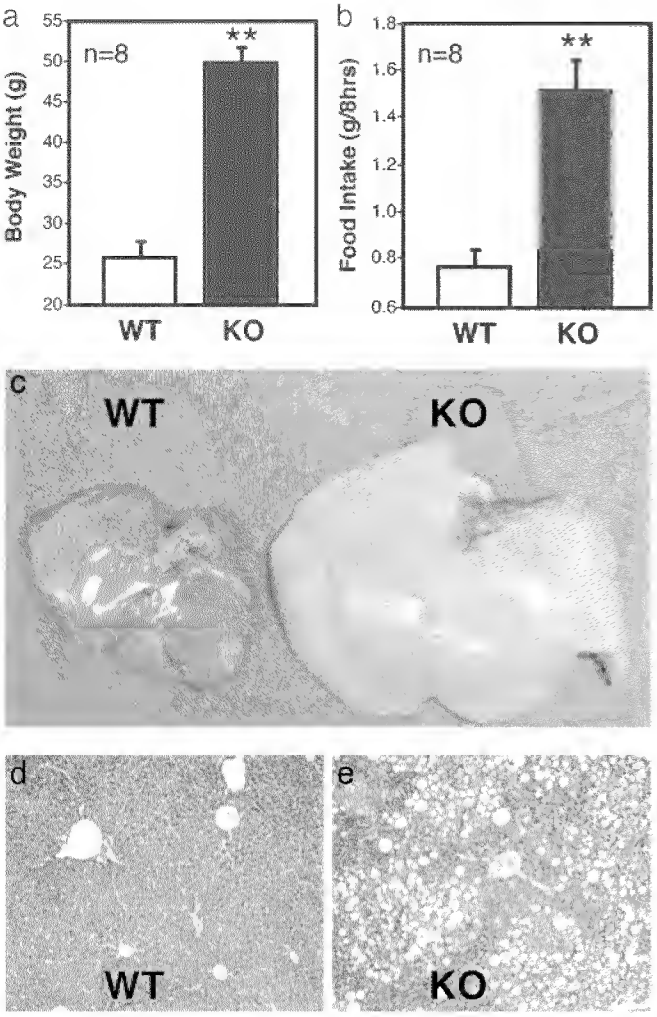

Fig. 2. Neural STAT3 deletion results in hyperphagia and fatty livers. $STAT3^{N-/-}$ animals are twice as heavy as WT animals (a) and consume twice as much food (*b*). Livers of KO animals are severely enlarged and fatty (*c*) and accumulated a large amount of fat (fatty liver) (*d* and e). (**, $P < 0.001$.)

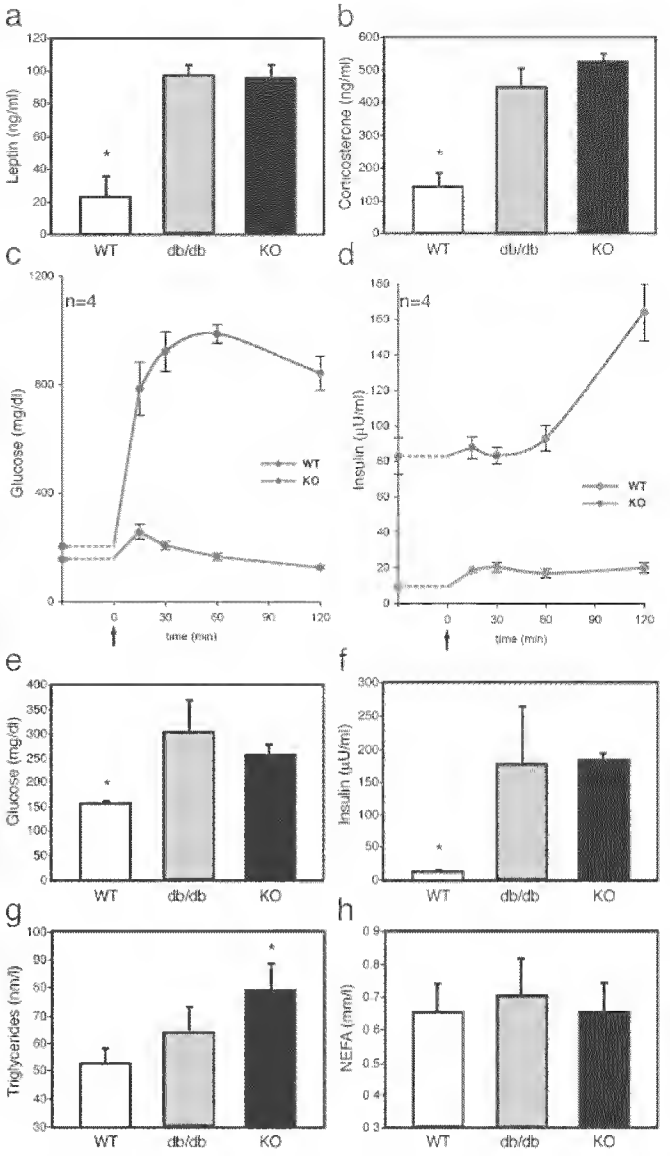

Fig. 4. $STAT3^{N-/-}$ animals are leptin-resistant and have increased corticosterone and glucose dysregulation. Leptin was increased significantly in $STAT3^{N-/-}$ and *db/db* animals (a), and corticosterone concentration was significantly increased as well (*b*). (*c* and *d*) Glucose tolerance tests were performed by measuring baseline glucose and insulin. Then an i.p. bolus of glucose (20%, 1 g/kg) was administered (arrow), and plasma was collected at the times indicated. (e and *f*) Fasting glucose and insulin were increased in $STAT3^{N-/-}$ and *db/db* animals. (*g*) Plasma triglycerides. (*h*) Nonesterified fatty acids. (*, $P < 0.005$.)

MTII (10 mg/kg), lowers food intake over a 4-h period (25, 39) and long-term application of MTII reverses obesity in *ob/ob* and *db/db* mice. MTII administration to $STAT3^{N-/-}$ mice completely reversed their hyperphagia over a 4-h period (Fig. 3). The food intake reduced to levels equal that of treated WT controls. This result suggests that the $STAT3^{N-/-}$ hyperphagia resulted from the down-regulation of anorexogenic peptides, consistent with studies of leptin-deficient mutants (40) as well as MC4R KO (39) and POMC KO (41). Moreover, plasma corticosterone levels were significantly elevated in $STAT3^{N-/-}$ mice (Fig. 4*b*), which is unique to *ob/ob* and *db/db* mutants but not to the other obese models (42). This further suggests a close genetic link between STAT3 and leptin signaling.

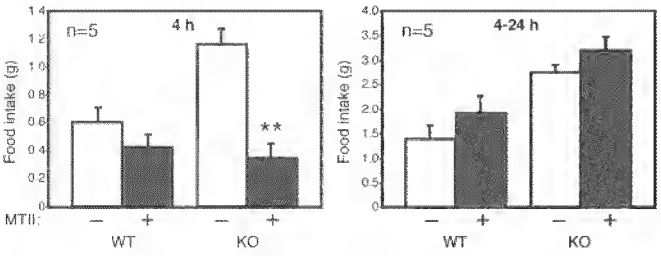

Fig. 3. Behavioral defects in $STAT3^{N-/-}$ animals are linked to a deficiency in the melanocortin system. Over a 4-h period, one i.p. administration of MTII (10 mg/kg) inhibits food intake in KO animals ($n = 5$) significantly over saline-injected controls. After 4 h, food intake returns to normal. (**, $P < 0.001$.)

$STAT3^{N-/-}$ Animals Are Diabetic. Glucose dysregulation and development of type 2 diabetes were evident in $STAT3^{N-/-}$ mice. Plasma fasting glucose concentrations in $STAT3^{N-/-}$ and *db/db* mice were equivalent and increased compared to littermates (Fig. 4*e*). The hyperglycemia was accompanied by severe hyperinsulinemia (Fig. 4*f*) in the $STAT3^{N-/-}$ animals. Plasma insulin concentrations were as much as 14- and 10-fold higher in the fed

and fasted state, respectively, suggesting severe insulin resistance. To characterize the dynamics of glucose metabolism with respect to insulin, we carried out a glucose tolerance test on fasted (14 h) animals. Basal glucose and insulin levels were measured before i.p. administration of a 20% glucose solution (1 g/kg). In $STAT3^{N-/-}$ mice, plasma glucose and insulin concentrations as measured by area under the curve (mg/dl/120 min) increased 5-fold after glucose challenge (glucose, $P < 0.0002$; insulin, $P < 0.003$) with a prolonged peak time. Basal insulin concentrations, which were 9- to 10-fold higher in mutants were not significantly induced by a dramatic increase of plasma glucose levels for the first hour but doubled during the second hour. In contrast, WT controls exhibited an immediate insulin induction (15 min, Fig. 4*d*) and a quick reduction of plasma glucose concentration. These observations revealed a severe alteration of the glucose/insulin dynamics in response to glucose challenge in $STAT3^{N-/-}$ animals. Plasma triglyceride but not nonesterified fatty acids were changed between groups probably indicating a peripheral effect of leptin (Fig. 4 *e* and *f*).

$STAT3^{N-/-}$ Animals Are Infertile with Reduced Linear Growth. Like *db/db* mutants, $STAT3^{N-/-}$ animals are infertile with accompanying hypogonadism in both male and female animals (Fig. 5 *a–c*). Heterozygous animals are fertile and both sexes were used for breeding resulting in normal litters. Fifteen $STAT3^{N-/-}$ animals (seven males and eight females) were housed with WT animals of the opposite sex with known fertility for 6–8 mo. No pregnancy was detected from any male or female $STAT3^{N-/-}$ mouse. Male $STAT3^{N-/-}$ animals showed a marked reduction in both testicular (Fig. 5*b*) and seminal vesicle size (Fig. 5*a*), whereas female $STAT3^{N-/-}$ mice showed a reduction in the size of the uterine horns (Fig. 5*c*). Normal gonadotropin-independent follicular development was observed in $STAT3^{N-/-}$ females, but corpa lutea were never observed indicating ovulation did not occur. This is consistent with the hypogonadotropic hypogonadism seen in leptin-deficient mice (43).

Moreover, the linear growth of $STAT3^{N-/-}$ mice as measured by snout-anus length was reduced (Fig. 5 *h* and *i*). Mutants are ≈8% shorter than their littermate controls, a level of reduction that is comparable with the linear growth reduction in *db/db* mice (≈5%). $STAT3^{N-/-}$ mice showed a marked reduction in POMC and an increase in NPY (Fig. 5 *d* and *e*) and AgRP (Fig. 5 *f* and *g*) by immunohistochemistry. Taken together, the $STAT3^{N-/-}$ model strongly argues a major role for STAT3-dependent leptin signaling in hypothalamic neuroendocrine function in reproduction and linear growth.

$STAT3^{N-/-}$ Animals Have Reduced Energy Expenditure. In leptin signaling mutant animals, both hyperphagia and lower energy expenditure contribute to their obese phenotype. To address this, we next asked whether $STAT3^{N-/-}$ mice had disrupted energy expenditure as measured by body temperature. In the fed state, $STAT3^{N-/-}$ animals showed a slightly but significantly lower body temperature (≈0.5°C) when compared with littermate controls suggesting a lower level of basal metabolism. Nevertheless, these animals were able to stabilize their body temperatures at a normal range by consuming twice as much food. After a 12-h fast, while littermate control mice maintained a normal body temperature, $STAT3^{N-/-}$ and *db/db* animals became significantly hypothermic as their body temperature dropped >4°C below normal (Fig. 6*a*), an effect that was reversed after 1.5 h of refeeding. Because body energy supply as measured by plasma glucose and fatty acid levels are not reduced during fast, these observations suggest that a constant feeding stimulation is essential for maintaining body temperature in the mutants.

The induction of body thermogenesis is controlled by the sympathetic nervous system in response to food or cold in brown

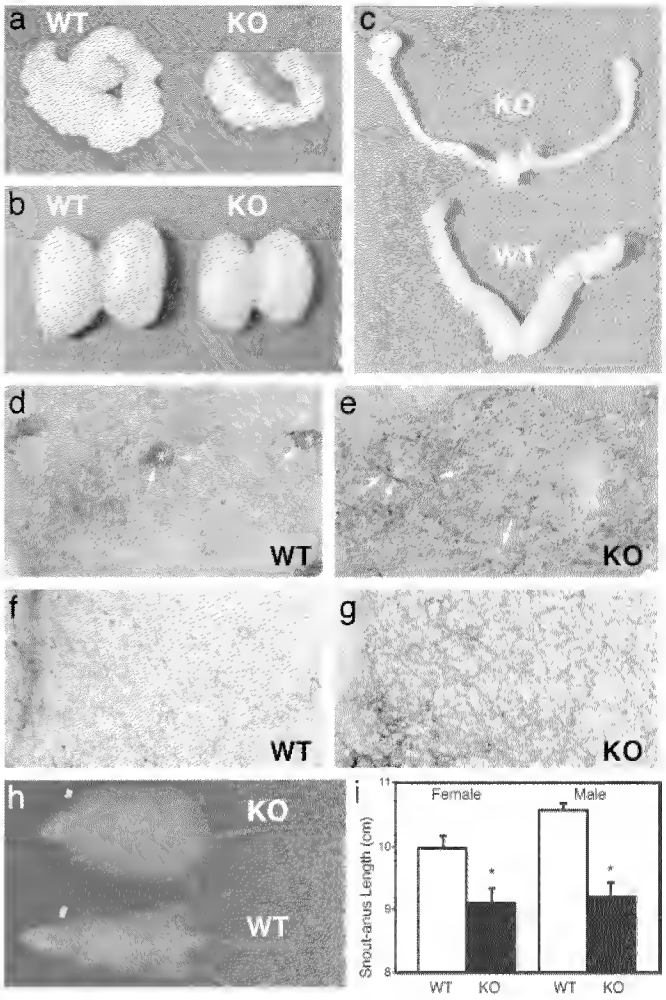

Fig. 5. $STAT3^{N-/-}$ animals are infertile, hypogonadal, and short. Seminal vesicles (a) as well as testes (*b*) are smaller in $STAT3^{N-/-}$ males. (*c*) Uterine horns of female KO mice are markedly decreased in size as well. (*d* and e) Immunocytochemistry of the lateral arcuate nucleus in WT and KO with anti-β-endorphin for POMC neurons diaminobenzidine (brown) and anti-NPY nickel diaminobenzidine (dark) (magnification, ×40). POMC staining (*) was not seen in KO animals. NPY neurons (arrows) were seen in direct contact with POMC neurons and overexpressed in KO animals. (*f* and *g*) KO animals showed overexpression of AgRP in the medial arcuate nucleus. WT and KO medial arcuate nuclei were stained by using anti-AgRP (Calbiochem) at 1:5,000. (*h*) An x-ray image of WT and KO animals showing decreased linear size and increased body mass. (*i*) Snout–anus measurements.

adipose tissue and white adipose tissue (44). In leptin mutants, such as *db/db* mice, sympathetic activity is reduced. To examine whether neuronal STAT3 disruption causes similar defects, we measured cold-induced thermogenesis. Animals were housed at 4°C for 3.5 h and body temperature was measured at 30-min intervals. Although control littermates were able to maintain their body temperature throughout the cold challenge, $STAT3^{N-/-}$ and *db/db* mice dropped ≈1°C in body temperature every 30 min until they reached 34°C and were able to stabilize this temperature throughout the rest of the experiment (Fig. 6*b*). These data are consistent with the decreased sympathetic activity seen in leptin signaling mutants but are different from the result obtained from the "β-less" triple β-adrenergic receptor KO mice, which fully disrupted β-adrenergic receptor function and animals fail to have any thermogenic response to cold challenge (45). Histological examination of $STAT3^{N-/-}$ animals revealed that the brown adipose tissue became diffuse and

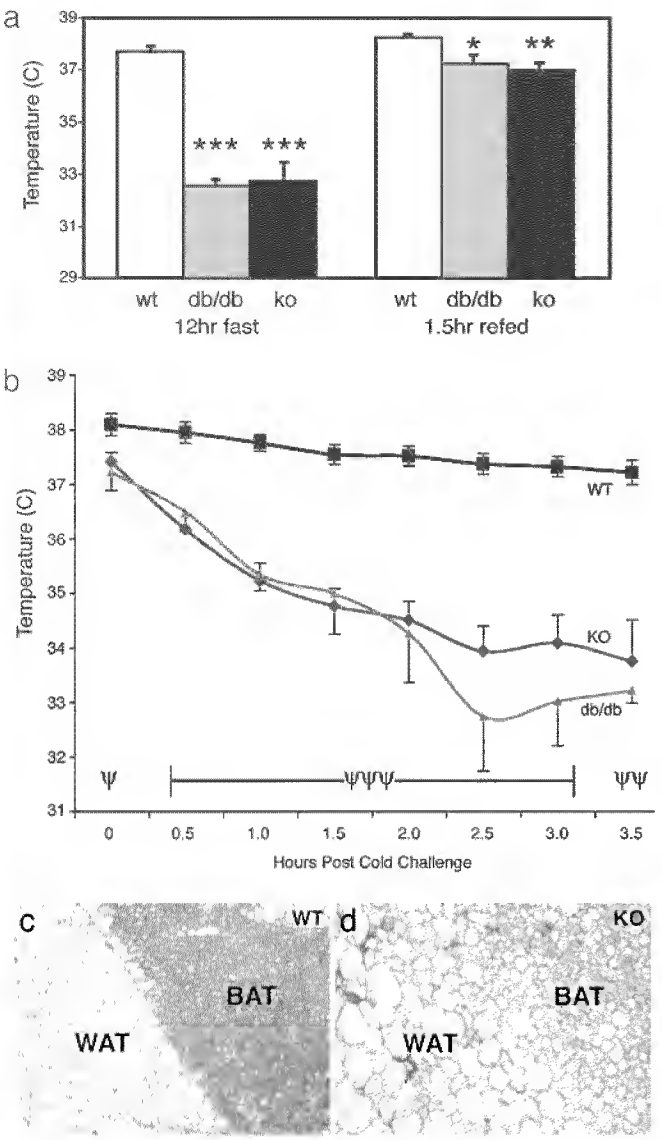

Fig. 6. Thermogensis and brown adipose tissue are altered in STAT3$^{N-/-}$ animals. (a) WT, *db/db*, and STAT3$^{N-/-}$ animals were fasted overnight, and the body temperatures were taken rectally. A 4°C drop in body temperature was seen after the fast in both *db/db* and KO animals, but body temperature was restored and maintained at 1.5 h of ad libitum refeeding. Note that, even at refeeding and fed status, temperature is significantly lower in both mutants (WT and KO, $n = 8$; *db/db*, $n = 4$). (*b*) Animals were subjected to a 4°C cold stress for 3.5 h. Body temperature dropped to ≈3°C below baseline temperature whereas WT animals maintained their body temperature. One *db/db* mutant died at the 3-h time point (WT and KO, $n = 6$; *db/db*, $n = 4$). (*c* and *d*) Hematoxylin and eosin staining of 10-μm frozen sections of brown and white adipose tissue. KO animals have larger white adipose cells and brown adipose tissue with more diffuse morphology resembling white adipose tissue in structure. (***, $P < 0.00001$; **, $P < 0.005$; *, $P < 0.012$) ($\psi\psi\psi$, $P < 0.00001$; $\psi\psi$, $P < 0.0003$; ψ, $P < 0.02$.)

resembled white adipose tissue in structure (Fig. 6*c*). The delineation between white and brown adipose tissue was less evident. This morphological change is less severe than that of β-less mice but is consistent with the impaired levels of thermogenesis in the β-less and STAT3$^{N-/-}$ animals.

Discussion

The acute phase response signaling/transcription factor STAT3 is broadly expressed in the CNS and is activated by a number of extracellular stimuli. We have shown that, during normal embryonic development and adulthood, the major function of neuronal STAT3 is for homeostatic regulation. There is a broad data set describing the effect of STAT3 on glial differentiation late in embryonic development (11–13). Our early deletion of STAT3 by using the nestin promoter surprisingly did not result in an absence of GFAP$^+$ astrocytes as expected (Q.G. and M.J.W., unpublished data). Therefore, *in vivo*, STAT3 may have a limited function during neural differentiation. The phenotype of the STAT3$^{N-/-}$ mouse closely resembles that of leptin-deficient mice. The restricted phenotype was surprising given the number of STAT3-activating cytokines produced in the brain. Although other STAT3-activating cytokines have weight reducing characteristics under artificial or pathological conditions (21, 22), the only candidate cytokine that can signal body energy stores efficiently in normal physiology is the fat-derived cytokine leptin. STAT3$^{N-/-}$ animals are hyperleptinemic but obese, and therefore leptin does not act to lower body weight in these animals.

The fact that the STAT3 deletion, which disrupts one distinct signaling output from the leptin receptor, can so closely resemble leptin deficiency is surprising and intriguing because recent studies have shown that in the hypothalamus, leptin activates multiple signaling events (24, 25). Specific inhibitors of some of these pathways can cause inhibitory actions to the effects of leptin. In addition, immediate electrical changes (27, 28) were also observed in hypothalamic neurons after leptin administration, which presumably is not the direct function of STAT3. Even recently, the role of STAT3 in hypothalamic signaling has come into question. Indeed, the conclusion from this study is contradictory to a recent report that concluded that STAT3 is not involved in neuroendocrinology including reproduction, and linear growth, and only moderately involved in glucose regulation (23). These conclusions were based on a receptor knock-in that mutated the putative STAT3 docking site (Y to S change at position 1,138 on the leptin receptor, LRb^{s1138}). We have found that the reproductive and growth characteristics of leptin receptor mutant mice are controlled by STAT3. The inconsistency between STAT3$^{N-/-}$ mice and LRb^{s1138} mice is probably due to the nature of the mutations, with STAT3$^{N-/-}$ mice ablating STAT3 directly and LRbs1138 having only diminished STAT3 activation by leptin (24). This is supported by *in vitro* data (24) and by other genetic models of leptin signaling such as lipodystrophic mice that have very low leptin levels and show the metabolic characteristics of leptin deficiency (46). However, these animals are fertile. STAT3$^{N-/-}$ animals also show the same neuropeptide levels as *db/db* animals indicating they are infertile via the same mechanism, lending further support for our model.

The infertility, decreased linear growth and high plasma corticosterone levels show that STAT3$^{N-/-}$ mice recapitulate the unique phenotypes of *db/db* mutants, which delineate STAT3$^{N-/-}$ and *db/db* mutants from other obese genetic models that often exhibit only a subset of the *db/db* phenotype. The fact that STAT3$^{N-/-}$ mutants exhibit all four characteristic defects (obesity, decreased linear growth, infertility, and high corticosterone) of *db/db* mutants provide convincing evidence that STAT3 mediates most, if not all, hypothalamic leptin function. This notion is further supported by comparative studies of energy expenditure between STAT3$^{N-/-}$ and *db/db* mutants measured by body temperature in response to fasting or cold stress. Therefore, the overlapping phenotypes between *db/db* mutants and STAT3$^{N-/-}$ mice unlikely resulted from a leptin-independent STAT3 function.

Leptin is not the only hormone that controls body weight and diabetes. There are multiple peripheral signals that can modify body weight independent of leptin. For example, insulin (29, 30) and long chain fatty acids (31, 32) regulate energy homeostasis within the hypothalamus. Insulin can act through insulin recep-

tor substrates (47, 48) and downstream pathways such as Akt/protein kinase B (49) to modulate energy homeostasis. How are these divergent pathways orchestrated? Are they organized in parallel or form convergent pathways to regulate energy balance? Because disruption of STAT3 causes all of the major phenotypes of leptin signaling, it is possible that different pathways activated by leptin or independent of leptin are convergent and function through STAT3. For example, both insulin and leptin activate phosphatidylinositol 3-kinase pathway in the hypothalamus. At least in some systems, the activation of this pathway requires STAT3 (50). It is also possible that leptin-STAT3 plays a dominant role in energy balance, whereas other pathways play modifying roles, which may be essential for age related and/or diet induced obesity and diabetes. Leptin is functional in humans, and leptin resistance in humans is rarely caused by direct defects on leptin or its receptor (51, 52). Therefore, the integration of these divergent pathways in energy homeostasis may be essential to garner a clear understanding, and better direct clinically relevant therapies. Further study of this model will address the interaction between Janus kinase/STAT signaling and other signaling pathways and elucidate the transcriptional control of neuropeptides and other down-stream target genes as well as the action of leptin within the CNS.

We thank Y. Xi for help with x-ray images. X.-Y.F. was a recipient of a Career Development Award from the National Institutes of Health. G.I.S. is an Investigator of Howard Hughes Medical Institute. This work was supported by National Institutes of Health Grants AI34522 and EY13607 (to X.-Y.F.), RO1DK-40936 and P30DK-45735 (to G.I.S.), and RR-014451 and DK-060711 (to T.L.H.).

1. Akira, S., Nishio, Y., Inoue, M., Wang, X. J., Wei, S., Matsusaka, T., Yoshida, K., Sudo, T., Naruto, M. & Kishimoto, T. (1994) *Cell* **77,** 63–71.
2. Zhong, Z., Wen, Z. & Darnell, J. E., Jr. (1994) *Science* **264,** 95–98.
3. Wegenka, U. M., Lutticken, C., Buschmann, J., Yuan, J., Lottspeich, F., Muller-Esterl, W., Schindler, C., Roeb, E., Heinrich, P. C. & Horn, F. (1994) *Mol. Cell. Biol.* **14,** 3186–3196.
4. Takeda, K., Noguchi, K., Shi, W., Tanaka, T., Matsumoto, M., Yoshida, N., Kishimoto, T. & Akira, S. (1997) *Proc. Natl. Acad. Sci. USA* **94,** 3801–3804.
5. Niwa, H., Burdon, T., Chambers, I. & Smith, A. (1998) *Genes Dev.* **12,** 2048–2060.
6. Takeda, K., Clausen, B. E., Kaisho, T., Tsujimura, T., Terada, N., Forster, I. & Akira, S. (1999) *Immunity* **10,** 39–49.
7. Welte, T., Zhang, S. S., Wang, T., Zhang, Z., Hesslein, D. G., Yin, Z., Kano, A., Iwamoto, Y., Li, E., Craft, J. E., *et al.* (2003) *Proc. Natl. Acad. Sci. USA* **100,** 1879–1884.
8. Yoo, J. Y., Huso, D. L., Nathans, D. & Desiderio, S. (2002) *Cell* **108,** 331–344.
9. Alonzi, T., Middleton, G., Wyatt, S., Buchman, V., Betz, U. A., Muller, W., Musiani, P., Poli, V. & Davies, A. M. (2001) *Mol. Cell. Neurosci.* **18,** 270–282.
10. Schweizer, U., Gunnersen, J., Karch, C., Wiese, S., Holtmann, B., Takeda, K., Akira, S. & Sendtner, M. (2002) *J. Cell Biol.* **156,** 287–297.
11. Bonni, A., Sun, Y., Nadal-Vicens, M., Bhatt, A., Frank, D. A., Rozovsky, I., Stahl, N., Yancopoulos, G. D. & Greenberg, M. E. (1997) *Science* **278,** 477–483.
12. Sun, Y., Nadal-Vicens, M., Misono, S., Lin, M. Z., Zubiaga, A., Hua, X., Fan, G. & Greenberg, M. E. (2001) *Cell* **104,** 365–376.
13. Takizawa, T., Nakashima, K., Namihira, M., Ochiai, W., Uemura, A., Yanagisawa, M., Fujita, N., Nakao, M. & Taga, T. (2001) *Dev. Cell* **1,** 749–758.
14. Moon, C., Yoo, J. Y., Matarazzo, V., Sung, Y. K., Kim, E. J. & Ronnett, G. V. (2002) *Proc. Natl. Acad. Sci. USA* **99,** 9015–9020.
15. Ghilardi, N., Ziegler, S., Wiestner, A., Stoffel, R., Heim, M. H. & Skoda, R. C. (1996) *Proc. Natl. Acad. Sci. USA* **93,** 6231–6235.
16. Darnell, J. E., Jr. (1996) *Proc. Natl. Acad. Sci. USA* **93,** 6221–6224.
17. Vaisse, C., Halaas, J. L., Horvath, C. M., Darnell, J. E., Jr., Stoffel, M. & Friedman, J. M. (1996) *Nat. Genet.* **14,** 95–97.
18. Friedman, J. M. & Halaas, J. L. (1998) *Nature* **395,** 763–770.
19. Elmquist, J. K., Ahima, R. S., Elias, C. F., Flier, J. S. & Saper, C. B. (1998) *Proc. Natl. Acad. Sci. USA* **95,** 741–746.
20. Elmquist, J. K., Ahima, R. S., Maratos-Flier, E., Flier, J. S. & Saper, C. B. (1997) *Endocrinology* **138,** 839–842.
21. Wallenius, V., Wallenius, K., Ahren, B., Rudling, M., Carlsten, H., Dickson, S. L., Ohlsson, C. & Jansson, J. O. (2002) *Nat. Med.* **8,** 75–79.
22. Lambert, P. D., Anderson, K. D., Sleeman, M. W., Wong, V., Tan, J., Hijarunguru, A., Corcoran, T. L., Murray, J. D., Thabet, K. E., Yancopoulos, G. D., *et al.* (2001) *Proc. Natl. Acad. Sci. USA* **98,** 4652–4657.
23. Bates, S. H., Stearns, W. H., Dundon, T. A., Schubert, M., Tso, A. W., Wang, Y., Banks, A. S., Lavery, H. J., Haq, A. K., Maratos-Flier, E., *et al.* (2003) *Nature* **421,** 856–859.
24. Banks, A. S., Davis, S. M., Bates, S. H. & Myers, M. G., Jr. (2000) *J. Biol. Chem.* **275,** 14563–14572.
25. Niswender, K. D., Morton, G. J., Stearns, W. H., Rhodes, C. J., Myers, M. G., Jr. & Schwartz, M. W. (2001) *Nature* **413,** 794–795.
26. Zhao, A. Z., Huan, J. N., Gupta, S., Pal, R. & Sahu, A. (2002) *Nat. Neurosci.* **5,** 727–728.
27. Spanswick, D., Smith, M. A., Groppi, V. E., Logan, S. D. & Ashford, M. L. (1997) *Nature* **390,** 521–525.
28. Cowley, M. A., Smart, J. L., Rubinstein, M., Cerdan, M. G., Diano, S., Horvath, T. L., Cone, R. D. & Low, M. J. (2001) *Nature* **411,** 480–484.
29. Bruning, J. C., Gautam, D., Burks, D. J., Gillette, J., Schubert, M., Orban, P. C., Klein, R., Krone, W., Muller-Wieland, D. & Kahn, C. R. (2000) *Science* **289,** 2122–2125.
30. Obici, S., Feng, Z., Karkanias, G., Baskin, D. G. & Rossetti, L. (2002) *Nat. Neurosci.* **5,** 566–572.
31. Obici, S., Feng, Z., Arduini, A., Conti, R. & Rossetti, L. (2003) *Nat. Med.* **9,** 756–761.
32. Loftus, T. M., Jaworsky, D. E., Frehywot, G. L., Townsend, C. A., Ronnett, G. V., Lane, M. D. & Kuhajda, F. P. (2000) *Science* **288,** 2379–2381.
33. Kano, A., Wolfgang, M. J., Gao, Q., Jacoby, J., Chai, G. X., Hansen, W., Iwamoto, Y., Pober, J. S., Flavell, R. A. & Fu, X. Y. (2003) *J. Exp. Med.* **198,** 1517–1525.
34. Tronche, F., Kellendonk, C., Kretz, O., Gass, P., Anlag, K., Orban, P. C., Bock, R., Klein, R. & Schutz, G. (1999) *Nat. Genet.* **23,** 99–103.
35. Graus-Porta, D., Blaess, S., Senften, M., Littlewood-Evans, A., Damsky, C., Huang, Z., Orban, P., Klein, R., Schittny, J. C. & Muller, U. (2001) *Neuron* **31,** 367–379.
36. Cohen, P., Zhao, C., Cai, X., Montez, J. M., Rohani, S. C., Feinstein, P., Mombaerts, P. & Friedman, J. M. (2001) *J. Clin. Invest.* **108,** 1113–1121.
37. Huszar, D., Lynch, C. A., Fairchild-Huntress, V., Dunmore, J. H., Fang, Q., Berkemeier, L. R., Gu, W., Kesterson, R. A., Boston, B. A., Cone, R. D., *et al.* (1997) *Cell* **88,** 131–141.
38. Bousquet, C., Zatelli, M. C. & Melmed, S. (2000) *J. Clin. Invest.* **106,** 1417–1425.
39. Marsh, D. J., Hollopeter, G., Huszar, D., Laufer, R., Yagaloff, K. A., Fisher, S. L., Burn, P. & Palmiter, R. D. (1999) *Nat. Genet.* **21,** 119–122.
40. Fan, W., Boston, B. A., Kesterson, R. A., Hruby, V. J. & Cone, R. D. (1997) *Nature* **385,** 165–168.
41. Yaswen, L., Diehl, N., Brennan, M. B. & Hochgeschwender, U. (1999) *Nat. Med.* **5,** 1066–1070.
42. Bray, G. A. & York, D. A. (1979) *Physiol. Rev.* **59,** 719–809.
43. Caprio, M., Fabbrini, E., Isidori, A. M., Aversa, A. & Fabbri, A. (2001) *Trends Endocrinol. Metab.* **12,** 65–72.
44. Lowell, B. B. & Spiegelman, B. M. (2000) *Nature* **404,** 652–660.
45. Bachman, E. S., Dhillon, H., Zhang, C. Y., Cinti, S., Bianco, A. C., Kobilka, B. K. & Lowell, B. B. (2002) *Science* **297,** 843–845.
46. Shimomura, I., Hammer, R. E., Richardson, J. A., Ikemoto, S., Bashmakov, Y., Goldstein, J. L. & Brown, M. S. (1998) *Genes Dev.* **12,** 3182–3194.
47. Sun, X. J., Wang, L. M., Zhang, Y., Yenush, L., Myers, M. G., Jr., Glasheen, E., Lane, W. S., Pierce, J. H. & White, M. F. (1995) *Nature* **377,** 173–177.
48. Withers, D. J., Gutierrez, J. S., Towery, H., Burks, D. J., Ren, J. M., Previs, S., Zhang, Y., Bernal, D., Pons, S., Shulman, G. I., *et al.* (1998) *Nature* **391,** 900–904.
49. Cho, H., Mu, J., Kim, J. K., Thorvaldsen, J. L., Chu, Q., Crenshaw, E. B., III, Kaestner, K. H., Bartolomei, M. S., Shulman, G. I. & Birnbaum, M. J. (2001) *Science* **292,** 1728–1731.
50. Pfeffer, L. M., Mullersman, J. E., Pfeffer, S. R., Murti, A., Shi, W. & Yang, C. H. (1997) *Science* **276,** 1418–1420.
51. Montague, C. T., Farooqi, I. S., Whitehead, J. P., Soos, M. A., Rau, H., Wareham, N. J., Sewter, C. P., Digby, J. E., Mohammed, S. N., Hurst, J. A., *et al.* (1997) *Nature* **387,** 903–908.
52. Clement, K., Vaisse, C., Lahlou, N., Cabrol, S., Pelloux, V., Cassuto, D., Gourmelen, M., Dina, C., Chambaz, J., Lacorte, J. M., *et al.* (1998) *Nature* **392,** 398–401.

Deletion of *Pten* in mouse brain causes seizures, ataxia and defects in soma size resembling Lhermitte-Duclos disease

Stéphanie A. Backman[1], Vuk Stambolic[2], Akira Suzuki[3], Jillian Haight[2], Andrew Elia[2], James Pretorius[4], Ming-Sound Tsao[5], Patrick Shannon[6], Brad Bolon[4], Gwen O. Ivy[7] & Tak W. Mak[1,2]

Published online: 19 November 2001, DOI: 10.1038/ng782

Initially identified in high-grade gliomas, mutations in the *PTEN* tumor-suppressor are also found in many sporadic cancers and a few related autosomal dominant hamartoma syndromes. PTEN is a 3′-specific phosphatidylinositol-3,4,5-trisphosphate ($PI(3,4,5)P_3$) phosphatase and functions as a negative regulator of PI3K signaling. We generated a tissue-specific deletion of the mouse homolog *Pten* to address its role in brain function. Mice homozygous for this deletion ($Pten^{loxP/loxP}$;*Gfap-cre*), developed seizures and ataxia by 9 wk and died by 29 wk. Histological analysis showed brain enlargement in $Pten^{loxP/loxP}$;*Gfap-cre* mice as a consequence of primary granule-cell dysplasia in the cerebellum and dentate gyrus. *Pten* mutant cells showed a cell-autonomous increase in soma size and elevated phosphorylation of Akt. These data represent the first evidence for the role of Pten and Akt in cell size regulation in mammals and provide an animal model for a human phakomatosis condition, Lhermitte-Duclos disease (LDD).

Introduction

Initially identified in glioblastomas, mutations of the *PTEN* tumor suppressor are also found in endometrial, prostate and breast cancers and melanomas (refs. 1,2; reviewed in ref. 3). PTEN functions as a $PI(3,4,5)P_3$ lipid phosphatase and antagonizes PI3K signaling[4]. Cells mutant for Pten show increased phosphorylation and activation of the serine/threonine kinase Akt accompanied by resistance to numerous apoptotic agents[5,6]. Increased proliferation is observed in Pten-null mouse embryos and stem cells[5,7].

PTEN mutations are also found in the autosomal dominant hamartoma syndromes Cowden disease and Bannayan-Riley-Ruvalcaba syndrome, which are thought to constitute a single syndrome[8–11]. Hallmark features of Cowden disease include the presentation early in life of hamartomatous overgrowths of various tissues, including skin, breast, intestine and brain, as well as a predisposition to develop breast and brain tumors late in life[12]. Lhermitte-Duclos disease is a component of Cowden disease involving a hamartoma of the brain and is characterized by overgrowth of hypertrophied granule cells in the cerebellum[13].

The majority of tumors associated with PTEN loss are of an advanced stage (reviewed in ref. 3). Although increased activation of Akt has been documented in glioblastomas[6], studies carried out using mouse models indicate that activation of other pathways such as Ras might be necessary to induce these high-grade tumors[14,15].

Deletion of *Pten* in mice results in embryonic lethality, whereas mice heterozygous with respect to *Pten* have a higher incidence of tumors in many organs but not in the brain[16–19]. To investigate the role of Pten function in development and tumorigenesis of the nervous system, we deleted *Pten* in the mouse brain using the Cre-*loxP* system. Although we used a *Gfap-cre* transgenic mouse (containing *cre* inserted into a glial fibrillary acidic protein (Gfap) promoter construct)[20] to target *Pten* deletion to the glial compartment, loss of Pten was restricted to neuronal cells. Pten mutant mice showed neurological defects including seizures and ataxia and died by 29 wk. Histological analyses showed brain enlargement and dysplasia of several neural cell populations, including enlarged soma in Pten-null neurons. Notably, Pten mutant mice share many similarities with persons suffering from the hamartoma syndrome Lhermitte-Duclos disease and offer a model in which to further study this disease.

Results

Deletion of *Pten* in cerebellum and dentate gyrus granule cells

A *Pten flox* mouse was generated with *loxP* sites flanking exons 4 and 5 of the mouse *Pten* locus (Fig. 1*a*). To specifically delete *Pten* in mouse brain, homozygous *Pten flox* mice ($Pten^{loxP/loxP}$)[21] were crossed with *Gfap-cre* transgenic mice[20]. To determine if Cre-mediated recombination of the *Pten* locus occurred in the brain

[1]*Department of Medical Biophysics, University of Toronto and Ontario Cancer Institute, 610 University Avenue, Toronto, Ontario M5G 2M9, Canada.* [2]*Amgen Research Institute, 620 University Avenue, Suite 706, Toronto, Ontario M5G 2C1, Canada.* [3]*Department of Molecular Cell Biology, Research Institute for Microbial Diseases, Osaka University, Yamadaoka 3-1, Suita, Osaka 565-0874, Japan.* [4]*Department of Pathology, Amgen Inc., One Amgen Center Drive, Thousand Oaks, California 91320-1799, USA.* [5]*Department of Laboratory Medicine and Pathobiology, University Health Network and University of Toronto, 610 University Avenue, Toronto, Ontario, M5G 2M9, Canada.* [6]*Division of Neuropathology, The Toronto Western Hospital and the University Health Care Network, 399 Bathurst St., Toronto, Ontario M5T 2S8, Canada.* [7]*Department of Psychology, University of Toronto, Scarborough Campus, 1265 Military Trail, Scarborough, Ontario M1C 1A4, Canada. Correspondence should be addressed to T.W.M. (tmak@oci.utoronto.ca).*

of *Pten*$^{loxP/loxP}$;*Gfap-cre* mice, we carried out Southern-blot analysis with genomic DNA isolated from brains of 8-wk *Pten*$^{loxP/loxP}$;*Gfap-cre* and *Pten*$^{+/loxP}$;*Gfap-cre* control mice. As indicated by the quantification of band intensity in Southern blot, Cre-mediated recombination at the *Pten*^{loxP} locus occurred in 47% of *Pten*$^{loxP/loxP}$;*Gfap-cre* genomic loci but in only 22% of *Pten*$^{+/loxP}$;*Gfap-cre* controls (Fig 1*b*). We confirmed recombination at the *Pten*^{loxP} locus in *Pten*$^{loxP/loxP}$;*Gfap-cre* brains by PCR amplification of a 849-bp band specific for the recombined *Pten* locus (Fig. 1*c*) using primers located upstream and downstream of the 5′ and 3′ *loxP* sites, respectively. We carried out Pten immunohistochemistry on brains from *Pten*$^{loxP/loxP}$;*Gfap-cre* and *Pten*$^{+/loxP}$;*Gfap-cre* mice to determine the pattern of Pten expression (Fig.1*d*,*e*). In *Pten*$^{+/loxP}$;*Gfap-cre* control mice, Pten was ubiquitously expressed, with prominent staining in Purkinje cells, pyramidal cells of the hippocampus and cortical neurons. We observed loss of Pten expression in brains of *Pten*$^{loxP/loxP}$;*Gfap-cre* mice in granule cells of the cerebellum and dentate gyrus (Fig. 1*d*,*e*), as well as some cortical neurons. The extent of *Pten* deletion (measured as the fraction of Pten-positive granule cells/total granule cells) was greater in the cerebellum (90±11%, n=3) than in the dentate gyrus, where the efficiency of *Pten* deletion was 35±14% (n=8) in *Pten*$^{loxP/loxP}$;*Gfap-cre* mice aged 8–14 wk.

We investigated the expression status of Pten in glial cells by comparing immunostaining in glial-rich regions of the *Pten*$^{+/loxP}$;*Gfap-cre* and *Pten*$^{loxP/loxP}$;*Gfap-cre* brains. Pten expression in isolated glial cells is very low or punctate and virtually undetectable (Fig. 2*c*), consistent with the previously reported lack of detection in murine astrocytes[22], whereas the white-matter tracts of the cerebellum, which include Gfap-positive processes (Fig. 2*a*,*b*), maintain a low level of expression in *Pten*$^{loxP/loxP}$;*Gfap-cre* mice (Fig. 2*d*). PTEN-null primary and immortalized cell lines from many organs, including glioblastoma cell lines, have elevated phosphorylation and activity of a serine/threonine kinase Akt[5–7,23–26]. Amounts of P-Akt were dramatically increased in the cerebellar granule-cell layer (Fig. 2*f*) and the dentate gyrus (Fig. 7*h*,*j*) of *Pten*$^{loxP/loxP}$;*Gfap-cre* mice as compared with control mice; however, P-Akt levels were unchanged in the white matter tracts of the cerebellum (Fig. 2*f*). Specific deletion of *Pten* in granule cells of the cerebellum and the dentate gyrus but, notably, not in astrocytes is consistent with the pattern of Cre-mediated recombination seen in *Rosa-lacZ* Cre reporter assays of the *Gfap-cre* parental line[20]. Thus, despite the expected Cre-mediated *Pten* recombination in astrocytes, both the reporter and the immunostaining data strongly suggest that *Pten* deletion is limited to neuronal cells in *Pten*$^{loxP/loxP}$;*Gfap-cre* mice. It is possible, however, that a low frequency of *Pten* recombination, undetectable by screening methods, occurs in glia.

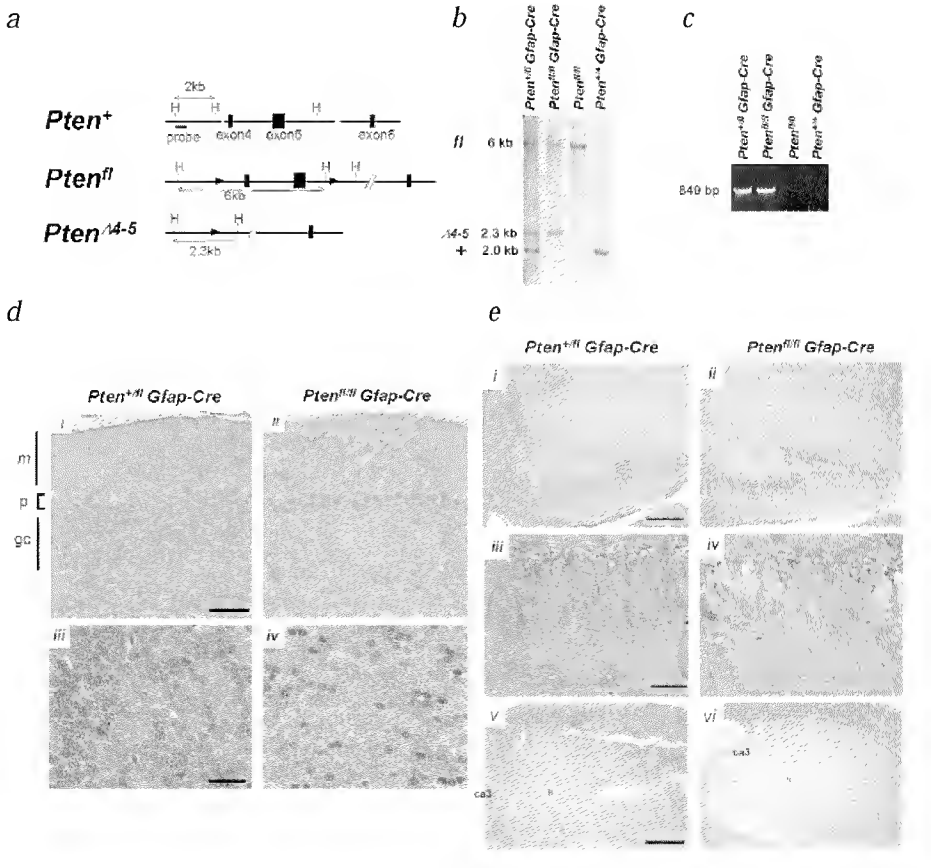

Fig. 1 Targeted conditional deletion of *Pten* in the brain. ***a***, Schematic representation of the mouse *Pten*$^{+}$ gene (middle) *Pten*^{loxP} locus with *loxP* sites flanking exons 4 and 5 and (bottom) the recombinant *Pten*$^{\Delta4-5}$ allele in which exons 4 and 5 were deleted by crossing the *Pten*^{loxP} allele with a *Gfap-cre* line[20]. Arrowheads denote positions of *loxP* sequences. H, *Hin*dIII. ***b***, Southern-blot genotypic analysis for brain-specific *Pten* deletion. Genomic DNA extracted from whole brain was digested with *Hin*dIII and hybridized with the 958-bp DNA probe (shown in *a*, top) to show bands (positions shown in *a*) for wildtype (*Pten*$^{+}$; 2-kb), non-recombined (*Pten*^{loxP}; 6 kb), and recombined (*Pten*$^{\Delta4-5}$; 2.3 kb) *Pten* alleles. ***c***, PCR confirmation of correct Cre-mediated recombination of the *Pten*^{loxP} locus. Primers situated upstream of the 5′ *loxP* site and downstream of the 3′ *loxP* site amplified an 849-bp product only upon Cre-mediated deletion of *Pten*$^{4-5}$. ***d–e***, Pten expression in cerebellum (*d*) and hippocampus (e) was lost in 4-wk *Pten*$^{loxP/loxP}$;*Gfap-cre* but not in age-matched *Pten*$^{+/loxP}$;*Gfap-cre* controls. In cerebellum (*d*, *i*) Pten in control brains (*i*, *iii*) was strongly expressed in neurons of the granule-cell (gc), molecular (m) and Purkinje-cell (p) layers relative to the distribution seen in mice with conditional *Pten* deletion (*ii*, *iv*). Panels *iii*, *iv* represent higher magnification of the internal granular cell layer shown in *i*, *ii*. Cells positive for *Pten* in the granule-cell layer of (*d*, *iv*) are glial cells and granule cells that have not undergone Cre-mediated recombination. Scale bars=50 μm (*i*, *ii*) and 25 μm (*iii*, *iv*). In dentate gyrus (e), Pten was widely expressed in granule cells of control mice at 4 (*i*, *iii*) and 10 (*v*) wk, whereas its distribution was modestly (*ii*, *iv*) to markedly (*vi*) reduced at 4 and 10 wk, respectively, in *Pten*$^{loxP/loxP}$;*Gfap-cre* mice. The dentate gyrus of 10-wk *Pten*$^{loxP/loxP}$;*Gfap-cre* mouse (*vi*) appears abnormal. The dentate gyrus area above and especially below the hilus (h) is expanded because of a lesion present in *Pten*$^{loxP/loxP}$;*Gfap-cre* mice by 10 wk. This lesion is further described in Fig. 7*d* and a higher magnification of Pten immunohistochemistry is in Fig. 7*n*. Panels *iii*, *iv* represent higher magnification of the granular cell layer shown in *i*, *ii*. Scale bars=100 μm (*i*, *ii*), 25 μm (*iii*, *iv*) and 0.5 mm (*v*, *vi*). 'ca3' denotes the cornu ammonis 3 as a point of reference.

Pten mutant mice have seizures, ataxia and macrocephaly

Pten$^{loxP/loxP}$;*Gfap-cre* mice are viable and appear healthy at birth. At an average age of 9 wk, these mice developed seizures and ataxia. Symptoms included episodes of front-paw tremors followed by spasms of hind legs (11/25 mice), ataxia (13/25) and sudden lethargy. None of these deficits were seen in age-matched *Pten*$^{+/loxP}$;*Gfap-cre* control mice during the monitoring period. All *Pten*$^{loxP/loxP}$;*Gfap-cre* mice monitored up to 29 wk died during this period (n=15; Fig. 3*a*), whereas the majority of *Pten*$^{+/loxP}$;*Gfap-cre* mice remained healthy, with no signs of motor dysfunction (25/27). Glioblastomas were excluded as a possible cause of death as these tumors were not present in *Pten*$^{loxP/loxP}$;*Gfap-cre* mice aged 4–19 wk (n=8, including four mice older than 9 wk).

Upon dissection, brains of *Pten*$^{loxP/loxP}$;*Gfap-cre* mice were substantially larger than those of age-matched *Pten*$^{+/loxP}$;*Gfap-cre* controls (Fig. 3*b*). Surface-area measurement of sagittal sections of isolated whole brains from 10–14-wk *Pten*$^{loxP/loxP}$;*Gfap-cre* mice showed a 43% increase in brain size in comparison to brains of age-matched *Pten*$^{+/loxP}$;*Gfap-cre* controls (Fig. 3*c*). We frequently saw hydrocephalus of the lateral ventricles in *Pten*$^{loxP/loxP}$;*Gfap-cre* mice (4/4; Fig. 3*b*).

Dysplasia in granule, Purkinje and molecular layer of Pten mutant cerebella

Presentation of motor dysfunction in the *Pten*$^{loxP/loxP}$;*Gfap-cre* mice coupled with significant cerebellar enlargement (Fig. 3*b*) warranted a detailed histological examination of the main motor-control centers in the cerebella of symptomatic *Pten*$^{loxP/loxP}$;*Gfap-cre* mice (10–14-wk). Analysis of Nissl-stained sections showed multifocal persistence of the external granular cell layer (EGCL) at the pial surface and heterotopic neuronal clusters scattered in the molecular layer in *Pten*$^{loxP/loxP}$;*Gfap-cre* cerebella (Fig. 4*b*). The molecular layer was thickened, especially at sites of heterotopic lesions (Fig. 4*b*). Immunohistochemistry for the neuronal marker microtubule-associated protein-2 (MAP-2) showed prominent disorganization and dysplasia in the molecular layer (Fig. 4*d*), and myelination was elevated as determined by staining for myelin-basic protein (Fig. 4*f*). Immunostaining for the Purkinje-cell marker calbindin showed partial loss of Purkinje cells, whereas those remaining were atrophic or dysplastic, as indicated by dendritic coarsening and axonal swelling (Fig. 4*h*). We also saw gliosis in the molecular layer (Fig. 5*d*). Although Purkinje-cell abnormalities were not restricted to regions of gliosis, they were more severe near these areas. Dysplastic neurons in the molecular layer were negative for calbindin and for glutamic acid decarboxylase (GAD), an enzyme present

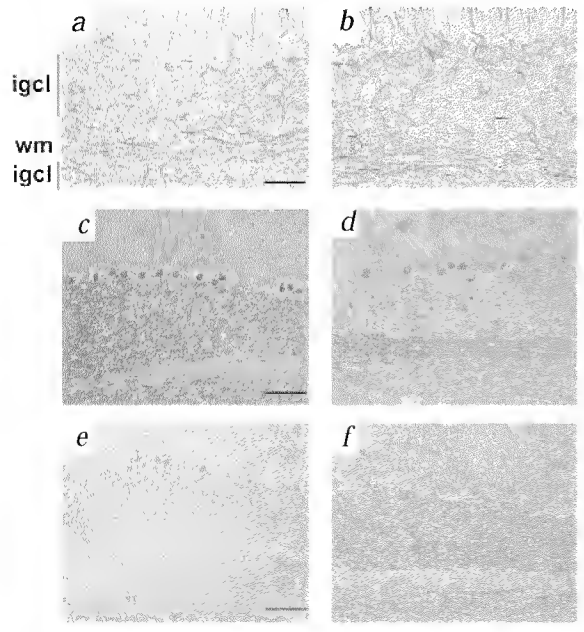

Fig. 2 Pten expression in glial cells of *Pten*$^{loxP/loxP}$;*Gfap-cre* mice aged 10 wk. *a,b*, Gfap immunohistochemistry. White-matter (wm) tracts of the cerebellum are rich in astrocytes in both *Pten*$^{+/loxP}$;*Gfap-cre* (**a**) and *Pten*$^{loxP/loxP}$;*Gfap-cre* mice (*b*). Increased Gfap immunoreactivity present in *Pten*$^{loxP/loxP}$;*Gfap-cre* mice is described further in Fig. 5*d* and accompanying text. *c,d*, Pten immunohistochemistry. Pten was expressed in wm of both *Pten*$^{+/loxP}$;*Gfap-cre* (*c*) and *Pten*$^{loxP/loxP}$;*Gfap-cre* brains (*d*). Notably, Pten is increased in *Pten*$^{loxP/loxP}$;*Gfap-cre* wm. *e,f*, P-Akt immunohistochemistry. Elevated activation of Akt in neurons of the internal granule-cell layer (igcl) of *Pten*$^{loxP/loxP}$;*Gfap-cre* mice (*f*) compared to *Pten*$^{+/loxP}$;*Gfap-cre* (*e*) brains, but not in the wm. All scale bars=50 μm.

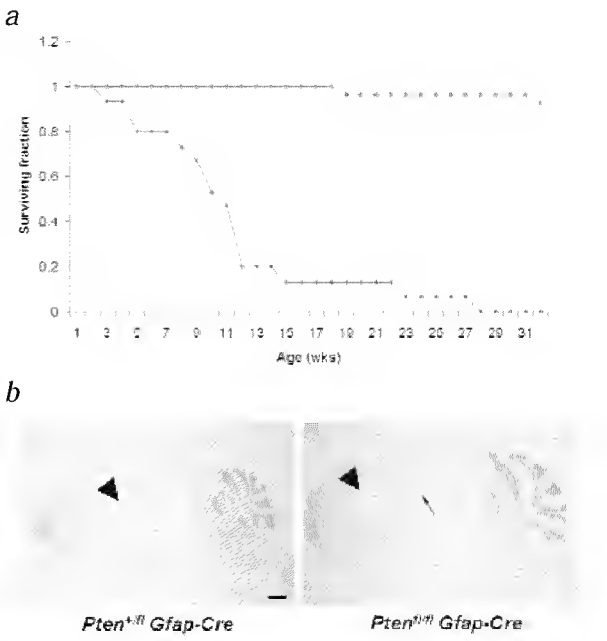

Fig. 3 Brain-specific conditional deletion of *Pten* results in premature death, macrocephaly and hydrocephalus. *a*, Survival of *Pten*$^{loxP/loxP}$;*Gfap-cre* mice (diamonds, n=15) was markedly decreased relative to that of *Pten*$^{+/loxP}$;*Gfap-cre* controls (boxes, n=27). *Pten*$^{loxP/loxP}$;*Gfap-cre* mice die at 10.7±1.9 wk, whereas the majority of *Pten*$^{+/loxP}$;*Gfap-cre* mice remain healthy. *b*, Conditional deletion of *Pten* in the brain was associated with marked macrocephaly (particularly prominent in the cerebellum), disorganization of the dentate gyrus in the hippocampus (arrow) and hydrocephalus of the lateral ventricle (arrowhead). Scale and staining as for a. *c*, Surface area of plane-matched sagittal brain sections. Average relative surface area of *Pten*$^{loxP/loxP}$;*Gfap-cre* brains (white bar; 2.81±0.335 mm^2 g^{-1}, n=4) was 43.3% greater than that of *Pten*$^{+/loxP}$;*Gfap-cre* brains (black bars; 1.96±0.12 mm^2 g^{-1}, n=4) by 10 wk (P=0.03). Average relative brain area was not significantly different between controls and Pten mutants at 4 wk (n=4, P=0.12). Values for *Pten*$^{loxP/loxP}$;*Gfap-cre* mice expressed as percentage of age-matched *Pten*$^{loxP/wt}$;*Gfap-cre*. Staining was with thionin-Nissl stain for neurons. Scale bar, 1 mm.

in the soma of stellate and basket interneurons of the molecular layer as well as in Purkinje cells[27,28] (Fig. 4*i–k*). The absence of calbindin and GAD staining in the aberrant neurons of the molecular layer, coupled with the extensive dysplasia of the EGCL and internal granular cell layers (IGCL; Fig. 4*a,b*), implies that the heterotopic cells belong to the granule-cell population.

In view of the fact that neural injury (with or without frank neurodegeneration) is accompanied by astrogliosis[29–32], we investigated abnormalities in Bergmann glia in the cerebellum. In many cases, astrogliosis was visible in close proximity to the affected heterotopic neurons (Fig. 5*d*), implying that the glial abnormalities are caused by the neuronal defects.

Immunohistochemical staining to detect the phosphorylated and activated form of Akt showed a dramatic increase in staining in the granule cells of the cerebellum of *Pten*$^{loxP/loxP}$;*Gfap-cre* mice, including the heterotopic cells (Fig. 5*a,b*). Elevated activity of Akt may cause an increase in proliferation or a decrease in cell death resulting in hypercellularity of the brain[33,34]. Judged by BrdU incorporation, the proportion of proliferating cells was less than 1% in both *Pten*$^{loxP/loxP}$;*Gfap-cre* mice and *Pten*$^{+/loxP}$;*Gfap-cre* mice (data not shown). The extent of apoptosis, determined by terminal deoxynucleotidyltransferase–mediated dUTP nick end labeling (TUNEL) staining, was also comparable in mice of the two genotypes (data not shown). Thus, the gross and microscopic neural defects did not result from late-stage alterations in proliferation or apoptosis in neuronal populations.

Normal proliferation and death in Pten mutant EGCL during development

The presence of heterotopic cells in the EGCL raises the possibility that this defect might arise during development. Lack of cell death or in hyperproliferation of immature granule cells could contribute to an increased number of EGCL cells that do not migrate to the IGCL in the first few weeks after birth (reviewed in ref. 35) and remain in this layer throughout adulthood. Increased cellularity could also contribute to the macrocephaly seen in the Pten mutants. Despite the normal appearance of the EGCL and molecular layer of Pten mutant brains in Nissl-stained sections of *Pten*$^{loxP/loxP}$;*Gfap-cre* mice (n=10; Fig. 6*b*), we saw loss of Pten expression accompanied by increased Akt phosphorylation (Fig. 6*d,f*) in the EGCL and outer part of the IGCL in lobules VIII–X of the cerebellum of *Pten*$^{loxP/loxP}$;*Gfap-cre* mice at postnatal day 10 (P10). However, proliferation and apoptosis in the EGCL and molecular layer were unchanged in *Pten*$^{loxP/loxP}$;*Gfap-cre* mice compared with controls (Fig. 6*g–k*). The presence of a normal-appearing EGCL without perturbations in proliferation or apoptosis in the Pten mutants indicates that the accumulation of granule cells at the pial surface and macrocephaly are not the results of increased cellularity in the developing EGCL.

Increased soma size in Pten-null neurons

Another mechanism by which loss of Pten in brains of *Pten*$^{loxP/loxP}$;*Gfap-cre* mice might lead to neuronal expansion and macrocephaly is through an increase in neuron size. *Pten*-null mutations in the *Drosophila* eye result in enlargement of mutant cells[36,37]. Pten is thought to regulate cell size in this system by antagonizing PI3K signaling via Akt[36–38]. As determined by surface area measurements, granule-cell soma from

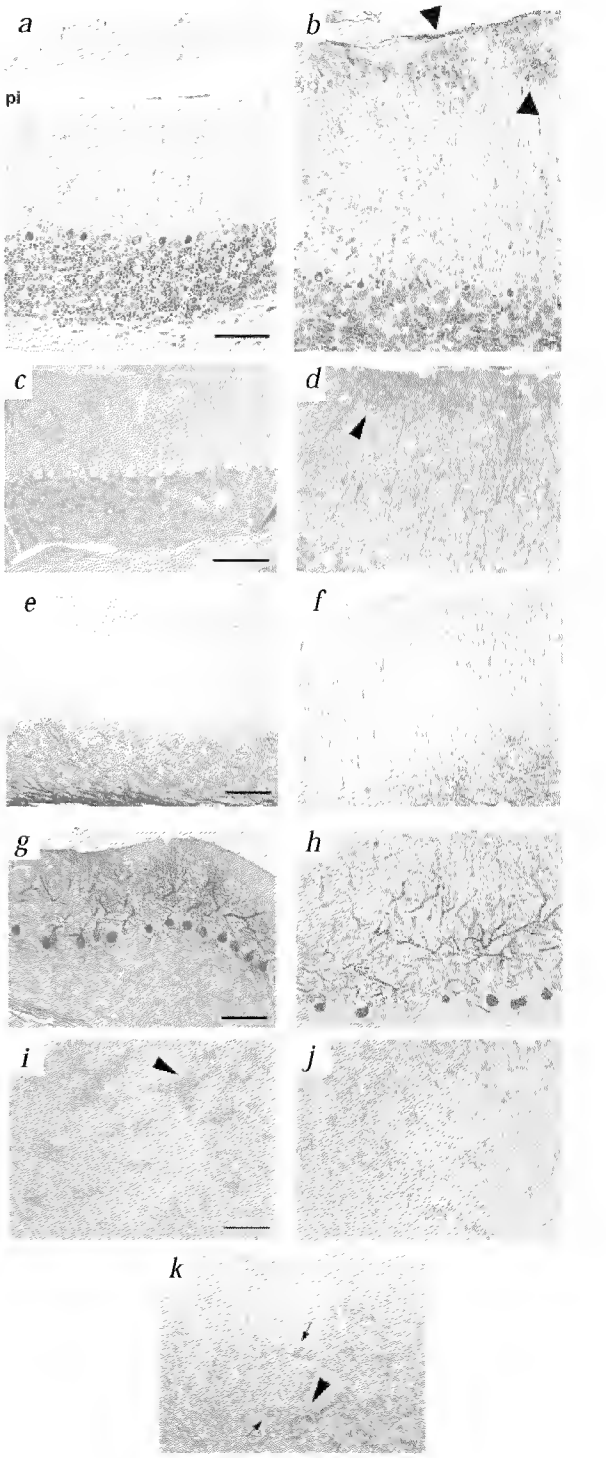

Fig. 4 Staining of cerebella of *Pten*$^{loxP/loxP}$;*Gfap-cre* mice and controls. Marked cerebellar dysplasia occurred in *Pten*$^{loxP/loxP}$;*Gfap-cre* mice (*b,d,f,h*) but not controls (*a,c,e,g*). ***a,b***, Thionin staining. Lesions in *Pten*$^{loxP/loxP}$;*Gfap-cre* mice (*b*) included thickening of the folia (particularly the molecular layer, ML); heterotopic clusters of dysplastic granule cells (arrowheads) persisting at the pial surface (pi) and scattered throughout the ML; Purkinje cell loss and atrophy; and dysplasia of the IGCL. ***c,d***, MAP-2 immunohistochemistry. In *Pten*$^{loxP/loxP}$;*Gfap-cre* mice (*d*), neurons in the ML are larger, more numerous and disorganized. Arrowhead denotes MAP-2 positive heterotopic neurons. ***e,f***, MBP immunohistochemistry. Myelination in the molecular layer was greater in *Pten*$^{loxP/loxP}$;*Gfap-cre* mice (*f*). ***g,h***, Calbindin immunohistochemistry. In mice lacking *Pten* (*h*), Purkinje-cell dendrites showed coarsened branching near heterotopic clusters of dysplastic neurons. Note that staining is absent in the heterotopic neurons. For *a–h*, scale bar=50 μm. ***i–k***, GAD immunohistochemistry in *Pten*$^{loxP/loxP}$;*Gfap-cre* brains; scale bar=20 μm. Granule cells of IGCL (*i*) and heterotopic neurons (*j*) of *Pten*$^{loxP/loxP}$;*Gfap-cre* brains are negative for GAD expression. Stellate and basket cells (arrows) as well as Purkinje-cell somas (arrowheads in *i* and *k*) express GAD (*k*).

Pten$^{loxP/loxP}$;*Gfap-cre* mice were approximately twofold larger than those from *Pten*$^{+/loxP}$;*Gfap cre* control brains at 10 wk (Fig. 5*e–g*). These data represent the first evidence for the role of Pten and Akt in cell-size regulation in mammalian cells.

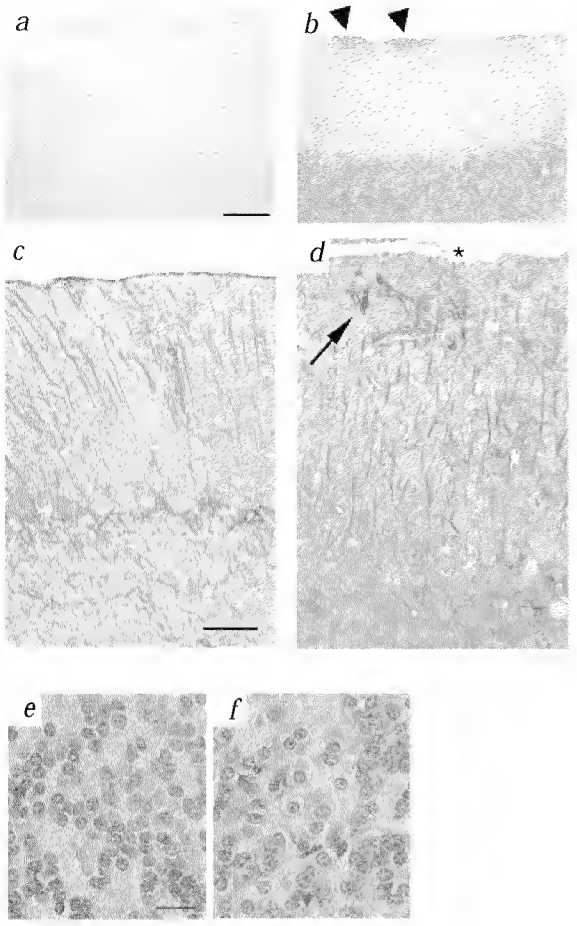

Fig. 5 Increased activation of Akt and granule soma size in *Pten*$^{loxP/loxP}$;*Gfap-cre* cerebella. ***a,b***, phospho-Akt (P-Akt) immunohistochemistry; scale bar=50 μm. Mice lacking *Pten* (*a*) have elevated levels of activated Akt in dysplastic granule cells of the IGCL and persistent external granular cell layer (arrowheads). ***c,d***, Gfap and P-Akt colorimetric co-immunohistochemistry; scale bar=20 μm. In *Pten*$^{+/loxP}$;*Gfap-cre* brains (*c*), Purkinje (blue) but not Bergmann glial cells (brown) express P-Akt. In mice lacking *Pten* (*d*), gliosis is evident, particularly below the asterisk. The majority of Bergmann glial cells are negative for P-Akt in the ML of *Pten*$^{loxP/loxP}$;*Gfap-cre*. Occasionally, P-Akt-positive glial processes (black, arrow) are present near heterotopic clusters of neurons. ***e,f***, Thionin staining; scale bar=10 μm. Dysplastic granule cells in the IGCL of *Pten*$^{loxP/loxP}$;*Gfap-cre* (*f*) mice were larger than those of control mice (*e*). ***g***, Average cerebellar granule-cell area of *Pten*$^{loxP/loxP}$;*Gfap-cre* mice (white bars; 13.50±0.42 μm^2, *n*=4) is greater than that of *Pten*$^{+/loxP}$;*Gfap-cre* mice (black bars; 6.94 ± 0.99 μm^2, *n*=4) at 10 wk (*P*<0.01). Average granule-cell area between *Pten*$^{loxP/loxP}$;*Gfap-cre* and *Pten*$^{+/loxP}$;*Gfap-cre* mice at 4 wk is not significantly different: *Pten*$^{loxP/loxP}$;*Gfap-cre* cell area is 8.40±2.9 μm^2 (*n*=4) and *Pten*$^{+/loxP}$;*Gfap-cre* cell area is 6.87±2.41 μm^2 (*n*=4, *P*=0.13).

Although heterotopic neurons and prominent molecular thickening are evident by 4 wk, the extent of Purkinje-cell abnormalities and astrogliosis is minimal at this age compared to 10 wk. Purkinje cell abnormalities at 10 wk are more severe and common than at 4 wk. The observed progression of Purkinje-cell and glial-cell abnormalities thus indicates that the initial site of neuronal dysplasia in the *Pten*$^{loxP/loxP}$;*Gfap-cre* mice is in the granule cells, whereas the Purkinje- and glial-cell aberrations are probably secondary effects. This is further supported by the fact that Cre-mediated deletion of *Pten* could not be detected in Purkinje cells or astrocytes of mice with mutated *Pten*. The well documented dependence of developing Purkinje cells and their dendrites on proper synaptic connections with granule cells supports such a view[39–42].

In addition to heterotopic cells and cells of the IGCL, P-Akt–positive processes were also present in the molecular layer of *Pten*$^{loxP/loxP}$;*Gfap-cre* mice (Fig. 5*b*). P-Akt–positive Purkinje cells were present in both control (Fig. 5*c*) and Pten mutant mice (data not shown). To determine if the P-Akt processes belonged to Bergmann glial cells, the predominant glial cell type in the molecular layer of the cerebellum, we carried out P-Akt/Gfap co-immunohistochemistry. Although the majority of Bergmann glial cells do not have increased P-Akt levels in *Pten*$^{loxP/loxP}$;*Gfap-cre* brains, there is occasional expression of P-Akt in this population (less than 1% of Bergmann glial cells) near sites of heterotopic neurons (Fig. 5*d*). Bergmann glial cells aid in the migration of granule cells from the pial surface to the IGCL[43]. It is possible that deletion of *Pten* in a minority of these cells affects their ability to aid in granule-cell migration, resulting in the sporadic accumulation of granule cells at the pial surface. Alternatively, it is possible that P-Akt is upregulated in gliotic Bergmann glial cells that are reacting to the neuronal lesion.

Dysplasia and neurodegeneration in Pten mutant hippocampus

In addition to changes in cerebellar granule cells, *Pten*$^{loxP/loxP}$;*Gfap-cre* mice also showed prominent loss of Pten in granule cells of the dentate gyrus. Few cells were affected at 4 wk relative to the marked, but not total, reduction in Pten-positive cells by 10 wk (Fig. 1*e*), paralleling the time course for the anatomic changes in the dentate gyrus of *Pten*$^{loxP/loxP}$;*Gfap-cre* mice. At 10 wk, symptomatic mice showed striking disorganization of the dentate gyrus characterized by marked undulation of the granule-cell layer of the dentate gyrus (Fig 7*d*). Intercellular spaces between granule-cell bodies, containing thick neuronal dendrites and astrocytes (data not shown), were expanded in *Pten*$^{loxP/loxP}$;*Gfap-cre* mice compared with the tightly packed conformation noted in the dentate gyrus of *Pten*$^{+/loxP}$;*Gfap-cre* mice (Fig. 7*k–l*). We saw prominent astrogliosis in the hippocampus and the sub-pial surface (Fig. 7*f*) and a reduction in pyramidal cell density of the cornu ammonis (Fig. 7*d*). This astrogliosis and neurodegeneration are consistent with mesial temporal sclerosis detected in some individuals with epilepsy[44]. As in the cerebellum, proliferation and apoptosis in the dentate gyrus were not significantly different between *Pten*$^{loxP/loxP}$; *Gfap-cre* and *Pten*$^{+/loxP}$;*Gfap-cre* mice (data not shown). Furthermore, granule cells of the dentate gyrus in *Pten*$^{loxP/loxP}$;*Gfap-cre* mice conformed to their cerebellar counterparts in having a greater surface area relative to those in *Pten*$^{+/loxP}$;*Gfap-cre* control brains (Fig. 7*m–o*).

Pten-null neurons show a cell-autonomous increase in soma size

Mosaic loss of Pten in the dentate gyrus of *Pten*$^{loxP/loxP}$;*Gfap-cre* mice allowed the assessment of neuronal soma size abnormalities relative to the adjacent cells that maintain wildtype expression of Pten (Fig. 7*m–o*). The average cell surface area of Pten-null granule

cells was approximately twofold larger than that of neighboring Pten-expressing granule cells. The fact that Pten-negative cells are enlarged whereas the immediate Pten-expressing neighbors are of normal size shows that the neuronal soma size phenotype resulting from *Pten* deletion is cell autonomous (Fig. 7*m,n*).

Discussion

Pathology of Pten mutant mice is similar to Lhermitte-Duclos disease

The seizures, ataxia, macrocephaly, thickened cerebellar folia, expansion and dysplasia of the granule cells into the molecular layer and its myelination, as well as the presence of large neuronal cells, dysplastic Purkinje cells and low proliferative index, seen in *Pten*$^{loxP/loxP}$;*Gfap-cre* mice resemble the hallmark symptoms of Lhermitte-Duclos disease (LDD), which is a component of the multiple hamartoma syndrome Cowden disease[13]. Significantly, Cowden disease is caused by a germline mutation in *PTEN*[8,13]. Lesions seen in the *Pten*$^{loxP/loxP}$;*Gfap-cre* mice can be categorized as hamartomas, as they are nodular overgrowths of mature cells of varying types appropriate to the tissue involved[45]. These mature cells include dysplastic granule cells, hypertrophied glial cells and oligodendrocytes with aberrant myelination. Causes of death from Lhermitte-Duclos disease include brainstem compression resulting from the cerebellar growth[46] and, as has been documented in one case, status epilepticus[47]. It is unlikely that the cerebellar lesion in *Pten*$^{loxP/loxP}$;*Gfap-cre* mice is severe enough to cause brainstem compression. *Pten*$^{loxP/loxP}$;*Gfap-cre* mice probably die from status epilepticus, cardiorespiratory problems resulting from their seizures or complications associated with hydrocephalus.

Whereas the LDD-like condition in mice appears only in the *Pten*-null genetic background, there is limited evidence for the loss of the second *PTEN* allele in LDD[48]. However, the high penetrance of an LDD-like condition in *Pten*$^{loxP/loxP}$;*Gfap-cre* mice implies that complete loss of PTEN expression is required for symptomatic LDD. Further investigations aimed at characterizing PTEN expression in individuals with LDD are needed to elucidate the relevance of the complete loss of PTEN in the pathogenesis of LDD. Considering the high degree of similarity in clinical presentation of individuals with LDD and *Pten*$^{loxP/loxP}$;*Gfap-cre* mice, these mice offer valuable insight into the progression of LDD. The data presented here imply that those with LDD may be clinically but not anatomically normal early in life (as seen in the 4-wk *Pten*$^{loxP/loxP}$;*Gfap-cre* mice) before developing clinical, and more pronounced morphologic, changes (similar to 10–14-wk mice). Proteus and Proteus-like syndrome are other conditions associated with *PTEN* mutations[49,50]. These diseases are characterized by hemihypertrophy, connective tissue and epidermal nevi, lipomas and vascular malformations[51]. Similar to the *Pten*$^{loxP/loxP}$;*Gfap-cre* mice and to individuals with LDD, individuals with Proteus syndrome occasionally present with macrocephaly and seizures, and histological analyses of brain tissue shows clusters of large neurons and areas of gliosis[51,52]. In light of the fact that granule-cell hypertrophy contributes to the macrocephaly in *Pten*$^{loxP/loxP}$;*Gfap-cre* mice and in persons with LDD, it is possible that neuron hypertrophy is also associated with the macrocephaly in Proteus and Proteus-like disease.

The phenotype seen in this study consists of granule-cell defects and the loss of Pten expression in these cells. Considering that an astrocyte-specific promoter, Gfap, was used to direct

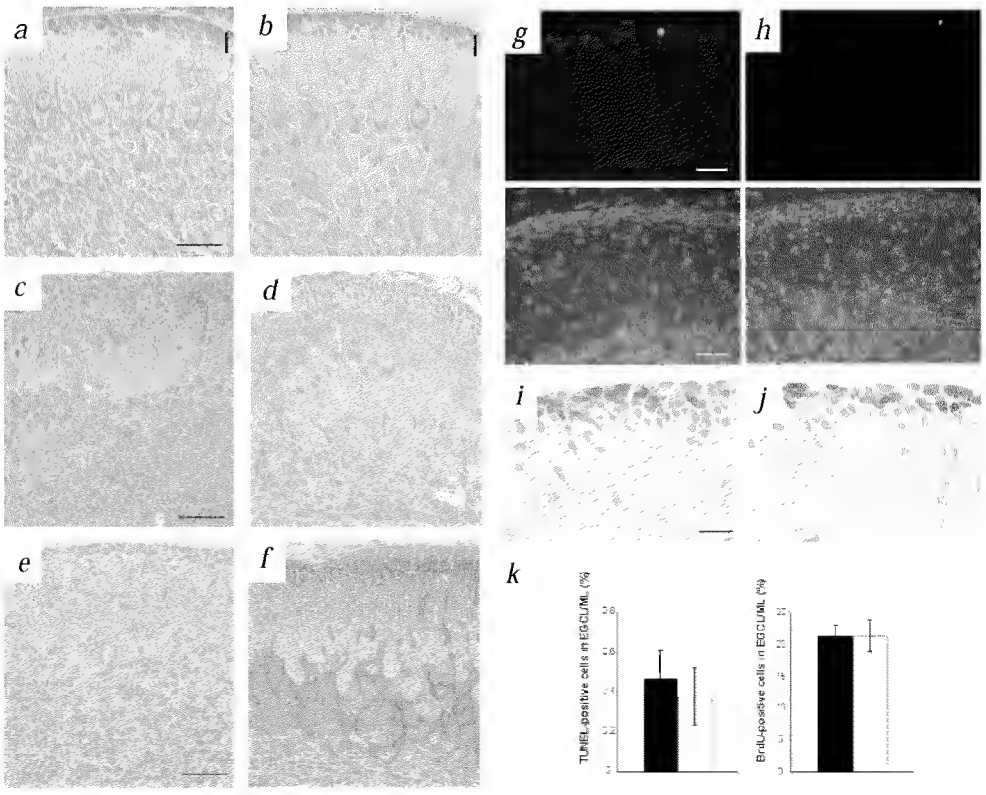

Fig. 6 Appearance, cell death and proliferation are normal in the EGCL of Pten mutant mice during postnatal development. ***a,b***, Thionin staining. The architecture of the EGCL and ML in cerebella of 10-day Pten mutant mice (*b*) was comparable to those of control mice (*a*; vertical line indicates location of the EGCL). ***c,d***, Pten immunohistochemistry. Pten expression was decreased in the EGCL and outer portion of the IGCL of *Pten*$^{loxP/loxP}$;*Gfap-cre* mice (*d*) compared to *Pten*$^{+/fl}$;*Gfap-cre* mice (*c*). ***e,f***, P-Akt immunohistochemistry. Elevated levels of activated Akt in the EGCL and outer portion of the IGCL in Pten mutant mice (*f*) compared with control mice (*e*). The extent of apoptosis is not significantly different between Pten mutant and control mice. ***g,h***, TUNEL FITC-fluorescence staining (upper) and DAPI counterstaining (lower). ***i,j***, BrdU immunohistochemistry. ***k***, Measurements of apoptosis and proliferation in EGCL/ML. Percentage of apoptotic cells in *Pten*$^{loxP/loxP}$;*Gfap-cre* EGCL/ML is 0.38±0.14 (*h*, white bar in *k*, left) as compared to 0.47±0.14 for *Pten*$^{+/loxP}$; *Gfap-cre* controls of the same age (*g*, black bar in *k*, left; n=4, P=0.69). Proliferation in EGCL/ML of Pten mutants (21.3±2.49%; *j*, white bar in *k*, right) was not significantly different compared to control mice (21.4±1.64%; n=4, P=0.98; *i*, black bar in *k*, right). Scale bars=20 μm (*a–h*), 10 μm (*i,j*).

Cre expression, it is possible that *Pten* deletion also occurred in astrocytes, affecting the granule-cell population in an indirect manner. However, Cre-mediated recombination is not detected in astrocytes of *Rosa-lacZ* reporter mice and granule soma size defects of Pten mutant mice are present in the context of morphologically normal glial cells at 4 wk, before alterations in the structure of the dentate gyrus appear (data not shown). In addition, the cell-autonomous effect of Pten loss in granule cells strongly implicates the granule cells as a primary source of the brain phenotype in Pten mutant mice. Considering that gliosis is frequently associated with seizures and neural insult[29,53], glial defects seen in Pten mutant mice are probably a consequence of the neuronal abnormalities in the dentate gyrus and the cerebellum.

Our results indicate that Pten has a pivotal role in the regulation of neuronal soma size in mammals. Consistent with studies in *Drosophila*, the cell-size phenotype caused by the loss of *Pten* is cell-autonomous[36]. Notably, the ability of Pten to regulate soma size might be restricted to neuronal cells in mammals, considering the absence of cell-size defects in mouse embryonic stem cells, embryonic fibroblasts or thymocytes mutated for *Pten* (V.S., A.S. and T.W.M., unpublished observations). Mice with a brain-targeted disruption of *Pten* provide an excellent animal model system for studying LDD and its underlying molecular mechanisms.

Methods

Genotype analysis. We isolated genomic DNA from mouse tail for PCR analysis. We genotyped the *Pten flox* allele using forward primer (5′–CTC CTCTACTCCATTCTTCCC–3′) and reverse primer (5′–ACTCCCACC AATGAA CAA AC–3′) that flank the 3′ *loxP* site. PCR products were 335-bp for the $Pten^{loxP}$ allele and 228-bp for the wildtype allele. We amplified the $Pten^{\Delta 4-5}$ allele using forward primer (5′–GTCACCAGGATG CTTCT GAC–3′) and reverse primer (5′–ACTATTGAACAGAATCA ACCC–3′). We genotyped for presence of the Cre allele using forward primer (5′–TCGCGATTATCT TCTATA TCTTCAG–3′) and reverse primer (5′–GCTCGACCAGTTTAGTTACCC–3′). We carried out Southern blot analysis of whole-brain genomic DNA as per Suzuki *et al.*[21].

Histology and immunohistochemistry. We perfused mice with 4% paraformaldehyde and post-fixed dissected brains for 24–48 h before paraffin embedding. For MAP-2 immunohistochemistry, we cryoprotected brains with 30% sucrose and froze them in OCT compound for cryostat sectioning. We carried out thionin Nissl staining and immunohistochemistry on 7-μm sections. We used the antibodies at the following dilutions: Pten (Neomarkers), 1:50; phospho-Akt (New England Biolabs), 1:50; Gfap

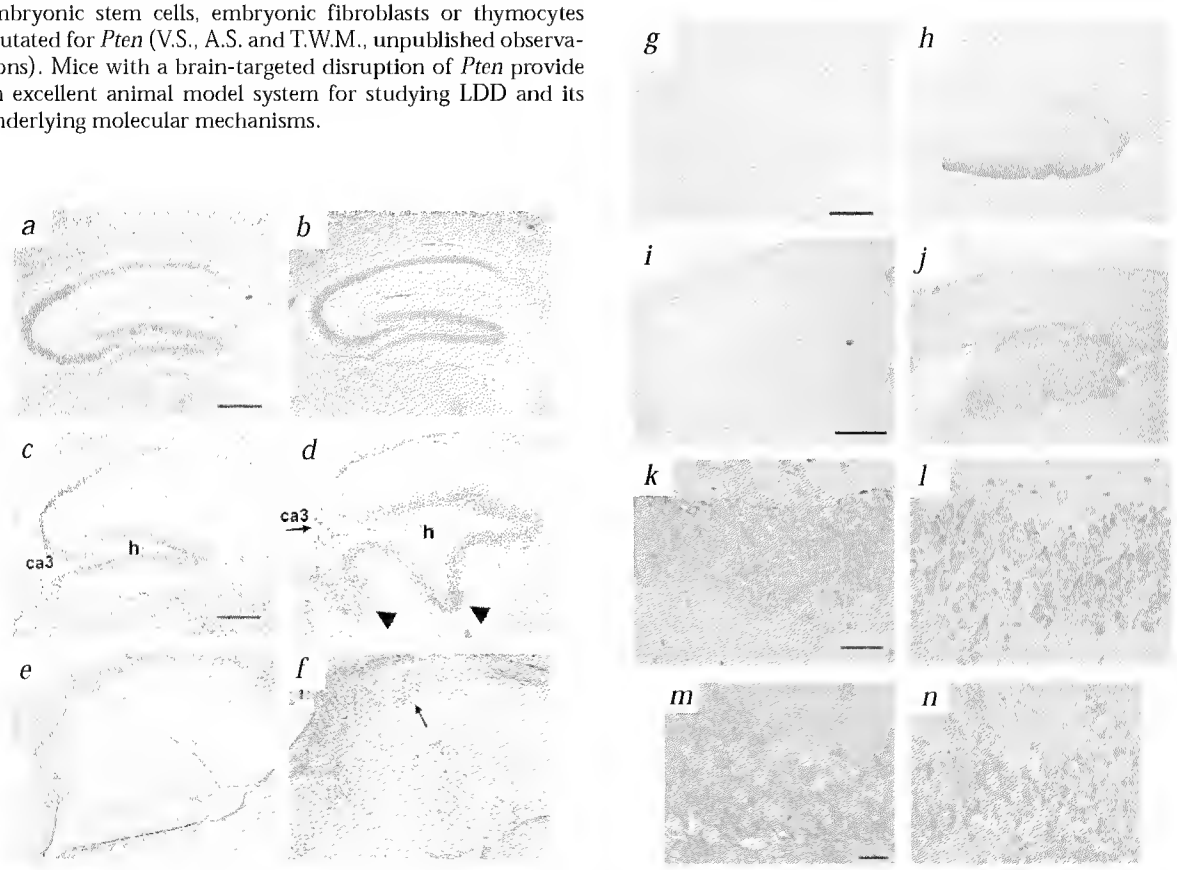

Fig. 7 Pronounced dysplasia of the dentate gyrus (DG) and CA3. *b,d,f,h,j,l*, sections from $Pten^{loxP/loxP}$;*Gfap-cre* mutated mice. *a,c,e,g,i,k*, Sections from control mice. *a–d*, Thionin staining; scale bar=100 μm (*a,b*), 0.5 mm (*c,d*). At 4 wk (*b*), DG morphology was comparable, but by 10 wk (*d*) the most pronounced DG feature in $Pten^{loxP/loxP}$;*Gfap-cre* mice was undulation of the granule-cell layer (arrowheads) and sclerosis of the pyramidal cell layer of the CA3 (ca3, arrow). *e,f*, Gfap immunhistochemistry. Astrogliosis was prominent in the hippocampus of $Pten^{loxP/loxP}$;*Gfap-cre* mice (*f*) near sclerotic pyramidal cells (arrow) and the hilus (h) of the DG. *g–j*, P-Akt immunohistochemistry; scale bar=100 μm (*a,b*) and 0.5 mm (*c,d*). Elevated levels of activated Akt in granule-cell pericarya and dendrites are visible in $Pten^{loxP/loxP}$;*Gfap-cre* mice at 4 (*h*) and 10 (*j*) wk. *k,l*, Thionin staining; scale bar=25 μm. *l*, Granule-cell soma in the DG of 10-week mutants (*l*) appeared larger and less densely packed. *m,n*, Pten immunohistochemistry; scale bar=25 μm. Pten-null granule cells of the dentate gyrus are larger than neighboring Pten-expressing cells in 4- (*m*) and 10-week (*n*) $Pten^{loxP/loxP}$;*Gfap-cre* mice. *o*, Average surface area of Pten-negative granule cells in 4- and 10-wk $Pten^{loxP/loxP}$;*Gfap-cre* mice (white bars; 64.05±6.94 μm² and 63.58±5.92 μm², respectively) were approximately twofold greater than the neighboring Pten-expressing (black bars) cells (26.69±1.72 μm² and 30.28±3.12 μm², respectively).

(Dako), 1:5,000; MAP-2 (Sigma), 1:250; calbindin (IDLabs), 1:100; MBP (Biogenics), 1:100) BrdU (Caltag), 1:1000; GAD (Chemicon), 1:200. We used biotinylated secondary antibodies plus streptavidin–peroxidase complex to detect primary antibodies, and used red AEC or Nova Red staining for all immunohistochemistry except P-Akt/Gfap co-immunohistochemistry, where we used blue DAB-Ni^{2+} and brown DAB, respectively. We used an *in situ* cell detection kit (Roche) for TUNEL staining. Briefly, we end-labeled DNA breaks using FITC-conjugated modified nucleotides.

BrdU and TUNEL experiments. We injected mice with 50 mg per kg of 5-bromo-2-deoxyuridine (BrdU) 5 h before killing for P10 pups and every 2 h over 12 h for 10–14-wk mice. We counted at least 400 cells from lobule X of the cerebellum for both BrdU and TUNEL analysis of P10 mice.

Cell and brain area measurements. We measured cell surface area of granule cells with a visible nucleus in a defined field on thionin-stained and Pten immunohistochemistry sections using Improvision Openlab scientific imaging software (version 2.1). We measured the surface area of five plane-matched sagittal brain sections per mouse, averaged and normalized for body mass.

Acknowledgments

We thank S. Baker for providing Gfap-cre mice and discussing data before publication, K. So, L. Yoong, S. Plyte, W. King, J. Henderson and J. Robertson for technical assistance and S. Pownall, A. Guha and M. Burnham for helpful comments and discussion. V.S. is a recipient of a postdoctoral fellowship from the Cancer Research Institute, New York. This work is supported by the National Cancer Institute of Canada and the Canadian Breast Cancer Research Initiative.

Received 27 September; accepted 5 November 2001.

1. Li, J. *et al.* PTEN, a putative protein tyrosine phosphatase gene mutated in human brain, breast, and prostate cancer. *Science* **275**, 1943–1947 (1997).
2. Steck, P.A. *et al.* Identification of a candidate tumour suppressor gene, MMAC1, at chromosome 10q23.3 that is mutated in multiple advanced cancers. *Nature Genet.* **15**, 356–362 (1997).
3. Simpson, L. & Parsons, R. PTEN: life as a tumor suppressor. *Exp. Cell. Res.* **264**, 29–41 (2001).
4. Maehama, T. & Dixon, J.E. The tumor suppressor, PTEN/MMAC1, dephosphorylates the lipid second messenger, phosphatidylinositol 3,4,5-trisphosphate. *J. Biol. Chem.* **273**, 13375–13378 (1998).
5. Stambolic, V. *et al.* Negative regulation of PKB/Akt-dependent cell survival by the tumor suppressor PTEN. *Cell* **95**, 29–39 (1998).
6. Haas-Kogan, D. *et al.* Protein kinase B (PKB/Akt) activity is elevated in glioblastoma cells due to mutation of the tumor suppressor PTEN/MMAC. *Curr. Biol.* **8**, 1195–1198 (1998).
7. Sun, H. *et al.* PTEN modulates cell cycle progression and cell survival by regulating phosphatidylinositol 3,4,5,-trisphosphate and Akt/protein kinase B signaling pathway. *Proc. Natl Acad. Sci. USA* **96**, 6199–6204 (1999).
8. Liaw, D. *et al.* Germline mutations of the PTEN gene in Cowden disease, an inherited breast and thyroid cancer syndrome. *Nature Genet.* **16**, 64–67 (1997).
9. Marsh, D.J. *et al.* Germline mutations in PTEN are present in Bannayan-Zonana syndrome [letter]. *Nature Genet.* **16**, 333–334 (1997).
10. Marsh, D.J. *et al.* Germline PTEN mutations in Cowden syndrome-like families. *J. Med. Genet.* **35**, 881–885 (1998).
11. Marsh, D.J. *et al.* PTEN mutation spectrum and genotype-phenotype correlations in Bannayan-Riley-Ruvalcaba syndrome suggest a single entity with Cowden syndrome. *Hum. Mol. Genet.* **8**, 1461–1472 (1999).
12. Eng, C. & Peacocke, M. PTEN and inherited hamartoma-cancer syndromes [letter]. *Nature Genet.* **19**, 223 (1998).
13. Wiestler, O.D., Padberg, G.W. & Steck, P.A. Cowden disease and dysplastic gangliocytoma of the cerebellum/Lhermitte-Duclos disease. in *Pathology and Genetics of Tumors of the Nervous System* (eds. Kleihues, P. & Cavenee, W.K.) 235–237 (IARCPress, Lyon, 2000).
14. Holland, E.C. *et al.* Combined activation of Ras and Akt in neural progenitors induces glioblastoma formation in mice. *Nature Genet.* **25**, 55–57 (2000).
15. Ding, H. *et al.* Astrocyte-specific expression of activated p21-ras results in malignant astrocytoma formation in a transgenic mouse model of human gliomas. *Cancer Res.* **61**, 3826–3836 (2001).
16. Di Cristofano, A., Pesce, B., Cordon-Cardo, C. & Pandolfi, P.P. Pten is essential for embryonic development and tumour suppression. *Nature Genet.* **19**, 348–355 (1998).
17. Suzuki, A. *et al.* High cancer susceptibility and embryonic lethality associated with mutation of the PTEN tumor suppressor gene in mice. *Curr. Biol.* **8**, 1169–1178 (1998).
18. Podsypanina, K. *et al.* Mutation of Pten/Mmac1 in mice causes neoplasia in multiple organ systems. *Proc. Natl Acad. Sci. USA* **96**, 1563–1568 (1999).
19. Stambolic, V. *et al.* High incidence of breast and endometrial neoplasia resembling human Cowden syndrome in *pten*$^{+/-}$ mice. *Cancer Res.* **60**, 3605–3611 (2000).
20. Kwon, C.H. *et al.* Pten regulates neuronal soma size: a mouse model for Lhermitte-Duclos disease. *Nature Genet.* **29**, 404–411 (2001).
21. Suzuki, A. *et al.* T cell-specific loss of Pten leads to defects in central and peripheral tolerance. *Immunity* **14**, 523–534 (2001).
22. Lachyankar, M.B. *et al.* A role for nuclear PTEN in neuronal differentiation. *J. Neurosci.* **20**, 1404–1413 (2000).
23. Myers, M.P. *et al.* The lipid phosphatase activity of PTEN is critical for its tumor supressor function. *Proc. Natl Acad Sci. USA.* **95**, 13513–13518 (1998).
24. Dahia, P.L. *et al.* PTEN is inversely correlated with the cell survival factor Akt/PKB and is inactivated via multiple mechanisms in haematological malignancies. *Hum. Mol. Genet.* **8**, 185–193 (1999).
25. Ramaswamy, S. *et al.* Regulation of G1 progression by the PTEN tumor suppressor protein is linked to inhibition of the phosphatidylinositol 3-kinase/Akt pathway. *Proc. Natl Acad. Sci. USA.* **96**, 2110–2115 (1999).
26. Bruni, P. *et al.* PTEN expression is reduced in a subset of sporadic thyroid carcinomas: evidence that PTEN-growth suppressing activity in thyroid cancer cells mediated by p27kip1. *Oncogene* **19**, 3146–3155 (2000).
27. Hampe, C.S. *et al.* A novel monoclonal antibody specific for the N-terminal end of GAD65. *J. Neuroimmunol.* **113**, 63–71 (2001).
28. Wuenschell, C.W., Fisher, R.S., Kaufman, D.L. & Tobin, A.J. *In situ* hybridization to localize mRNA encoding the neurotransmitter synthetic enzyme glutamate decarboxylase in mouse cerebellum. *Proc. Natl Acad. Sci. USA.* **83**, 6193–6197 (1986).
29. Norenberg, M.D. Astrocyte responses to CNS injury. *J. Neuropathol. Exp. Neurol.* **53**, 213–220 (1994).
30. Karle, J., Woldbye, D.P. & Diemer, N.H. $GABA_A$ receptor antisense epilepsy: histological changes following infusion of antisense oligodeoxynucleotide to $GABA_A$ receptor $\gamma 2$ subunit into rat hippocampus. *Neurol. Res.* **23**, 39–46 (2001).
31. Nishio, S., Morioka, T., Hisada, K. & Fukui, M. Temporal lobe epilepsy: a clinicopathological study with special reference to temporal neocortical changes. *Neurosurg. Rev.* **23**, 84–89 (2000).
32. Khurgel, M. *et al.* Activation of astrocytes during epileptogenesis in the absence of neuronal degeneration. *Neurobiol. Dis.* **2**, 23–35 (1995).
33. Datta, S.R., Brunet, A. & Greenberg, M.E. Cellular survival: a play in three Akts. *Genes. Dev.* **13**, 2905–2927 (1999).
34. Stambolic, V., Mak, T.W. & Woodgett, J.R. Modulation of cellular apoptotic potential: contributions to oncogenesis. *Oncogene* **18**, 6094–6103 (1999).
35. Goldowitz, D. & Hamre, K. The cells and molecules that make a cerebellum. *Trends Neurosci.* **21**, 375–382 (1998).
36. Huang, H. *et al.* PTEN affects cell size, cell proliferation and apoptosis during *Drosophila* eye development. *Development* **126**, 5365–5372 (1999).
37. Goberdhan, D.C., Paricio, N., Goodman, E.C., Mlodzik, M. & Wilson, C. *Drosophila* tumor suppressor PTEN controls cell size and number by antagonizing the Chico/PI3-kinase signaling pathway. *Genes. Dev.* **13**, 3244–3258 (1999).
38. Scanga, S.E. *et al.* The conserved PI3'K/PTEN/Akt signaling pathway regulates both cell size and survival in *Drosophila*. *Oncogene* **19**, 3971–3977 (2000).
39. Rakic, P. Role of cell interaction in development of dendritic patterns. *Adv. Neurol.* **12**, 117–134 (1975).
40. Privat, A. & Drian, M.J. Postnatal maturation of rat Purkinje cells cultivated in the absence of two afferent systems: an ultrastructural study. *J. Comp. Neurol.* **166**, 201–243 (1976).
41. Sotelo, C. & Arsenio-Nunes, M.L. Development of Purkinje cells in absence of climbing fibers. *Brain Res.* **111**, 289–295 (1976).
42. Morrison, M.E. & Mason, C.A. Granule neuron regulation of Purkinje cell development: striking a balance between neurotrophin and glutamate signaling. *J. Neurosci.* **18**, 3563–3573 (1998).
43. Voogd, J. & Glickstein, M. The anatomy of the cerebellum. *Trends Neurosci.* **21**, 370–375 (1998).
44. Babb T, B.W. Pathological findings in epilepsy. in *Surgical Treatment of Epilepsies* (ed. Engel, J.) 511–540 (Raven Press, New York, 1987).
45. Dorland, W.A. *Dorland's Illustrated Medical Dictionary*, 2088 (WB Saunders, New York, 2000).
46. Vinchon, M. *et al.* Association of Lhermitte-Duclos and Cowden disease: report of a new case and review of the literature. *J. Neurol. Neurosurg. Psychiatry* **57**, 699–704 (1994).
47. Roessmann, U. & Wongmongkolrit, T. Dysplastic gangliocytoma of cerebellum in a newborn. Case report. *J. Neurosurg.* **60**, 845–847 (1984).
48. Iida, S. *et al.* A heterozygous frameshift mutation of the PTEN/MMAC1 gene in a patient with Lhermitte-Duclos disease—only the mutated allele was expressed in the cerebellar tumor. *Int. J. Mol. Med.* **1**, 925–929 (1998).
49. Zhou, X.P. *et al.* Germline and germline mosaic PTEN mutations associated with a Proteus-like syndrome of hemihypertrophy, lower limb asymmetry, arteriovenous malformations and lipomatosis. *Hum. Mol. Genet.* **9**, 765–768 (2000).
50. Zhou, X. *et al.* Association of germline mutation in the PTEN tumour suppressor gene and Proteus and Proteus-like syndromes. *Lancet* **358**, 210–211 (2001).
51. Biesecker, L.G. *et al.* Proteus syndrome: diagnostic criteria, differential diagnosis, and patient evaluation. *Am. J. Med. Genet.* **84**, 389–395 (1999).
52. Griffiths, P.D., Welch, R.J., Gardner-Medwin, D., Gholkar, A. & McAllister, V. The radiological features of hemimegalencephaly including three cases associated with proteus syndrome. *Neuropediatrics* **25**, 140–144 (1994).
53. Steward, O., Torre, E.R., Tomasulo, R. & Lothman, E. Seizures and the regulation of astroglial gene expression. *Epilepsy. Res. Suppl.* **7**, 197–209 (1992).